Dynamical properties of piecewise-smooth stochastic models

Yaming Chen

School of Mathematical Sciences

Queen Mary University of London

Submitted in partial fulfilment of the requirements

of the Degree of Doctor of Philosophy

September 2014

I, Yaming Chen, confirm that the research included within this thesis is my own work or that where it has been carried out in collaboration with, or supported by others, that this is duly acknowledged below and my contribution indicated. Previously published material is also acknowledged below.

I attest that I have exercised reasonable care to ensure that the work is original, and does not to the best of my knowledge break any UK law, infringe any third party's copyright or other Intellectual Property Right, or contain any confidential material.

I accept that the College has the right to use plagiarism detection software to check the electronic version of the thesis.

I confirm that this thesis has not been previously submitted for the award of a degree by this or any other university.

Signature: Yaming Chen

Date: 24/09/2014

Details of collaboration and publications:

- Y. Chen, A. Baule, H. Touchette, W. Just. Weak-noise limit of a piecewise-smooth stochastic differential equation. Physical Review E 88, 052103 (2013).
- Y. Chen, W. Just. First-passage time of Brownian motion with dry friction. Physical Review E 89, 022103 (2014).
- Y. Chen, W. Just. On large deviation properties of Brownian motion with dry friction. Accepted for publication in Physical Review E.

Abstract

Piecewise-smooth stochastic systems are widely used in engineering science. However, the theory of these systems is only in its infancy. In this thesis, we take as an example the Brownian motion with dry friction to illustrate dynamical properties of these systems with respect to three interesting topics: (i) weak-noise approximations, (ii) first-passage time (FPT) problems and (iii) functionals of stochastic processes. Firstly, we investigate the validity and accuracy of weak-noise approximations for piecewise-smooth stochastic differential equations (SDEs), taking as an illustrative example the Brownian motion with pure dry friction. For this model, we show that the weak-noise approximation of the path integral correctly reproduces the known propagator of the SDE at lowest order in the noise power, as well as the main features of the exact propagator with higher-order corrections, provided that the singularity of the path integral is treated with some heuristics. We also consider a smooth regularisation of this piecewise-constant SDE and study to what extent this regularisation can rectify some of the problems encountered in the non-smooth case. Secondly, we provide analytic solutions to the FPT problem of the Brownian motion with dry friction. For the pure dry friction case, we find a phase transition phenomenon in the spectrum which relates to the position of the exit point and affects the tail of the FPT distribution. For the model with dry and viscous friction, we evaluate quantitatively the impact of the corresponding stick-slip transition and of the transition to ballistic exit. We also derive analytically the distributions of the maximum velocity till the FPT for the dry friction model. Thirdly, we generalise the so-called backward Fokker-Planck technique and obtain a recursive ordinary differential equation for the moments of functionals in the Laplace space. We then apply the developed results to analyse the local time, the occupation time and the displacement of the dry friction model. Finally, we conclude this thesis and state some related unsolved problems.

Contents

List of Figures

Acknowledgement

Thanks must first go to my main supervisor: Dr. Wolfram Just. I have been fortunate enough to be supervised by him, who has had the patience to allow me to advance at my own pace and choosing. This thesis would not have been possible without his help, support and patience.

I would like to thank Dr. Hugo Touchette and Dr. Adrian Baule for many interesting and very helpful discussions. Many thanks are also due to all of the members of the School of Mathematical Sciences at Queen Mary University of London for making my stay as a research student such an enjoyable one.

I would also like to thank my family and friends. Without their support it is hard to imagine that I can make such an effort to pursue a PhD degree abroad. In particular, I thank Prof. Songhe Song of NUDT who encouraged me to study in the UK.

Finally, let me thank the grant agency that funded my work: the Chinese Scholarship Council (CSC).

Chapter 1

Introduction

Dynamical systems with discontinuities are frequently used for the phenomenological modelling in applied science and engineering. The impact of such discontinuities on dynamical behaviour has attracted recently considerable attention from the general dynamical systems point of view (see, e.g., Ref. [65]). These dynamical systems are usually modelled by piecewise-smooth differential equations, the study of which is a relatively recent topic in the field of dynamical systems [34, 12, 65, 13, 25]. The dynamics generated by these equations displays many unexpected phenomena, including stick-slip transitions associated, for instance, with dry friction forces [16, 32, 73, 11], and bifurcations that do not appear in the standard classification of catastrophes of smooth dynamical systems [65, 13, 25]. They also show, in the case of systems with discontinuous derivatives or forces (so-called Filippov systems [34]), multivalued solutions for a given initial condition, leading to a loss of determinism [49].

In this thesis, we want to go beyond the deterministic dynamical systems setup and intend to study stochastic versions of piecewise-smooth dynamical systems perturbed by noises, which are also used as models of physical and biological systems. Stochastic differential equations (SDEs) with piecewise-smooth drifts are commonly used, for instance, in stochastic or Brownian ratchets [80, 79, 66], which serve as models of diffusion and transport in a variety of biological motors [75, 37]. Another important class of problem concerns diffusion of solid objects on solid surfaces, which can be modelled phenomenologically using piecewise-smooth SDEs with dry friction forces [21, 5, 30, 48]. The dynamics in this case shows stick-slip transitions, as in the noiseless case, but also new features due to the noise, such as directed motion in the absence of a mean force

bias [7] and noise-dependent decay of correlation functions [88]. Non-Gaussian statistics are found by the studies of stochastic systems with dry friction [53, 30, 48, 69, 86, 85]. Some of these features have also been shown in experiments, such as those investigated recently by Chaudhury *et al.* [23, 42, 40, 41] and Gnoli *et al.* [38, 37].

For a few simple piecewise-constant or piecewise-linear SDEs, exact solutions of the propagator (also called transition probability distribution) are known (see, e.g., Refs. [21, 10, 51, 95, 18, 88, 83]). Some studies have also looked at the large deviations of SDEs with discontinuous drift (so-called SDEs with discontinuous statistics) [56, 24, 15, 43]. However, the theory of piecewise-smooth SDEs is only in its infancy compared to its noiseless counterpart. From the previous disconnected studies it is not clear how non-smooth SDEs can be studied with techniques developed and used for smooth systems. More efforts need to be done to understand the interrelation between noise and discontinuities.

In this thesis, we focus on dynamical properties of piecewise-smooth SDEs with respect to three interesting topics: (i) weak-noise approximations, (ii) first-passage time (FPT) problems and (iii) functionals of stochastic processes. The reason to consider these three topics is explained as follows. Firstly, the weak-noise limit is particularly interesting from a physical point of view because a piecewise-smooth system does not necessarily behave continuously with the magnitude of a force or noise and therefore may behave in a non-trivial way in the limit of vanishing noise. While weak-noise approximation has been widely used for smooth systems, it is not clear how to apply this approximation for non-smooth systems. Moreover, the validity of a weak-noise approximation for non-smooth systems needs to be checked. Secondly, FPT problems are of great importance and are relevant in quite diverse disciplines, like mathematical finance [60], biological modelling [90], complex media [72, 26], and others. However, the effect of discontinuities on a FPT problem is not clear. Exact results for the FPT problems of piecewise-smooth SDEs, to the best of my knowledge, are not available in the literature. Thirdly, functionals of a process have been investigated intensively in the past and have found numerous applications in physics [61]. Nevertheless, to find stochastic properties of functionals is usually nontrivial and analytic results of this topic are limited, especially for piecewise-smooth systems. Therefore, it is meaningful to study the functional problems of piecewise-smooth SDEs, which are often used in science and engineering.

1.1 Brownian motion with dry friction

To address our purpose, we take as an example the model of Brownian motion with dry (also called solid or Coulomb) friction [21, 30, 48]. This dry friction model is used to describe the motion of a solid object moving over a vibrating plate subjected to a dry friction force in addition to the viscous friction force commonly studied since the works of Einstein and Langevin [36]. The main property of the dry friction is that a certain threshold force should be applied to move the solid object resting on the plate. The simplest way to model such a phenomenon mathematically is to consider a velocity dependent force $-\mu\sigma(v)$, where $\mu > 0$ is a constant coefficient, denoting the strength of the force, and $\sigma(v)$ denotes the sign of the velocity v, i.e.,

$$\sigma(v) = \begin{cases} -1 & \text{for } v < 0, \\ 0 & \text{for } v = 0, \\ 1 & \text{for } v > 0. \end{cases} \tag{1.1}$$

Instead of a horizontal plate considered by de Gennes [30], an inclined plate is considered in this thesis following the experiment setups in Refs. [23, 42, 40] (see Fig. 1.1 and also Ref. [88]). Then there is a biased force acting on the solid object due to the gravity in addition to the dry and viscous friction forces. Moreover, we vibrate the plate as shown in Fig. 1.1 randomly, namely, we add a noise to the plate. In the present thesis, we confine our investigation to the Gaussian white noise. For convenience, we assume the mass of the solid object to be one without loss of generality. Therefore, a simple description of the velocity of the object in the reference frame of the plate can be described phenomenologically by the Newtonian law, which reads

$$\dot{v}(t) = -\mu\sigma(v(t)) - \gamma v(t) + b + \sqrt{D}\xi(t), \tag{1.2}$$

where the dot denotes the derivative with respect to time t. Here $\mu > 0$ represents the dry friction coefficient, $\gamma \geqslant 0$ denotes the linear viscous friction coefficient, b is a constant biased force, and $D > 0$ is the strength of the Gaussian white noise $\xi(t)$ with zero mean

$$\langle \xi(t) \rangle = 0 \tag{1.3}$$

and δ correlation

$$\langle \xi(t)\xi(t') \rangle = 2\delta(t - t'), \tag{1.4}$$

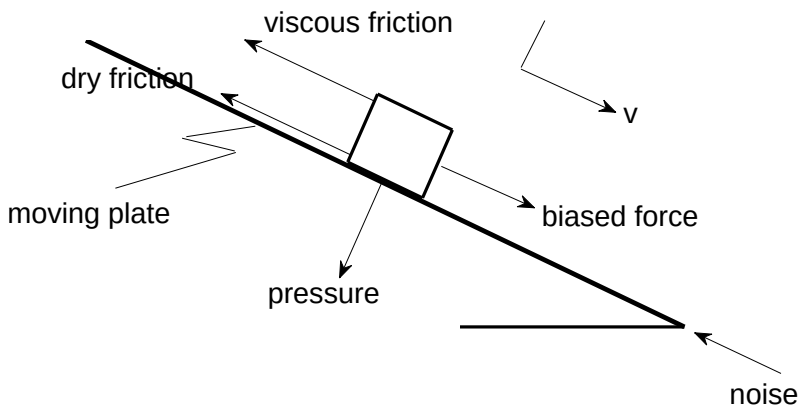

Figure 1.1: Model of Brownian motion with dry friction.

where $\langle \cdots \rangle$ stands for the average over all possible realisations of the noise and δ is the Dirac delta function.

Since the motion of two solid objects over each other is a ubiquitous problem in nature [59, 7, 8, 92, 78], the dry friction model (1.2) is important to understand the underlying dynamics of the motion. Mathematically, Eq. (1.2) is a special case of the following generic Langevin equation [76]

$$\dot{v}(t) = -\Phi'(v(t)) + \sqrt{D}\xi(t), \tag{1.5}$$

where $\Phi(v)$ is the potential of the drift and the prime denotes the derivative with respect to v. Since the noise considered here is additive, it does not matter whether Eq. (1.5) is interpreted in terms of Ito integral or Stratonovich integral (see, e.g., Ref. [36]). Moreover, since we are here concerned with the Gaussian white noise $\xi(t)$, the propagator of the velocity satisfies the following Fokker-Planck equation [76]

$$\frac{\partial}{\partial t}p(v,t|v_0,0) = \frac{\partial}{\partial v}[\Phi'(v)p(v,t|v_0,0)] + D\frac{\partial^2}{\partial v^2}p(v,t|v_0,0) \tag{1.6}$$

with initial condition $p(v,0|v_0,0) = \delta(v-v_0)$. Here $p(v,t|v_0,0)$ represents the probability density that $v(t) = v$ given the initial condition $v(0) = v_0$. Corresponding to Eq. (1.2), the potential in Eq. (1.6) reads

$$\Phi(v) = \mu|v| + \gamma v^2/2 - bv. \tag{1.7}$$

Since the force for the dry friction model (1.2) is piecewise-linear, the corresponding Fokker-Planck equation can be solved by using spectral decomposition method [76, 36, 88] or Laplace transform [89].

When the viscous force and the bias force vanish (i.e., $\gamma = 0$ and $b = 0$), Eq. (1.2) reduces to the pure dry friction case (also called Brownian motion with two-valued drift [83])

$$\dot{v}(t) = -\mu\sigma(v(t)) + \sqrt{D}\xi(t). \tag{1.8}$$

Mathematically, it is the simplest piecewise-smooth SDE whose time-dependent propagator $p(v, t|v_0, 0)$ can be expressed in closed analytic form:

$$p(v, t|v_0, 0) = \frac{\mu}{D}\,\hat{p}\left(\frac{\mu}{D}v, \frac{\mu^2}{D}t\middle|\frac{\mu}{D}v_0, 0\right), \tag{1.9}$$

where

$$\hat{p}(x, \tau|x', 0) = \frac{e^{-\tau/4}}{2\sqrt{\pi\tau}}\,e^{-(|x|-|x'|)/2}\,e^{-(x-x')^2/(4\tau)} + \frac{e^{-|x|}}{4}\left[1 + \operatorname{erf}\left(\frac{\tau - (|x| + |x'|)}{2\sqrt{\tau}}\right)\right] \tag{1.10}$$

is the propagator in non-dimensional units and

$$\operatorname{erf}(z) = 2\int_0^z e^{-t^2}dt/\sqrt{\pi} \tag{1.11}$$

is the error function. This propagator can be obtained by explicitly solving the corresponding time-dependent Fokker-Planck equation (see, e.g., Refs. [51, 52, 88]). Taking the limit $t \to \infty$ of $p(v, t|v_0, 0)$, we obtain the stationary probability density function of Eq. (1.8):

$$p(v) = \frac{\mu}{2D}\,e^{-\mu|v|/D}, \tag{1.12}$$

which solves the corresponding time-independent Fokker-Planck equation of Eq. (1.8).

For the model (1.2) with dry and viscous forces (with or without bias), the associated time-dependent propagator in closed analytic form is not known. However, we can solve the corresponding Fokker-Planck equation (1.6) to obtain the propagator in terms of the so-called parabolic cylinder function (see appendix A.9) by using spectral decomposition method [88] or Laplace transform [89].

1.2 Outline of this thesis

The rest of this thesis consists of six chapters and an appendix. Chapter 2 is about pedagogical contributions, which are the essential theories to understand the main content of this thesis. Even though they are well documented in the literature, we summarise some of the main derivations for the purpose of making the presentation self-contained. The other five chapters are the author's own work, which are largely from the three papers listed at the beginning of this thesis.

In chapter 3, we investigate how non-smooth SDEs can be studied with techniques developed and used for smooth systems. As an example, we focus on the validity and accuracy of weak-noise approximations for non-smooth systems. We address the question by using path integral representation of propagators and the corresponding saddle-point approximation of these integrals. In particular, we take the pure dry friction model (1.8) as an example to investigate the validity of the weak-noise approximation and some problems encountered in the non-smooth setup. For the model (1.8), we show that the weak-noise approximation of the path integral correctly reproduces the known propagator of the SDE at lowest order in the noise power. If some heuristics are used to treat the singularity of the path integral, the weak-noise approximation can also reproduce the main features of the exact propagator with higher-order corrections. Furthermore, to remove this singularity we consider a smooth regularisation of the pure dry friction model and study to what extent this regularisation can rectify some of the problems encountered in the non-smooth case.

In chapter 4, we take the dry friction model (1.2) as an example to investigate the interrelation between discontinuity and noise in FPT problems. For this model with or without viscous friction, we provide analytic solutions to the FPT problems using two different but closely related approaches. One is based on eigenfunction decompositions and the other is on the backward Kolmogorov equation. For the pure dry friction case, we find a phase transition phenomenon in the spectrum related to the position of the exit point. This phenomenon finally results in different decay rates of the FPT distribution. For the full model, we observe two additional transitions, i.e., the stick-slip transition and the transition to ballistic exit. The impact of both transitions is evaluated quantitatively.

In chapter 5, we provide analytic solutions of the distributions of the maximum velocity till the FPT for the dry friction model. This problem is closely related to the

FPT problem investigated in chapter 4. We first solve the corresponding problem for the pure dry friction case so as to address all the techniques used in the piecewise-smooth systems. Then we present the corresponding solution for the full model.

In chapter 6, we first show that the moments of functionals of a generic Langevin equation satisfy a recursive ordinary differential equation in the Laplace space. Then for three important functionals (i.e., local time, occupation time and displacement), we present some general results of the corresponding moments for the generic Langevin equation. Finally, we apply the developed results to solve the corresponding functionals of the dry friction model. Some analytic results of this model are obtained explicitly.

In chapter 7, concluding remarks are drawn from the previous chapters. In addition, we give comments on some interesting unsolved problems.

To make this thesis more readable, some details of the derivations are put in the appendix.

1.3 A note to the examiners of this thesis

Chapters 3–6 are my own work. The main content of chapter 3 comes from the publication: Y. Chen, A. Baule, H. Touchette, W. Just, Weak-noise limit of a piecewise-smooth stochastic differential equation, Physical Review E 88, 052103 (2013), chapter 4 from the publication: Y. Chen, W. Just, First-passage time of Brownian motion with dry friction, Physical Review E 89, 022103 (2014), and chapter 6 from the paper: Y. Chen, W. Just, On large deviation properties of Brownian motion with dry friction, accepted for publication in Physical Review E. In these papers, I did most of the calculations and the co-authors contributed to the writing and interpretation. Chapter 5 is written by myself under the supervision of my main supervisor: Dr. Wolfram Just, which has not been summarised as a paper and submitted to elsewhere.

Chapter 2

Preliminaries

To keep the presentation self-contained we summarise in this chapter some preliminary theoretical considerations even though they are well documented in the literature. These theories are necessary to understand the main results of this thesis. In Sec. 2.1, we summarise the essential features of path integral formulations of the propagator of SDEs and their weak-noise approximations, which will be used in chapter 3 to investigate the pure dry friction case. In Sec. 2.2, we revisit two different but closely related approaches to FPT problems. One is based on a spectral decomposition method and the other is on the backward Kolmogorov equation, both of which will be used to address the FPT problem of Brownian motion with dry friction in chapter 4. In Sec. 2.3, we recall the derivation of the distribution of the maximum velocity till the FPT. This derivation will be used to solve the corresponding problem of the dry friction model in chapter 5. Finally, we present in Sec. 2.4 the backward Fokker-Planck technique of functionals, which will be used in chapter 6.

2.1 Weak-noise approximation of path integrals

Path integral formulations of the propagator of SDEs and their expansion for weak-noise are well established in the literature. To set the notation and to keep the thesis self-contained, we summarise here the essential features, following the formulation presented in Ref. [22]. Let us consider the one-dimensional Langevin equation (1.5). We can write down the conditional probability distribution $p(v_t, t|v_0, 0)$ by using the path integral

formula [22],

$$p(v_t,t|v_0,0)=\int_{(v_0,0)}^{(v_t,t)}\mathcal{D}[v]J[v]e^{-\int_0^t[\dot{v}+\Phi'(v)]^2ds/(4D)}, \tag{2.1}$$

where $\int\mathcal{D}[v]$ denotes the Wiener measure and the Jacobian term

$$J[v]=\exp\left(\frac{1}{2}\int_0^t\Phi''(v)ds\right) \tag{2.2}$$

originates from a transformation $\xi(t)\to v(t)$. Putting the two exponentials in Eq. (2.1) together, we thus express the kernel of the path integral in terms of the action

$$S[v]=\int_0^t L(v(s),\dot{v}(s))ds=\int_0^t\left\{[\dot{v}(s)+\Phi'(v(s))]^2-2D\Phi''(v(s))\right\}ds. \tag{2.3}$$

All trajectories contribute to the path integral (2.1), but for small D, the largest contribution will come from the trajectory with smallest action. At lowest order in D, this contribution is found by minimising the action

$$S^{(0)}[v]=\int_0^t\left[\dot{v}(s)+\Phi'(v(s))\right]^2ds, \tag{2.4}$$

which does not take the contribution of Jacobian into account since it is multiplied by D. The corresponding boundary value problem determined by the Euler-Lagrange equation reads

$$\ddot{v}^{(0)}(s)=\Phi'(v^{(0)}(s))\Phi''(v^{(0)}(s)),\quad v^{(0)}(0)=v_0,\quad v^{(0)}(t)=v_t. \tag{2.5}$$

Given the path minimising the action (2.4), the leading order approximation of the propagator is thus given by

$$p^{(0)}(v_t,t|v_0,0)=N_1e^{-S^{(0)}[v^{(0)}]/(4D)}, \tag{2.6}$$

where N_1 is a (time-dependent) normalisation.

A simple way to improve the approximation (2.6) is to evaluate the action of Eq. (2.3) with the Jacobian using the optimal path $v^{(0)}$ [see Eq. (2.5)]. This leads to the expression

$$p^{(0;1)}(v_t,t|v_0,0)=N_2e^{-S[v^{(0)}]/(4D)}. \tag{2.7}$$

A more coherent approach, perhaps, which keeps the spirit of the saddle-point approximation (SPA) and ensures positivity of the propagator, is to evaluate the minimising

path with the Jacobian, leading to the following Euler-Lagrange equation:

$$\ddot{v}^{(1)}(s) = \Phi'(v^{(1)}(s))\Phi''(v^{(1)}(s)) - D\Phi'''(v^{(1)}(s)), \quad v^{(1)}(0) = v_0, \quad v^{(1)}(t) = v_t. \tag{2.8}$$

In this case, the corresponding first-order expression for the propagator is given by

$$p^{(1)}(v_t, t|v_0, 0) = N_3 e^{-S[v^{(1)}]/(4D)}. \tag{2.9}$$

In general, it is not possible to solve the boundary value problem of the Euler-Lagrange equations (2.5) or (2.8) analytically. Hence, numerical methods such as the shooting method must be used. In this case, it is useful to respect the underlying Hamiltonian structure of the Euler-Lagrange problem by using symplectic integration methods [46], which preserve the Hamiltonian

$$H^{(0)}(v, p_v) = p_v^2/2 - [\Phi'(v)]^2/2 \tag{2.10}$$

without the Jacobian or

$$H(v, p_v) = p_v^2/2 - \{[\Phi'(v)]^2 + D\Phi''(v)\}/2 \tag{2.11}$$

with the Jacobian. Here $p_v = \dot{v}$. In this case, a symplectic Euler scheme (see appendix A.2.1), for example, can be applied to integrate the corresponding canonical equations of motion.

2.2 Remarks on first-passage time problems

In an abstract setting the FPT is defined as the time when a stochastic process, often governed by a SDE, exits a given region for the first time (see Fig. 2.1). The theory of FPT problems is well documented in the literature, and suitable expositions can be found in standard textbooks, e.g., Ref. [76]. Here we just summarise the essential ideas not only for the convenience of the reader but also to address the few technical issues related to piecewise-smooth drifts. We will focus on the Langevin equation

$$\dot{v}(t) = -\Phi'(v(t)) + \xi(t), \tag{2.12}$$

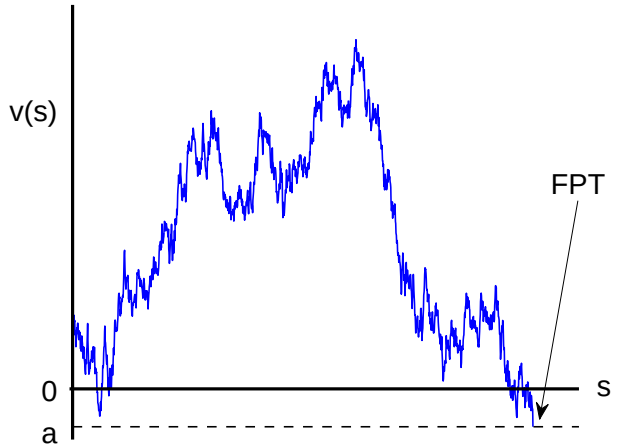

Figure 2.1: Illustration of the FPT by using a sample of the process $v(s)$, starting at $s = 0$. The given exit region is chosen to be (a, ∞) with $a < 0$.

where the potential $\Phi(v)$ is smooth everywhere apart from $v = 0$ where its derivative may have a discontinuity, and $\xi(t)$ is the Gaussian white noise that satisfies Eqs. (1.3) and (1.4). In the following, we will present two different but closely related approaches based on a spectral decomposition method on the one hand and on the backward Kolmogorov equation on the other. The given region here is chosen to be (a, ∞) with a being a negative constant. However, it is straightforward to generalise the following theories to other types of regions.

2.2.1 Spectral decomposition

For the stochastic dynamics according to Eq. (2.12) on the interval (a, ∞) it is well known that the corresponding distribution of the FPT for orbits starting at $v(0) = v_0 \in (a, \infty)$ is given by (see Ref. [76])

$$f(T, v_0) = -\frac{\partial}{\partial T} \int_a^\infty p(v, T|v_0, 0) dv, \tag{2.13}$$

where the propagator $p(v, t|v_0, 0)$ satisfies the corresponding Fokker-Planck equation

$$\frac{\partial}{\partial t} p(v, t|v_0, 0) = \frac{\partial}{\partial v} \left[\Phi'(v) p(v, t|v_0, 0)\right] + \frac{\partial^2}{\partial v^2} p(v, t|v_0, 0), \tag{2.14}$$

with an initial condition

$$p(v,0|v_0,0) = \delta(v - v_0), \tag{2.15}$$

an absorbing boundary condition at the left interval endpoint

$$p(a,t|v_0,0) = 0, \tag{2.16}$$

and a reflecting boundary, i.e., a vanishing probability current (see, e.g., Ref. [36]) at infinity,

$$\left[\Phi'(v)p(v,t|v_0,0) + \frac{\partial}{\partial v}p(v,t|v_0,0)\right]\Big|_{v\to\infty} = 0. \tag{2.17}$$

To get the solution $p(v,t|v_0,0)$ we follow a spectral decomposition method for piecewise-smooth systems used, e.g., in Ref. [88], and first solve the associated eigenvalue problem of Eqs. (2.14)–(2.16),

$$-\Lambda u_\Lambda(v) = [\Phi'(v)u_\Lambda(v)]' + u_\Lambda''(v), \tag{2.18}$$

with the (formal) boundary conditions

$$u_\Lambda(a) = 0, \qquad [\Phi'(v)u_\Lambda(v) + u_\Lambda'(v)]\big|_{v\to\infty} = 0, \tag{2.19}$$

which follow from Eqs. (2.16) and (2.17). Since we are here concerned with a piecewise-smooth potential $\Phi(v)$, we have to solve Eq. (2.18) on the two domains $v > 0$ and $v < 0$, respectively, and have to apply suitable matching conditions, i.e.,

$$u_\Lambda(0-) = u_\Lambda(0+) \tag{2.20}$$

coming from the continuity of the eigenfunction and

$$\Phi'(0-)u_\Lambda(0-) + u_\Lambda'(0-) = \Phi'(0+)u_\Lambda(0+) + u_\Lambda'(0+) \tag{2.21}$$

from the continuity of the probability current, which can be obtained by integrating Eq. (2.18) on the interval $(-\varepsilon,\varepsilon)$ in the limit $\varepsilon \to 0$. As in the standard case of Fokker-Planck equations with reflecting boundary conditions the eigenfunctions of the Fokker-Planck operator and the eigenfunctions of the formally adjoint problem are related to each other by an exponential factor containing the potential $\Phi(v)$ (see Ref. [76]). Furthermore, both types of eigenfunctions are mutually orthogonal sets and thus result

in the orthogonality relations:

$$\int_a^\infty u_{\Lambda_m}(v)u_{\Lambda_n}(v)e^{\Phi(v)}dv = Z_{\Lambda_n}\delta_{mn}, \tag{2.22}$$

$$\int_a^\infty u_{\Lambda}(v)u_{\Lambda'}(v)e^{\Phi(v)}dv = Z_{\Lambda}\delta(\Lambda-\Lambda'), \tag{2.23}$$

depending on whether the eigenvalue is contained in the discrete or continuous part of the spectrum. These conditions implicitly take the reflecting boundary at infinity into account [see Eq. (2.19) and also Ref. [36]]. Furthermore, it is worth to mention that the reasoning for Fokker-Planck equations with reflecting boundary conditions can be also applied to map the eigenvalue problem to a formally Hermitian positive operator (see Refs. [76, 36]). Thus all eigenvalues are positive; in particular, they are real. Finally, the solution of Eq. (2.14) is given by (see Ref. [94] for an accessible account on the completeness of the spectrum)

$$p(v,t|v_0,0) = e^{\Phi(v_0)}\left(\sum_n u_{\Lambda_n}(v_0)u_{\Lambda_n}(v)e^{-\Lambda_n t}/Z_{\Lambda_n} + \int u_\Lambda(v_0)u_\Lambda(v)e^{-\Lambda t}/Z_\Lambda d\Lambda\right), \tag{2.24}$$

where the sum is taken over the discrete eigenvalues and the integral is taken over the continuous part of the spectrum. The normalisation factors Z_{Λ_n} and Z_Λ are determined by Eqs. (2.22) and (2.23), respectively.

2.2.2 Backward Kolmogorov equation

It is well known that the propagator $p(v,t|v_0,0)$, which determines the FPT distribution (2.13), obeys the backward Kolmogorov equation (see, e.g., Ref. [36])

$$\frac{\partial}{\partial t}p(v,t|v_0,0) = -\Phi'(v_0)\frac{\partial}{\partial v_0}p(v,t|v_0,0) + \frac{\partial^2}{\partial v_0^2}p(v,t|v_0,0) \tag{2.25}$$

with the initial condition (2.15), an absorbing boundary condition at $v_0 = a$,

$$p(v,t|a,0) = 0, \tag{2.26}$$

and a reflecting boundary condition at infinity [36],

$$\frac{\partial}{\partial v_0}p(v,t|v_0\to\infty,0) = 0. \tag{2.27}$$

Hence, according to Eq. (2.13) we can derive from Eq. (2.25) that the FPT distribution also obeys a backward Kolmogorov equation:

$$\frac{\partial}{\partial T} f(T, v_0) = -\Phi'(v_0) \frac{\partial}{\partial v_0} f(T, v_0) + \frac{\partial^2}{\partial v_0^2} f(T, v_0) \tag{2.28}$$

with an initial condition

$$f(0, v_0) = 0 \qquad \text{for } v_0 > a. \tag{2.29}$$

The two boundary conditions (2.26) and (2.27) translate into

$$f(T, a) = \delta(T) \tag{2.30}$$

at the left interval endpoint, and into

$$\frac{\partial}{\partial v_0} f(T, v_0 \to \infty) = 0 \tag{2.31}$$

at infinity. If we use the Laplace transform

$$\tilde{f}(s, v_0) = \int_0^\infty f(T, v_0) e^{-sT} dT, \tag{2.32}$$

the partial differential equation (2.28) turns into the ordinary boundary value problem

$$\frac{\partial^2}{\partial v_0^2} \tilde{f}(s, v_0) - \Phi'(v_0) \frac{\partial}{\partial v_0} \tilde{f}(s, v_0) - s\tilde{f}(s, v_0) = 0, \tag{2.33}$$

where Eq. (2.30) obviously results in

$$\tilde{f}(s, a) = 1. \tag{2.34}$$

As for the other boundary condition we observe that the Laplace transform (2.32) converges uniformly in v_0 for s being in the right half plane, as the integral converges absolutely at $s = 0$. Hence Eq. (2.31) yields

$$\frac{\partial}{\partial v_0} \tilde{f}(s, v_0 \to \infty) = 0 \qquad \text{for } \mathrm{Re}(s) > 0. \tag{2.35}$$

Intuitively the two boundary conditions (2.34) and (2.35) take care of the fact that on the one hand the FPT is δ distributed in the limit $v_0 \to a$ and that on the other hand

the particle cannot exit the given region (a, ∞) at infinity. In addition, Eq. (2.33) should be solved for $v_0 > 0$ and $v_0 < 0$ separately with matching conditions at $v_0 = 0$:

$$\tilde{f}(s, 0-) = \tilde{f}(s, 0+), \qquad \frac{\partial}{\partial v_0}\tilde{f}(s, 0-) = \frac{\partial}{\partial v_0}\tilde{f}(s, 0+), \tag{2.36}$$

where the first condition follows from the solution $\tilde{f}(s, v_0)$ being continuous at $v_0 = 0$ and the second one is derived by integrating Eq. (2.33) across $v_0 = 0$ [see also Eq. (2.21)].

The approach via the backward Kolmogorov equations enables us to obtain the Laplace transform of the FPT distribution in closed analytic form. Even though it may not be possible to perform the inverse transform by analytical means to compute $f(T, v_0)$, by taking derivatives the moments of the FPT, $\langle T^n \rangle$, are then easily evaluated as

$$\langle T^n \rangle = (-1)^n \frac{\partial^n}{\partial s^n}\tilde{f}(s, v_0)\bigg|_{s=0} \qquad \text{for } n = 1, 2, 3, \ldots. \tag{2.37}$$

2.3 Maximum velocity till the first-passage time

For the FPT problem considered in the previous section, we study here the distribution of the maximum velocity (MVD) till the FPT (see Fig. 2.2). The given exit region is till chosen to be (a, ∞) with $a < 0$. Following the method used in Ref. [54], we summarise the derivation of the MVD till the FPT. Let us first denote the maximum velocity as v_m, which is a random variable. Then given an initial value $v(0) = v_0$, using the Markov property of the process $v(t)$ we can obtain the following equation of the probability:

$$Pr(v < v_m | v_0) = \langle Pr(v < v_m | v_0 + \Delta v) \rangle_{\Delta v}, \tag{2.38}$$

where $Pr(v < v_m | v_0)$ represents the probability that $v < v_m$ till the FPT given that $v(0) = v_0$, Δv is an increment and $\langle \cdots \rangle_{\Delta v}$ denotes the average over all possible realisations of Δv. The right hand side of Eq. (2.38) can be expanded with respect to the increment Δv to obtain

$$\begin{aligned}\langle Pr(v < v_m | v_0 + \Delta v) \rangle_{\Delta v} = Pr(v < v_m | v_0) + \langle \Delta v \rangle_{\Delta v} \frac{\partial}{\partial v_0} Pr(v < v_m | v_0) \\ + \frac{\langle (\Delta v)^2 \rangle_{\Delta v}}{2} \frac{\partial^2}{\partial v_0^2} Pr(v < v_m | v_0) + \langle O((\Delta v)^3) \rangle_{\Delta v}.\end{aligned} \tag{2.39}$$

Then substituting Eq. (2.39) into Eq. (2.38) results in

$$\langle \Delta v \rangle_{\Delta v} \frac{\partial}{\partial v_0} Pr(v < v_m | v_0) + \frac{\langle (\Delta v)^2 \rangle_{\Delta v}}{2} \frac{\partial^2}{\partial v_0^2} Pr(v < v_m | v_0) + \langle O((\Delta v)^3) \rangle_{\Delta v} = 0. \quad (2.40)$$

From Eq. (2.12), we obtain

$$\Delta v = v(\Delta t) - v_0 = -\Phi'(v_0)\Delta t + \int_0^{\Delta t} \xi(s) ds + O((\Delta t)^2). \quad (2.41)$$

Hence, it follows from the properties (1.3) and (1.4) of the noise $\xi(t)$ that

$$\langle \Delta v \rangle_{\Delta v} = -\Phi'(v_0)\Delta t + O((\Delta t)^2), \quad (2.42)$$

$$\langle (\Delta v)^2 \rangle_{\Delta v} = 2\Delta t + O((\Delta t)^2), \quad (2.43)$$

$$\langle (\Delta v)^3 \rangle_{\Delta v} = O((\Delta t)^2). \quad (2.44)$$

Therefore, by substituting Eqs. (2.42)–(2.44) into Eq. (2.40) it is easy to derive that

$$\frac{\partial^2}{\partial v_0^2} Pr(v < v_m | v_0) - \Phi'(v_0) \frac{\partial}{\partial v_0} Pr(v < v_m | v_0) = 0 \qquad \text{for } v_m > a, \quad (2.45)$$

where a stands for the exit point. The suitable boundary conditions for Eq. (2.45) are

$$Pr(v < v_m | v_0 = a) = 1, \quad (2.46)$$

$$Pr(v < v_m | v_0 = v_m) = 0, \quad (2.47)$$

which are easy to observe according to the meaning of the notation $Pr(v < v_m | v_0)$.

Since we are here concerned with the piecewise-smooth potential $\Phi(v_0)$, we have to solve Eq. (2.45) for the two domains $v_0 > 0$ and $v_0 < 0$, respectively. And then we have to match the solution by using the condition coming from the continuity of the probability when v_0 changes sign,

$$Pr(v < v_m | v_0 \to 0-) = Pr(v < v_m | v_0 \to 0+), \quad (2.48)$$

and the one coming form the integral of Eq. (2.45) across zero [see also Eq. (2.21)],

$$\frac{\partial}{\partial v_0} Pr(v < v_m | v_0 \to 0-) = \frac{\partial}{\partial v_0} Pr(v < v_m | v_0 \to 0+). \quad (2.49)$$

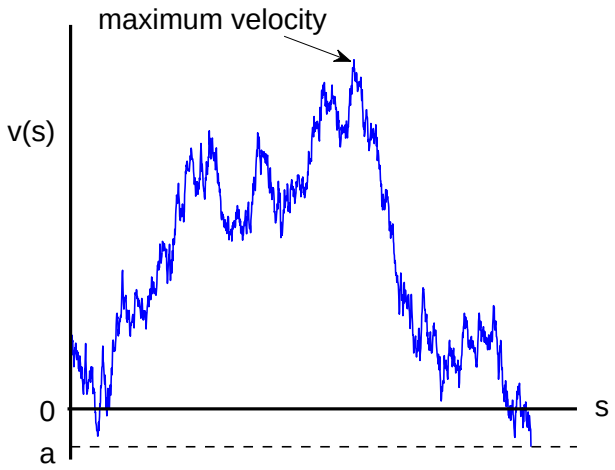

Figure 2.2: Illustration of the maximum velocity till the first-passage time by using a sample of the process $v(s)$, starting at $s = 0$. The given exit region is chosen to be (a, ∞) with $a < 0$.

2.4 Functionals with positive support

Since functionals of a process $v(t)$ are related to many practical problems, it is important to know their statistical properties. Here we revisit the backward Fokker-Planck technique developed for positive support functionals by Majumdar and Comtet [63]. For the process $v(t)$ obeying the Langevin equation (2.12), let us consider the functional

$$T = \int_0^t U(v(\tau))d\tau, \tag{2.50}$$

where $U(v)$ is a prescribed positive function. Since the functional T depends on both t and v_0, we denote its distribution as $p(T, t, v_0)$. Then according to the backward Fokker-Planck technique, we can derive an ordinary differential equation for this distribution in the double Laplace space. In the following, we summarise the main derivations. Let us first introduce the Laplace transform

$$\tilde{p}(\alpha, t, v_0) = \int_0^\infty e^{-\alpha T} p(T, t, v_0)dT = \left\langle e^{-\alpha \int_0^t U(v(\tau))d\tau} \right\rangle, \tag{2.51}$$

where $\langle \cdots \rangle$ represents the average over all possible realisations of v. Then we have

$$\begin{aligned}\tilde{p}(\alpha, t+\Delta t, v_0) &= \left\langle e^{-\alpha \int_0^{t+\Delta t} U(v(\tau))d\tau} \right\rangle \\ &= \left\langle e^{-\alpha \int_0^{\Delta t} U(v(\tau))d\tau - \alpha \int_{\Delta t}^{t+\Delta t} U(v(\tau))d\tau} \right\rangle \\ &= \left[1 - \alpha U(v_0)\Delta t + O((\Delta t)^2)\right] \langle \tilde{p}(\alpha, t, v_0 + \Delta v)\rangle_{\Delta v}, \end{aligned} \tag{2.52}$$

where $\langle \cdots \rangle_{\Delta v}$ denotes the average over all possible realisations of Δv [see Eq. (2.41)].

Using Eqs. (2.42)–(2.44), we can expand $\langle \tilde{p}(s, t, v_0 + \Delta v)\rangle_{\Delta v}$ to obtain

$$\langle \tilde{p}(\alpha, t, v_0 + \Delta v)\rangle_{\Delta v} = \tilde{p}(\alpha, t, v_0) - \Phi'(v_0)\frac{\partial \tilde{p}(\alpha, t, v_0)}{\partial v_0}\Delta t + \frac{\partial^2 \tilde{p}(\alpha, t, v_0)}{\partial v_0^2}\Delta t + O((\Delta t)^2). \tag{2.53}$$

Therefore, substituting Eq. (2.53) into (2.52) and letting $\Delta t \to 0$ we obtain a partial differential equation for the distribution $\tilde{p}(\alpha, t, v_0)$:

$$\frac{\partial}{\partial t}\tilde{p}(\alpha, t, v_0) = -\alpha U(v_0)\tilde{p}(\alpha, t, v_0) - \Phi'(v_0)\frac{\partial}{\partial v_0}\tilde{p}(\alpha, t, v_0) + \frac{\partial^2}{\partial v_0^2}\tilde{p}(\alpha, t, v_0). \tag{2.54}$$

Furthermore, if one uses the Laplace transform

$$q(\alpha, s, v_0) = \int_0^\infty e^{-st}\tilde{p}(\alpha, t, v_0)dt, \tag{2.55}$$

Eq. (2.54) reduces to the following ODE:

$$\frac{\partial^2}{\partial v_0^2}q(\alpha, s, v_0) - \Phi'(v_0)\frac{\partial}{\partial v_0}q(\alpha, s, v_0) - (\alpha U(v_0) + s)q(\alpha, s, v_0) = -1. \tag{2.56}$$

The appropriate boundary conditions for $q(\alpha, s, v_0 \to \pm\infty)$ are to be derived from the observation that if the particle starts at $v_0 \to \pm\infty$ it will never cross the origin in finite time (see Sec. 6.2).

As an important result, we will show in Sec. 6.1 that the results presented here can be generalised to handle functionals with general support.

Chapter 3

Weak-noise limit of the pure dry friction case

In this chapter, we will investigate how non-smooth SDEs can be studied with techniques developed and used for smooth systems in a practical way by studying the pure dry friction model (1.8). Here we focus on two of such techniques, namely, the path integral representation of propagators and the corresponding weak-noise approximation. Since the time-dependent propagator $p(v_t, t|v_0, 0)$ of this model is known exactly [see Eq. (1.9)], it is a good starting point for benchmarking results about non-smooth SDEs. Note that the propagator $p(v_t, t|v_0, 0)$ (1.9) and the stationary distribution $p(v)$ (1.12) are symmetric under the changes $v_0 \to -v_0$ and $v(t) \to -v(t)$ due to the symmetric force $\sigma(v)$. Thus we can confine the analysis to the case $v_0 > 0$ without loss of generality.

This chapter is arranged as follows. In Sec. 3.1, we compare the exact result (1.9), which is valid for any noise power D, with various weak-noise approximations of the path integral representation of $p(v_t, t|v_0, 0)$ in order to test the validity and accuracy of these approximations and to discuss subtle singularities arising in the path integral when dealing with discontinuous drifts. Related path integrals were studied in Refs. [6, 9] for a non-exactly solvable model of dry friction. For the pure dry friction model, we will see that the weak-noise approximation gives the correct propagator at the lowest order in D, as well as its main features with higher-order corrections, provided that some heuristics are used to treat the singularities of the path integral.

To treat the singularity of the system in a more explicit and systematic way, we then

consider in Sec. 3.2 a regularised version of the pure dry friction model, given by

$$\dot{v}(t) = -\mu \tanh\left(\frac{v(t)}{\varepsilon}\right) + \sqrt{D}\,\xi(t), \tag{3.1}$$

which recovers the original model (1.8) in the limit $\varepsilon \to 0$. Although we do not have an explicit expression for the propagator of this smooth (but nonlinear) model, we show with Langevin simulations that the weak-noise approximation of the path integral, which is now well-defined and shows no singularity, reproduces the main features of the propagator at different orders of approximation, with roughly the same accuracy as for the singular model. The regularised model also allows us to obtain analytical results about the optimal path of the system, as presented in Sec. 3.3, which is the most probable path singled out by the weak-noise approximation, and the so-called action functional or quasi-potential, obtained by approximating the propagator at the lowest order in D with the optimal path [44, 87, 35]. In addition, from these analytical results we are able to study the evolution of the propagator of the regularised model in the weak-noise limit. A summary of this chapter drawn from these results is finally given in Sec. 3.4.

3.1 Piecewise-smooth model

In this section, we compare the exact propagator of the piecewise-constant SDE (1.8) with various approximations of the path integral representation of this propagator, so as to discuss the validity of these approximations for a non-smooth SDE. From Sec. 2.1 we know that the path integral of Eq. (2.20) has the form

$$p(v_t, t|v_0, 0) = \int_{(v_0,0)}^{(v_t,t)} \mathcal{D}[v]\, J[v]\, e^{-S^{(0)}[v]/(4D)}, \tag{3.2}$$

and involves two terms: the action functional [see Eq. (2.4)]

$$S^{(0)}[v] = \int_0^t [\dot{v}(s) + \mu\sigma(v(s))]^2\, ds, \tag{3.3}$$

which is a measure of the probability of a path $\{v(s)\}_{s=0}^t$ in velocity space, and the Jacobian functional

$$J[v] = \exp\left(\mu \int_0^t \delta(v(s))\, ds\right), \tag{3.4}$$

which is the Jacobian of the transformation $\xi(t) \to v(t)$. Here $\delta(v)$ is the Dirac delta function.

For non-smooth SDEs, two problems arise in the path integral (3.2). The first is that, since the noiseless system $\dot{v} = -\mu\sigma(v)$ admits in general piecewise-linear trajectories that are continuous but non-differentiable at points where $v(t)$ vanishes, the minimisation of the action must also be carried over these trajectories, which means that care must be taken of the $\dot{v}$ term in $S^{(0)}[v]$. The second problem is that the Jacobian (3.4) is singular. Below we show how to treat this singular contribution and how its inclusion or non-inclusion in the saddle-point approximation of the path integral determines different orders of approximation of the propagator as $D \to 0$.

3.1.1 Zeroth-order saddle-point approximation

The lowest-order approximation of the propagator $p(v_t, t|v_0, 0)$ is obtained in the noiseless limit $D \to 0$ by finding the path $\{v^{(0)}(s)\}_{s=0}^{t}$ that minimises the action $S^{(0)}[v]$ so as to write

$$p^{(0)}(v_t, t|v_0, 0) = Ne^{-S^{(0)}[v^{(0)}]/(4D)}, \tag{3.5}$$

where N is a normalisation constant. We refer to this approximation as the zeroth-order saddle-point approximation or SPA(0) for short. The rationale for this approximation is that, in the limit $D \to 0$, the path integral (3.2) is dominated by the probability of the optimal path $\{v^{(0)}(s)\}_{s=0}^{t}$ having minimal action. The Jacobian $J[v]$ can be neglected at this level of approximation, since it does not depend on D.

The Euler-Lagrange equation associated with the minimisation of $S^{(0)}[v]$ in the regions $v > 0$ and $v < 0$ is simply [see Eq. (2.5)]

$$\ddot{v}^{(0)} = 0 \tag{3.6}$$

and leads to straight paths

$$v_{\mathrm{d}}^{(0)}(s) = (v_t - v_0)s/t + v_0, \tag{3.7}$$

which we call direct paths. As mentioned above, in addition to these paths, we must consider paths that follow the attractor $v = 0$, since these paths appear in the noiseless system. As a result, the minimisation of $S^{(0)}[v]$ must be carried out over all continuous and piecewise-linear paths consisting of direct paths and paths following the $v = 0$

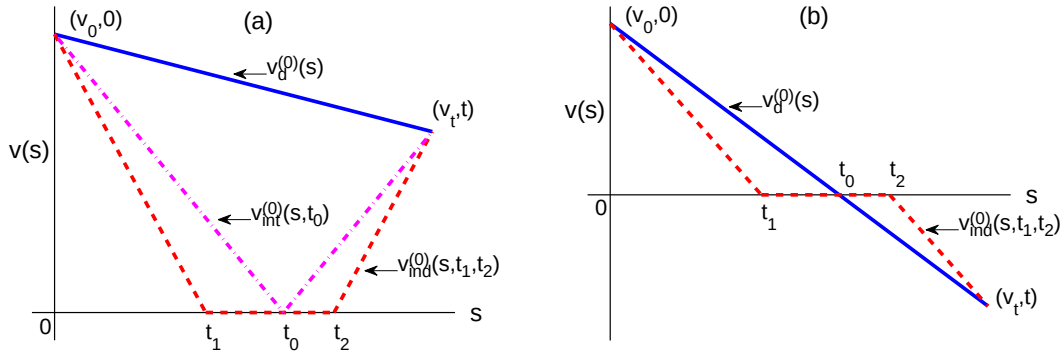

Figure 3.1: Different paths considered for minimising the action (3.3) for (a) $v_t > 0$ and (b) $v_t < 0$. Here $v_{\mathrm{d}}^{(0)}$ denotes the direct path (3.7), $v_{\mathrm{ind}}^{(0)}$ the indirect path (3.9), and $v_{\mathrm{int}}^{(0)}$ the intermediate path (3.9) with $t_1 = t_2 = t_0$.

axis. This situation differs from smooth SDEs, for which the minimisation is generally over all continuously differentiable paths, and leads us to define two important heuristic principles for dealing with non-smooth SDEs: (i) the action of a path must be evaluated as the sum of the actions of all its linear (or in general smooth) parts without regard to its joining (non-smooth) points and (ii) any part of a path on the $v = 0$ axis (or, in general, on an attractor of the noiseless system) must have a zero action, in analogy with smooth systems.

In the present model, two types of optimal paths arise from the action minimisation. The first consists of direct paths $v_{\mathrm{d}}^{(0)}(s)$, found above, which directly link the positive initial velocity v_0 to a final velocity v_t (see Fig. 3.1), and whose action is

$$S^{(0)}[v_{\mathrm{d}}^{(0)}] = \begin{cases} (v_t - v_0 + \mu t)^2/t - 4\mu v_t & \text{for } v_t < 0, \\ (v_t - v_0 + \mu t)^2/t & \text{for } v_t > 0. \end{cases} \tag{3.8}$$

The second type of paths are the piecewise-linear paths mentioned above, consisting of two straight lines in the region $v > 0$ or $v < 0$ connected by a straight line at $v = 0$. The equation of these so-called indirect paths is

$$v_{\mathrm{ind}}^{(0)}(s, t_1, t_2) = \begin{cases} (t_1 - s)v_0/t_1 & \text{for } s < t_1, \\ 0 & \text{for } t_1 < s < t_2, \\ (s - t_2)v_t/(t - t_2) & \text{for } s > t_2, \end{cases} \tag{3.9}$$

where $t_1 < t_2$ are arbitrary times at which a path reaches $v = 0$ (see Fig. 3.1). Following

the two principles above, we evaluate the action of these paths in a piecewise way with $S^{(0)}[0] = 0$ and minimise it for $t_1 < t_2$ to obtain

$$S^{(0)}[v^{(0)}_{\mathrm{ind}}] = 4\mu|v_t| \tag{3.10}$$

for $t_1 = v_0/\mu$ and $t_2 = t - |v_t|/\mu$. Since we require $t_1 < t_2$, the lower bound is reached only if $|v_t| < \mu t - v_0$. Note that paths arising in the limit case where $t_1 = t_2 \equiv t_0$ with $v_0 v_t < 0$ corresponds to direct paths, whereas those that just "bounce" on the $v = 0$ axis, i.e., $t_1 = t_2 \equiv t_0$ but $v_0 v_t > 0$ are called intermediate paths $v^{(0)}_{\mathrm{int}}(s, t_0)$ [see Fig. 3.1(a)] and have a minimal action equal to

$$S^{(0)}[v^{(0)}_{\mathrm{int}}] = (|v_t| + v_0 - \mu t)^2/t + 4\mu|v_t| \tag{3.11}$$

for $t_0 = v_0 t/(v_0 + |v_t|)$.

It can be easily checked that any piecewise-linear paths other than those considered above have a greater action, and so cannot be optimal. Since $S^{(0)}[v^{(0)}_{\mathrm{d}}] \leqslant S^{(0)}[v^{(0)}_{\mathrm{int}}]$ holds for any endpoint (v_t, t), we know that the intermediate paths can not be the optimal paths in the present approximation, but will be useful when we treat the Jacobian in the next subsection. In addition, for $v_t < 0$ we have $-4\mu v_t \leqslant S^{(0)}[v^{(0)}_{\mathrm{d}}]$, whereas for $v_t > 0$ we have $4\mu v_t \leqslant S^{(0)}[v^{(0)}_{\mathrm{d}}]$ if and only if $v_t \leqslant (\sqrt{v_0} - \sqrt{\mu t})^2$. Therefore, combining these informations and the condition that $S^{(0)}[v^{(0)}_{\mathrm{ind}}]$ attains the lower bound $4\mu|v_t|$ [see Eq. (3.10)], i.e., $|v_t| < \mu t - v_0$, we can write the equation of the optimal path as

$$v^{(0)}(s) = \begin{cases} v^{(0)}_{\mathrm{d}}(s) & \text{for } t < v_0/\mu, \\ v^{(0)}_{\mathrm{ind}}(s, v_0/\mu, t - |v_t|/\mu) & \text{for } t > v_0/\mu \text{ and } v_t \in [v^-(t), v^+(t)], \\ v^{(0)}_{\mathrm{d}}(s) & \text{for } t > v_0/\mu \text{ and } v_t \notin [v^-(t), v^+(t)], \end{cases} \tag{3.12}$$

where the limits of the velocity interval are defined by

$$v^-(t) = v_0 - \mu t, \qquad v^+(t) = \left(\sqrt{v_0} - \sqrt{\mu t}\right)^2. \tag{3.13}$$

This shows that, if the endpoint (v_t, t) lies in the area bounded by $v^-(s)$ and $v^+(s)$ with $s > v_0/\mu$, as shown in Fig. 3.2, then the optimal path is an indirect path, otherwise it is a direct path.

The SPA(0) approximation of the propagator is obtained from this result by substi-

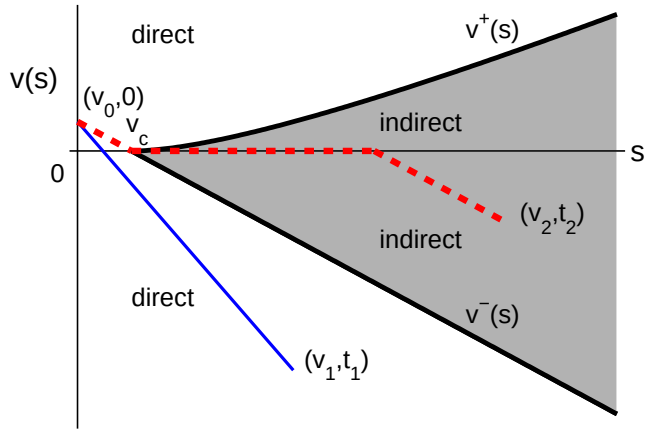

Figure 3.2: Regions in the $v_t - t$ plane for which the optimal path of the action at leading order, Eq. (3.3), is given by an indirect (direct) path [shaded (white)] [see Eqs. (3.13)]. Here $v_c = v_0/\mu$ denotes the tip of the region.

tuting the corresponding action in Eq. (3.5). For $t < v_0/\mu$, we find

$$p^{(0)}(v_t, t|v_0, 0) = N_1 \begin{cases} \exp[-(v_t - v_0 + \mu t)^2/(4Dt) + \mu v_t/D] & \text{for } v_t < 0, \\ \exp[-(v_t - v_0 + \mu t)^2/(4Dt)] & \text{for } v_t > 0, \end{cases} \tag{3.14}$$

whereas for $t > v_0/\mu$, we find

$$p^{(0)}(v_t, t|v_0, 0) = N_2 \begin{cases} \exp[-(v_t - v_0 + \mu t)^2/(4Dt) + v_t/D] & \text{for } v_t < v^-(t), \\ \exp[-(v_t - v_0 + \mu t)^2/(4Dt)] & \text{for } v_t > v^+(t), \\ \exp(-\mu|v_t|/D) & \text{for } v_t \in [v^-(t), v^+(t)], \end{cases} \tag{3.15}$$

where N_1 and N_2 are normalisation factors. This result is compared in Fig. 3.3 with the exact propagator. There we see that SPA(0) is a good approximation of $p(v_t, t|v_0, 0)$ at short and long times, but does not capture the bimodal structure of the propagator arising when the optimal path hits the origin for times close to $t = v_0/\mu$. While a kink (non-smooth point) of the exact propagator shows up at time $t < v_0/\mu$ in the region $v_t > 0$ [see Fig. 3.3(b)], the corresponding kink of the SPA(0) only appears at time $t > v_0/\mu$ [see Fig. 3.3(c) as well as Eqs. (3.14) and (3.15)]. For comparison, we also show in Fig. 3.3 the result of the propagator obtained from Langevin simulations of the SDE using the standard Euler-Maruyama integration scheme [55] (see also appendix

A.2.1). The application of this scheme is stable for the piecewise-smooth SDE and only requires that we choose the integration time step small enough, so that we can reproduce the cusp seen in its propagator.

We will see in the next subsection that the inclusion of the Jacobian in the saddle-point approximation enables us to reproduce this bimodality more accurately. An important remark, before we get to that part, is that the SPA(0) yields the same approximation as the exact propagator (1.9) in the noiseless limit. Indeed, it is not difficult to verify that the limit

$$I(v_t,t|v_0,0)=\lim_{D\to 0}-4D\,\ln p(v_t,t|v_0,0)=\lim_{D\to 0}-4D\,\ln\hat{p}\left(\frac{\mu}{D}v_t,\frac{\mu^2}{D}t\,\middle|\,\frac{\mu}{D}v_0,0\right), \tag{3.16}$$

which defines in the Freidlin-Wentzell large deviation theory [35] the so-called pseudo- or quasi-potential $I(v,t|v_0,0)$, is equal to the SPA(0) action (see appendix A.1 for the proof and also Fig. 3.4 for numerical comparisons). This means that the bimodal structure of the exact propagator (1.9) at time $t<v_0/\mu$ disappears when $D\to 0$ [see Eq. (3.14)]. In this piecewise case, the different optimal paths that we have found can be associated, in the weak-noise limit, to two different physical modes of motion of the noiseless system: direct paths represent slip motion, whereas indirect paths represent stick motion [6, 9]. For any fixed value of v_t, the optimal path will always be an indirect path if the time is sufficiently large, which means that all optimal paths are indirect paths in the limit $t\to\infty$.

3.1.2 Corrected action with zeroth-order path

One way to correct the SPA(0) is to use the candidate optimal paths obtained before but to evaluate their action by including the Jacobian in the action [see Eq. (2.3)]:

$$S[v]=\int_0^t\left\{[\dot{v}(s)+\mu\sigma(v(s))]^2-4D\mu\delta(v)\right\}ds. \tag{3.17}$$

This defines a first-order saddle-point approximation, referred to as SPA(1), of the propagator that retains the optimal paths of SPA(0) but includes the subdominant correction of the Jacobian, which is multiplied by D.

To obtain this approximation, we need to evaluate how the contribution arising from the δ function in Eq. (3.17) changes the action for the different paths considered. For direct paths $v_{\rm d}^{(0)}(s)$, there is obviously only a contribution when the $v=0$ axis is crossed,

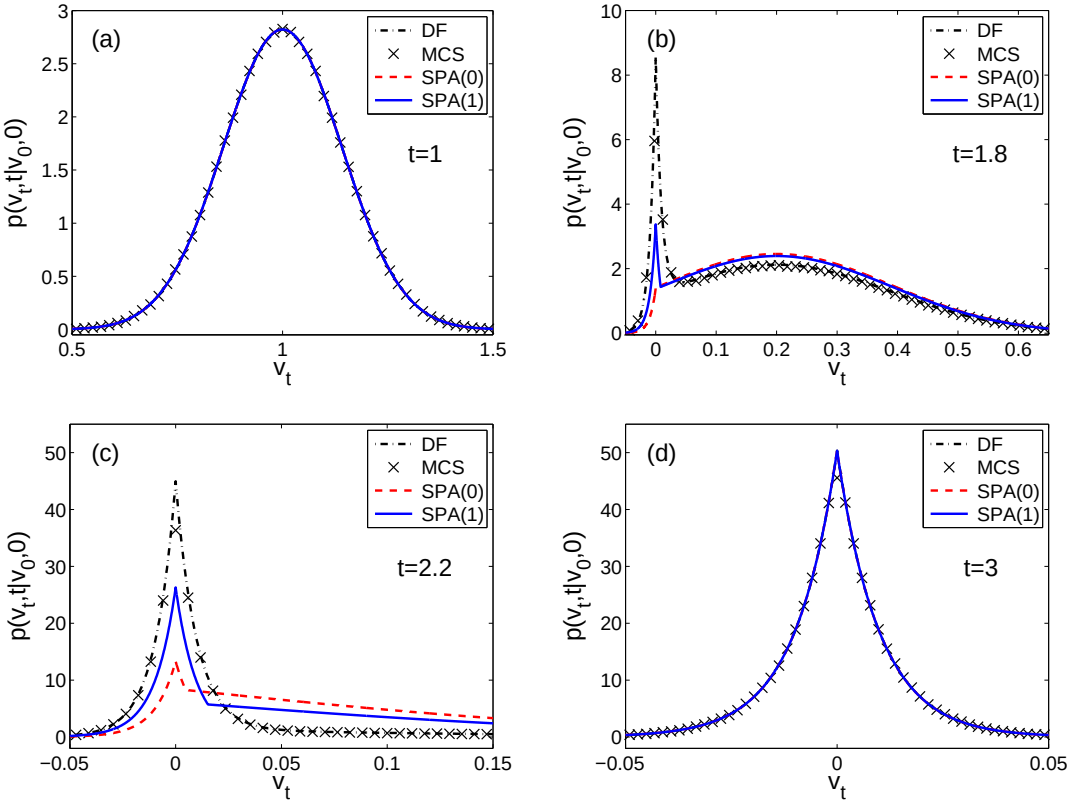

Figure 3.3: Propagator of the dry friction model (1.8) for initial velocity $v_0 = 2$, $\mu = 1$, $D = 0.01$ and different values of time: (a) $t = 1$, (b) $t = 1.8$, (c) $t = 2.2$, and (d) $t = 3$. Here DF denotes the exact analytical result (1.9), MCS the Monte Carlo simulation of Eq. (1.8) with step-size 0.0001 and an ensemble of 10^6 realisations, SPA(0) the leading order saddle-point approximation [see Eqs. (3.14) and (3.15) in Sec. 3.1.1], and SPA(1) the higher order saddle-point approximation [see Eqs. (3.19), (3.21) and (3.23) in Sec. 3.1.2].

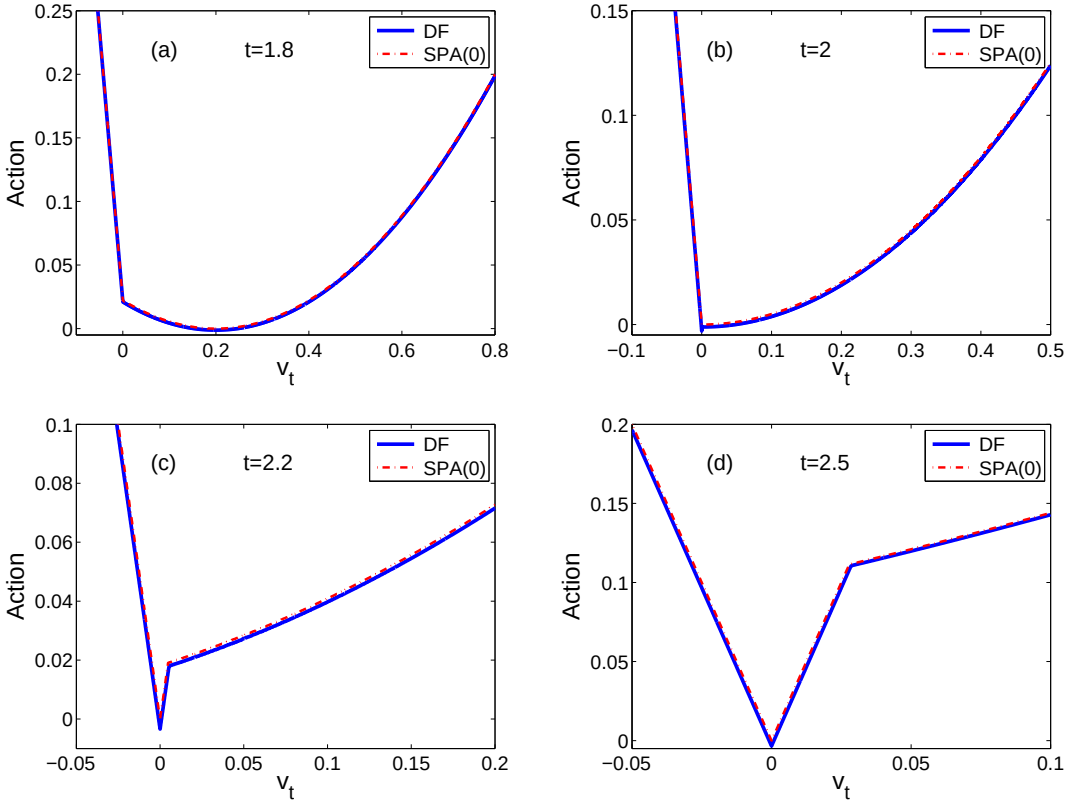

Figure 3.4: Comparison of the actions of the SPA(0) [see Eqs. (3.14) and (3.15)] and of the analytic solution (1.9) for initial velocity $v_0 = 2$, $\mu = 1$, $D = 0.0001$ and different values of time: (a) $t = 1.8$, (b) $t = 2$, (c) $t = 2.2$, and (d) $t = 2.5$. Here DF denotes the action of the exact analytical result (1.9) and SPA(0) the action of the leading order saddle-point approximation [see Eqs. (3.14) and (3.15)].

so that

$$\int_0^t \delta(v_{\mathrm{d}}^{(0)})ds = \begin{cases} t/(v_0 - v_t) & \text{for } v_t < 0, \\ 0 & \text{for } v_t > 0. \end{cases} \tag{3.18}$$

Thus, the corresponding corrected action of Eq. (3.8) is

$$S[v_{\mathrm{d}}^{(0)}] = \begin{cases} (v_t - v_0 + \mu t)^2/t - 4\mu v_t - 4D\mu t/(v_0 - v_t) & \text{for } v_t < 0, \\ (v_t - v_0 + \mu t)^2/t & \text{for } v_t > 0. \end{cases} \tag{3.19}$$

For intermediate paths $v_{\mathrm{int}}^{(0)}(s, t_0)$, the evaluation of the Jacobian term is straightforward as well. Any sensible representation of the δ function will result in a symmetric average of the inverse slopes of the path, leading to

$$\int_0^t \delta(v_{\mathrm{int}}^{(0)})ds = \frac{1}{2\left|\dot{v}_{\mathrm{int}}^{(0)}(t_0-, t_0)\right|} + \frac{1}{2\left|\dot{v}_{\mathrm{int}}^{(0)}(t_0+, t_0)\right|} = \frac{t}{v_0 + |v_t|}, \tag{3.20}$$

where we have used the condition $t_0 = v_0 t/(v_0 + |v_t|)$. Hence, it follows from Eqs. (3.17) and (3.20) that

$$S[v_{\mathrm{int}}^{(0)}] = (|v_t| + v_0 - \mu t)^2/t + 4\mu|v_t| - 4D\mu t/(v_0 + |v_t|). \tag{3.21}$$

Indirect paths $v_{\mathrm{ind}}^{(0)}(s, t_1, t_2)$ require a closer inspection: these paths vanish over an entire interval of time, so that the contribution originating from the Jacobian is ill defined. To treat this, we follow the previous principle that paths on the attractor do not contribute to the action and define the following two additional heuristic principles: (iii) parts of indirect paths on the attractor are not considered as contributing to the Jacobian and (iv) non-vanishing parts of indirect paths contribute, as for intermediate paths, to the Jacobian in a weighted average way. With these principles, the corrected action of indirect paths is finite and equal to

$$\int_0^t \delta(v_{\mathrm{ind}}^{(0)})ds = \frac{1}{2\left|\dot{v}_{\mathrm{ind}}^{(0)}(t_1-, t_1, t_2)\right|} + \frac{1}{2\left|\dot{v}_{\mathrm{ind}}^{(0)}(t_2+, t_1, t_2)\right|} = \frac{1}{\mu}, \tag{3.22}$$

where we have used the conditions $t_1 = v_0/t$ and $t_2 = t - |v_t|/\mu$. Thus, the corresponding action (3.17) can be evaluated as

$$S[v_{\mathrm{ind}}^{(0)}] = 4\mu|v_t| - 4D \qquad \text{for } |v_t| < \mu t - v_0. \tag{3.23}$$

By properly comparing the corrected actions (3.19), (3.21) and (3.23), we can determine which path is minimal depending on v_t and t to obtain the corresponding propagator $p^{(0;1)}(v_t, t|v_0, 0)$ [see Eq. (2.7)]. The result of this minimisation is shown in Fig. 3.3 as SPA(1). We see that the inclusion of the Jacobian correction qualitatively improves the propagator as compared to the lowest-order approximation, SPA(0) of Sec. 3.1.1, even though there are still some deviations in the transient regime where the exact propagator shows a bimodality. Especially, at time $t < v_0/\mu$ the SPA(1) has already shown up the kink corresponding to that of the exact propagator in the region $v_t > 0$ [see Fig. 3.3(b)]. This phenomenon is different with that of the SPA(0), which does not have such a kink at $t < v_0/\mu$. As we know, this kink is an artifact of weak-noise approximations and are smoothed in the exact propagator by the finite diffusion.

3.1.3 Corrected action with corrected path

The SPA(1) corrects the SPA(0) by including the Jacobian term in the action, while using the optimal paths of SPA(0), i.e., the paths that minimise the zeroth-order action $S^{(0)}[v]$. As a further correction to this approximation, it is tempting to obtain the optimal paths by minimising the corrected action $S[v]$ with the Jacobian, thus constructing a "full" first-order approximation.

Unfortunately, this approach does not work as the action turns out to diverge for $v_t = 0$. To see this, evaluate the action of Eq. (3.17) for an intermediate path $v_{\mathrm{int}}^{(0)}$ with a kink at $t_0 = t/2$ (see Fig. 3.5):

$$S[v_{\mathrm{int}}^{(0)}] = 2\mu(|v_t| - v_0) + \mu^2 t + 2(v_0^2 + v_t^2)/t - D\mu t\,(1/v_0 + 1/|v_t|)\,. \tag{3.24}$$

This value is an upper bound for the minimum of the action, which determines the density according to Eq. (2.9). The problem of this result is that $S[v_{\mathrm{int}}^{(0)}] \to -\infty$ when $v_t \to 0$, leading to a (non-integrable) singularity for the propagator $p(v_t, t|v_0, 0)$ at $v_t = 0$. Thus the approximation scheme based on obtaining the optimal paths from $S[v]$ results in a non-normalisable expression, which implies that a "full" first-order SPA is not possible for the SDE of Eq. (1.8). It is clear that this problem will also arise in any SDE having, as in Eq. (1.8), points where the force of the SDE is discontinuous. One way to approach this problem is to explore regularisations of such discontinuities.

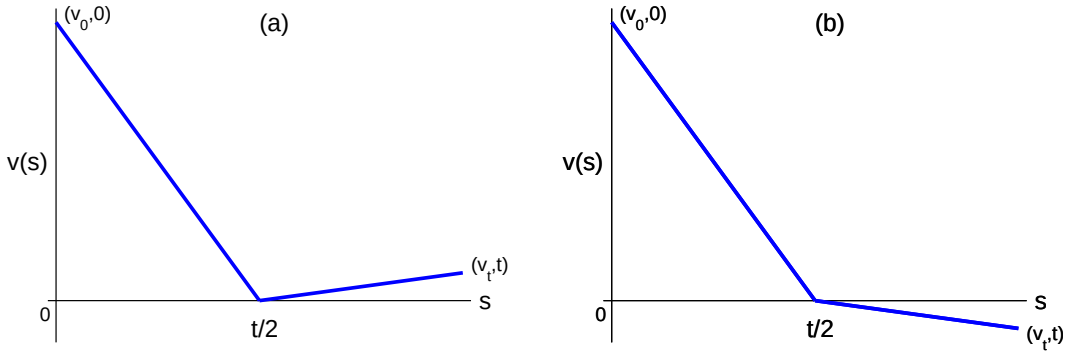

Figure 3.5: Intermediate paths $v_{\text{int}}^{(0)}(s, t_0)$ with $t_0 = t/2$ for (a) $v_t > 0$ and (b) $v_t < 0$.

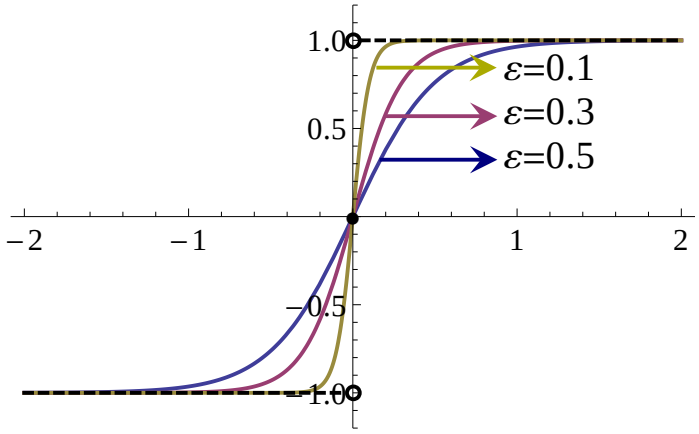

Figure 3.6: Comparison of the sign function $\sigma(v)$ (dashed) and the hyperbolic tangent function $\tanh(v/\varepsilon)$ (solid) for three different values of ε.

3.2 Regularised SDE

As seen in the previous section, the weak-noise approximation of the path integral for non-smooth SDEs faces some difficulties related to the minimisation of the action and the singularity of the Jacobian term. To treat these problems, we now consider the regularised SDE of Eq. (3.1) in which the discontinuous drift $\sigma(v)$ is replaced by the smooth drift $\tanh(v/\varepsilon)$ involving the additional (small) parameter ε (see Fig. 3.6). For this smooth SDE, the aforementioned difficulties do not occur: we can minimise the action over smooth differentiable paths and the Jacobian is well defined. In this section, we are interested in understanding the weak-noise properties of this regularised SDE.

To investigate the regularised model, we introduce non-dimensional units:

$$u = v/\varepsilon, \qquad \tau = \mu t/\varepsilon. \tag{3.25}$$

Equation (3.1) is then simply written as (see appendix A.3.1)

$$\dot{u}(\tau) = -\tanh(u(\tau)) + \sqrt{\widetilde{D}}\,\xi(\tau), \tag{3.26}$$

where $\widetilde{D} = D/(\varepsilon\mu)$ is now the only parameter of the model, called the effective diffusion constant. An important point to note is that the two limits $\varepsilon \to 0$ and $D \to 0$ do not commute. In the following, we will be interested in the smooth model for small and moderate effective noise amplitudes.

As mentioned at the beginning of this chapter, the propagator of the regularised model does not have a known closed analytic form. Thus, for benchmarking the weak-noise approximation results, we need to resort to numerical simulations obtained by the Euler-Maruyama scheme (see appendix A.2.1), which accurately reproduce, as for the piecewise-smooth SDE, all the features of the propagator, provided that we choose the integration time step small enough.

As before, the leading order of the weak-noise approximation of Eq. (3.26) is determined by the action [see Eqs. (2.4) and (2.6)]

$$S^{(0)}[u] = \int_0^\tau [\dot{u}(s) + \tanh(u(s))]^2\, ds \tag{3.27}$$

evaluated for the solution of the Euler-Lagrange boundary value problem [see Eq. (2.5)]

$$\ddot{u}^{(0)}(s) = \tanh(u^{(0)}(s))/\cosh^2(u^{(0)}(s)), \quad u^{(0)}(0) = u_0, \quad u^{(0)}(\tau) = u_\tau. \tag{3.28}$$

The leading order may be improved by taking consistently first-order contributions into account. The propagator (2.9) is then determined by the action [see Eq. (2.3)]

$$S[u] = \int_0^\tau \left\{ [\dot{u}(s) + \tanh(u(s))]^2 - 2\widetilde{D}/\cosh^2(u(s)) \right\} ds \tag{3.29}$$

evaluated at the first-order path that obeys the boundary value problem (2.8)

$$\ddot{u}^{(1)}(s) = \left(1 + 2\widetilde{D}\right) \tanh(u^{(1)}(s))/\cosh^2(u^{(1)}(s)), \quad u^{(1)}(0) = u_0, \quad u^{(1)}(\tau) = u_\tau. \tag{3.30}$$

The two boundary value problems (3.28) and (3.30) just differ by a rescaling of time,

and can be solved by using a numerical shooting method (see Sec. 2.1).

Figure 3.7 compares the numerical Monte Carlo simulations of Eq. (3.26) with the zeroth- and first-order weak-noise approximations for small and moderate noise amplitudes. We see that, while the short and long time behaviours are captured well by the lowest-order approximation, substantial transient deviations are visible when the maximum of the propagator approaches the origin. The first-order approximation is in fact able to deal with such a feature, even for substantial noise amplitudes. Thus, the scheme outlined above can be considered as a candidate to deal with the weak-noise limit even in systems which mimic the discontinuous drift.

Naturally, from our study of the discontinuous model, we cannot expect the weak-noise approximation to yield the full propagator of the smooth model in the asymptotic limit $\varepsilon \to 0$. However, it should be possible to obtain, at a quantitative level, the main features of the propagator for suitable small values of D and ε. Of course, an improved scheme such as the first-order approximation needs to be applied, as one cannot rely on extremely small values of the effective diffusion to cover cases which are sufficiently close to a discontinuous drift. Indeed, Fig. 3.8 shows that this is the case if we translate the results obtained via Eqs. (3.29) and (3.30) to the dimensional units via Eq. (3.25). The SPA(1) performs well in short time and is also able to capture the main profiles of the piecewise-smooth SDE in moderate and long times. Larger deviations between the discontinuous and the regularised results appear only in a neighbourhood of size ε of the discontinuity. Hence, we may conclude that, in these particular cases, a suitable regularisation and first-order saddle-point approximation is able to capture the essential features of the piecewise-smooth SDE.

To close this section, let us comment on the kinks appearing in the quasi-potential corresponding to the minimised action. Since Eqs. (3.28) and (3.30) only differ by a rescaling of time and since we are here mainly concerned with the essential structure of the quasi-potential, we just focus on the simple zeroth-order approximation (3.27) and (3.28). Figure 3.9 shows the solution of the boundary value problem using the shooting method for a given value of u_0. At some finite value of τ, the boundary value problem develops a cusp singularity, beyond which three solutions occur in a finite interval of u_τ values, corresponding to smooth versions of the previously-identified direct, indirect and intermediate paths. For instance, we take two typical endpoints from Fig. 3.9(c) and compare their optimal paths with the dry friction case (1.8) in the original scale [see Eqs. (3.25) and (3.1)], as shown in Fig. 3.10. Even though these two kinds of optimal

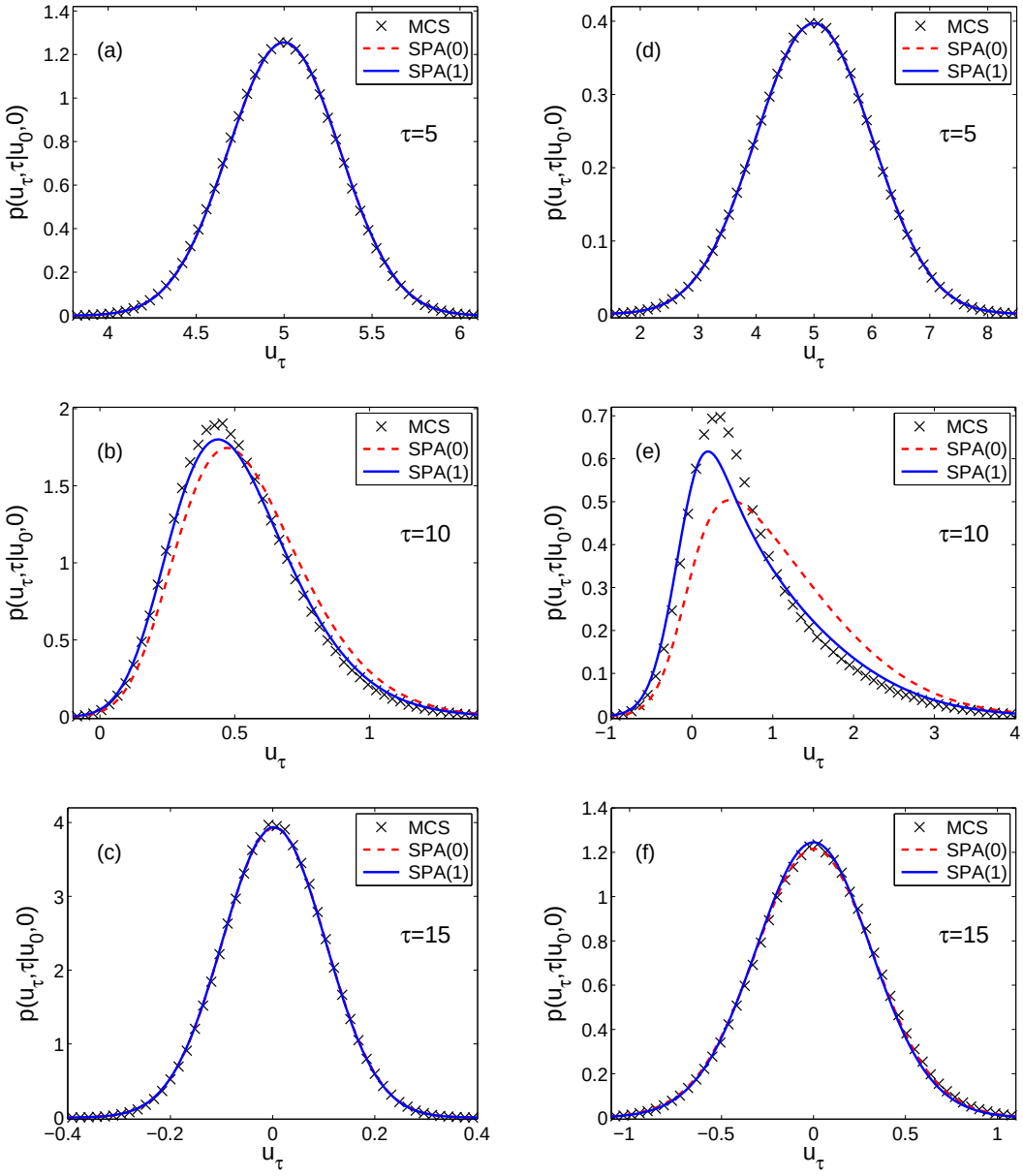

Figure 3.7: Propagator of Eq. (3.26) for small and moderate values of the effective diffusion, (a)–(c) $\widetilde{D} = 0.01$ and (d)–(f) $\widetilde{D} = 0.1$, initial condition $u_0 = 10$ and three different values of τ. Here MCS denotes the Monte Carlo simulations of the Langevin equation (3.26) with time step 0.005 and an ensemble of 10^6 realisations, SPA(0) the lowest order of the saddle-point approximation using the action of Eq. (3.27) [see also Eq. (2.6)], and SPA(1) the first order of the saddle-point approximation using the action of Eq. (3.29) [see also Eq. (2.5)].

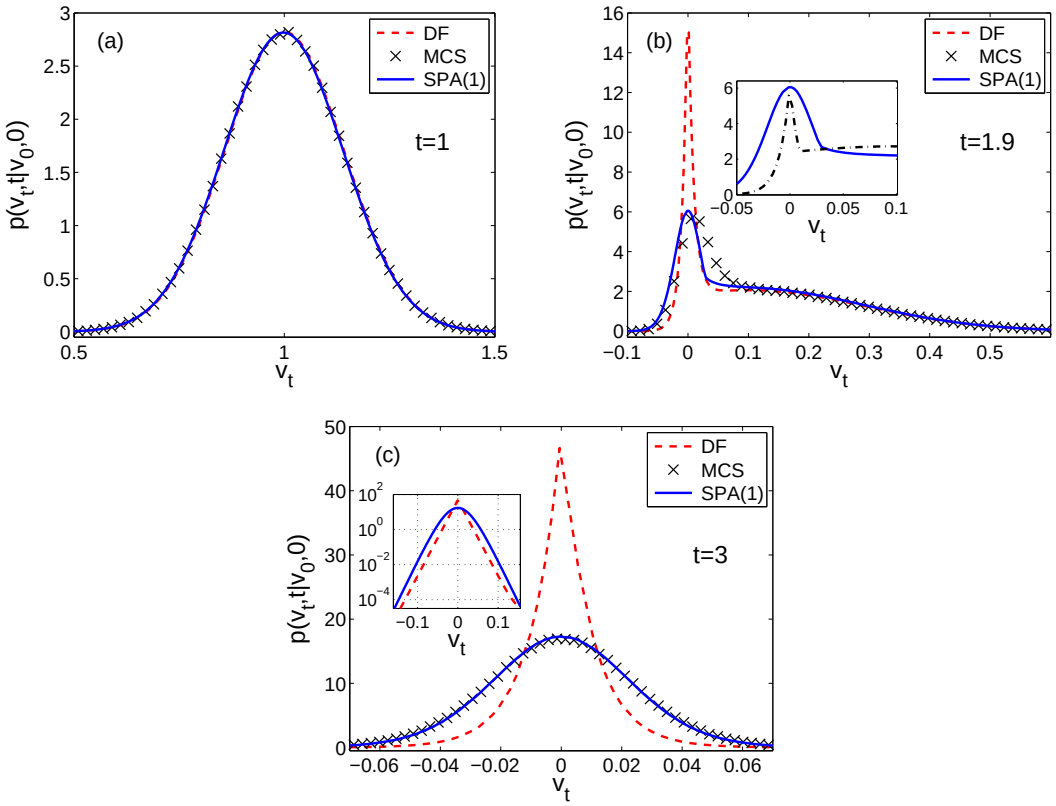

Figure 3.8: Comparison of the propagators of the dry friction model (1.8) and of the regularised scheme (3.1) for $\mu = 1$, $D = 0.01$, $\varepsilon = 0.05$, initial condition $v_0 = 2$ and three different values of time: (a) $t = 1$, (b) $t = 1.9$, and (c) $t = 3$. Here DF denotes the analytical result for the propagator of the dry friction model [see Eq. (1.9], MCS the Monte Carlo simulation of the Langevin equation (3.1) with time-step 0.005 and an ensemble of 10^6 realisations, and SPA(1) the first-order saddle-point approximation scheme using the action of Eq. (3.29). The inset in (b) shows the SPA(1) of the smooth case (solid line) and the SPA(1) of the dry friction case [dashed line, see Eqs. (3.19), (3.21), and (3.23)]. Both of these graphs have a kink which matches the structure appearing in the exact solution of the dry friction model (DF). The inset in (c) shows the data for DF and SPA(1) on a larger scale in a semi-logarithmic plot. Large quantitative deviations appear only in a neighbourhood of size ε of the discontinuity.

paths differ from each other, they have the same path structure.

A non-unique solution to the boundary value problem implies that the actual optimising path has to be determined from minimising Eq. (3.27) among the three possible paths. In our case, Fig. 3.9 shows that the optimal path is either a direct or an indirect path, as for the piecewise-constant SDE. The intermediate path is always a saddle point of the action, which implies that the quasi-potential consists of two analytic branches, with a kink appearing when the type of optimal paths changes [see Figs. 3.8(b), 3.11(b) and 3.11(c)]. The kink, which also shows up in the numerical solution of the Fokker-Planck equation, is an important feature of the quasi-potential: it appears at finite time and then moves to larger u_τ values [see Fig. 3.11(c)]. This feature, which is related to the convergence of the propagator towards the stationary distribution, is studied in detail next.

3.3 Analytic properties of the action

The previous analysis was mainly based on a numerical solution of the boundary value problem (3.28) and the evaluation of the corresponding action integral (3.27) (see Ref. [20] for a related numerical study). In this section, we try to obtain further insights into the weak-noise limit by studying some analytical properties of the quasi-potential, focusing on the zeroth-order approximation of the action. The first-order approximation of the action can be analysed along similar lines.

3.3.1 Action integral

The Euler-Lagrange equations (3.28) are equivalent to a conservative system with Hamiltonian

$$H(u, p_u) = p_u^2/2 - \tanh^2(u)/2, \tag{3.31}$$

where $p_u = \dot{u}$ [see Eq. (2.10)]. The phase portrait of this system, shown in Fig. 3.12, is important to understand the structure of the boundary value problem. The origin in phase space is a hyperbolic equilibrium point. Regions of positive and negative energy, respectively, are bounded by the separatrix of this fixed point. Solutions of the equation of motion (3.28) are given by constant energy levels

$$\dot{u} = p_u = \pm\sqrt{\tanh^2(u) + 2H}, \tag{3.32}$$

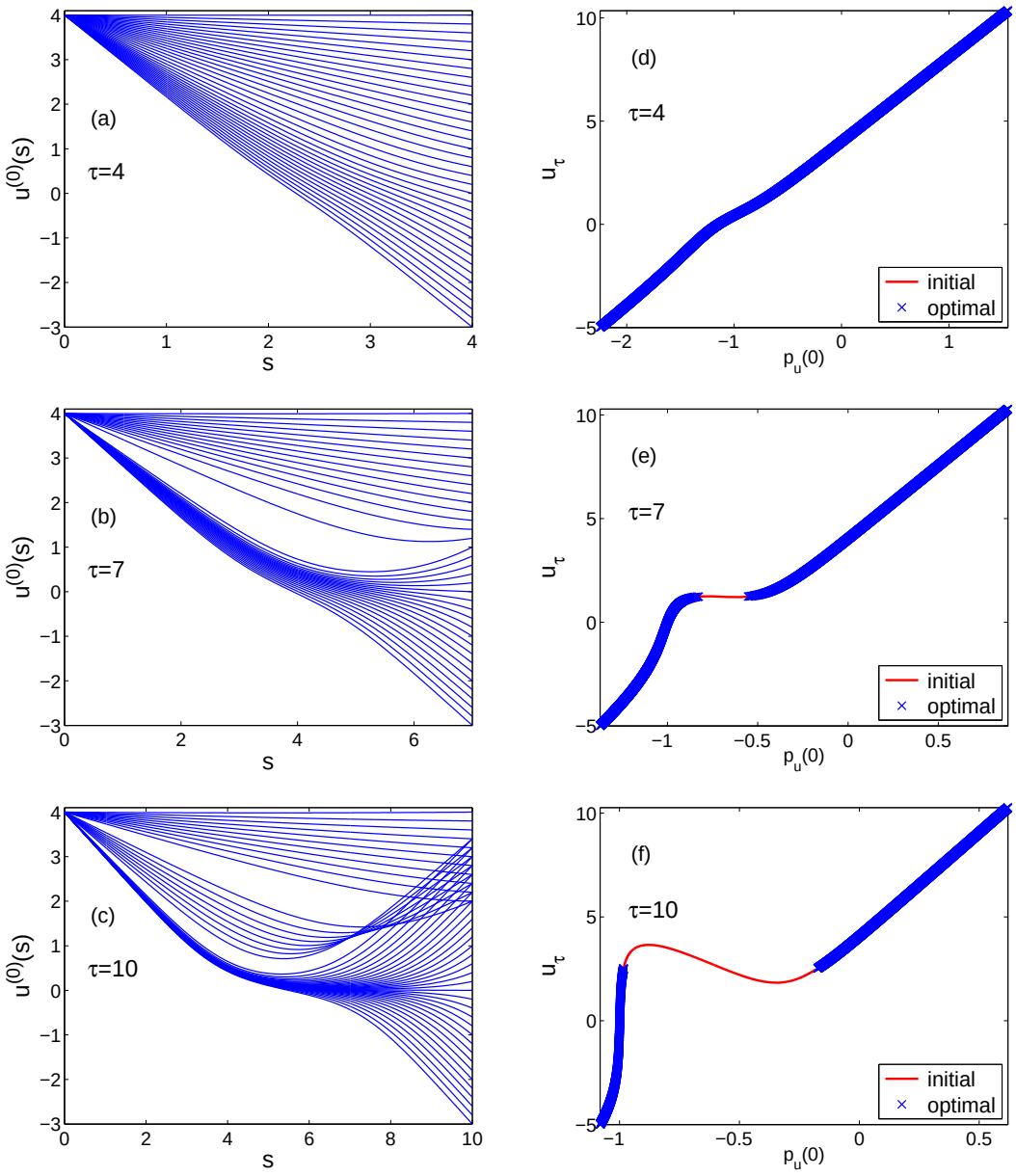

Figure 3.9: Solution of the boundary value problem (3.28) with the shooting method for the given value $u_0 = 4$ and three different values of τ. (a)–(c) Solutions of the differential equation (3.28) for different values of the initial slope $\dot{u}^{(0)}(0) = p_u(0)$. (d)–(f) Dependence of the final value $u_\tau = u^{(0)}(\tau)$ on the initial condition $\dot{u}^{(0)}(0) = p_u(0)$ of the differential equation (3.28), indicated by the solid line. The symbols indicate the solution which minimises the action (3.27).

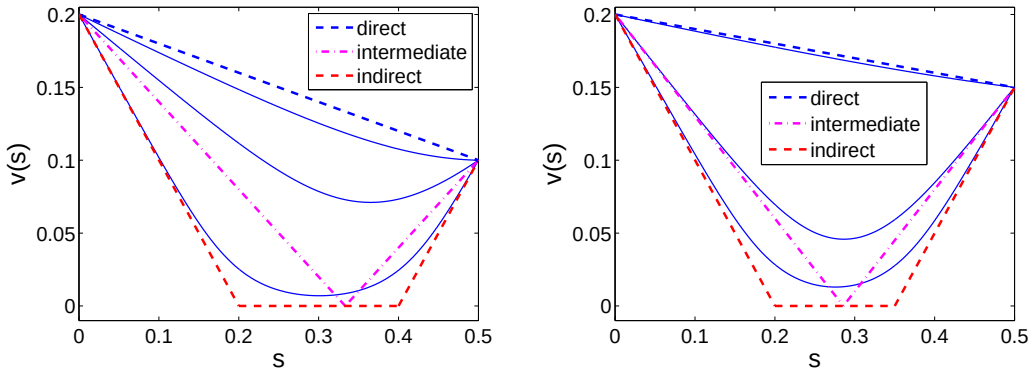

Figure 3.10: Comparison of the optimal paths of the dry friction model (1.8) (dashed) and of the regularised model (3.1) (solid) for two typical endpoints taken from Fig. 3.9(c).

where the sign determines whether the path is in the positive or negative momentum region of phase space. The zeroth-order action (3.27) for a path with energy H, starting at u_0 and terminating at u_τ can then be written as

$$S^{(0)}[u] = S(u_0, u_\tau, \tau, H) = 2\int_{u_0,H}^{u_\tau} p_u(s)du(s) + 2\ln\left(\frac{\cosh(u_\tau)}{\cosh(u_0)}\right) - 2H\tau \tag{3.33}$$

if we take the expression (3.31) for the Hamiltonian into account. The duration τ of this path from u_0 to u_τ is evaluated as

$$\tau = \int_{u_0,H}^{u_\tau} \frac{du(s)}{p_u(s)} \tag{3.34}$$

and allows us to express the energy in Eq. (3.33) in terms of the time. Thus the problem has been reduced to evaluating two integrals and solving algebraic equations. To take care of the correct sign in Eq. (3.32), we have to distinguish three cases, according to the sign of the terminal point u_τ.

Case 1: $u_\tau < 0 < u_0$

As can be seen from the phase portrait of Fig. 3.13(a), there is for given energy $H > 0$ a unique path connecting the two boundary points. Along this path Eq. (3.32) holds

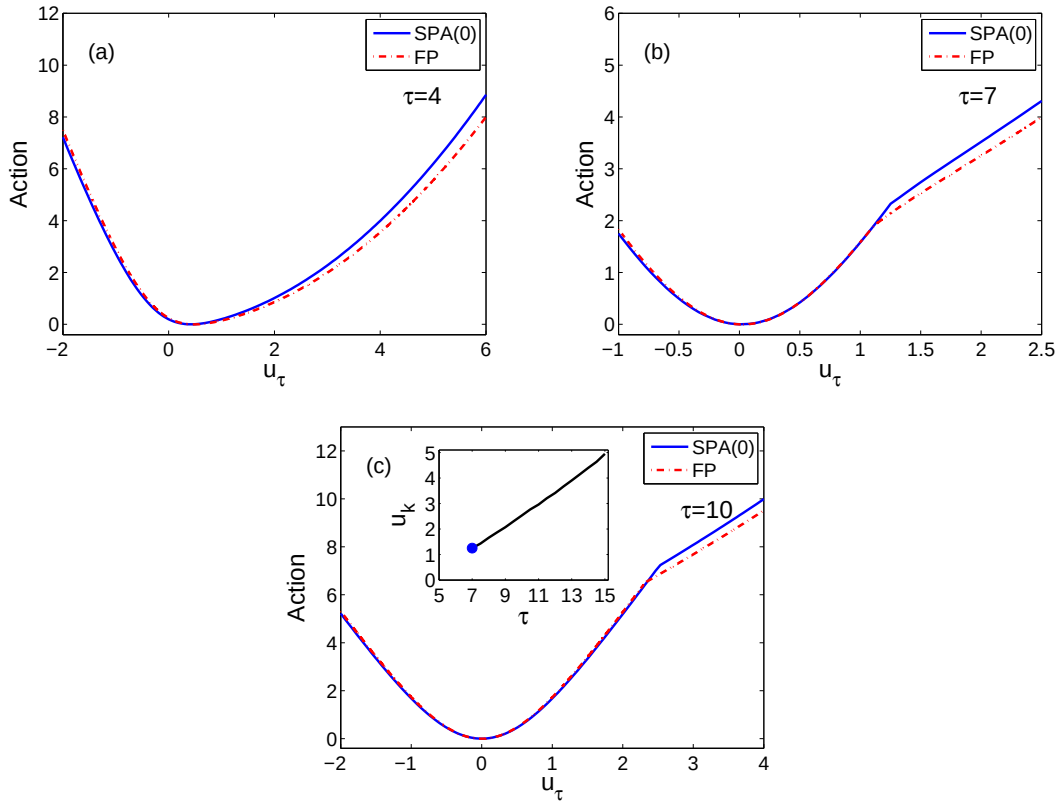

Figure 3.11: Quasi-potential of the regularised model (3.26) for initial condition $u_0 = 4$, $D = 0.0001$ and three different values of time: (a) $\tau = 4$, (b) $\tau = 7$, and (c) $\tau = 10$. Here FP (dashed line) denotes the potential $-4D \ln p(u_\tau, \tau | u_0, 0)$ computed by numerical integration of the corresponding Fokker-Planck equation (see appendix A.2.3 for the numerical scheme) and SPA(0) (solid line) the result of the leading order SPA, i.e., minimised action (3.27). The inset in (c) shows the position of the kink u_k as a function of the time τ, as obtained from SPA(0). The closed circle shows the time and the position where the kink emerges (see also Fig. 3.16).

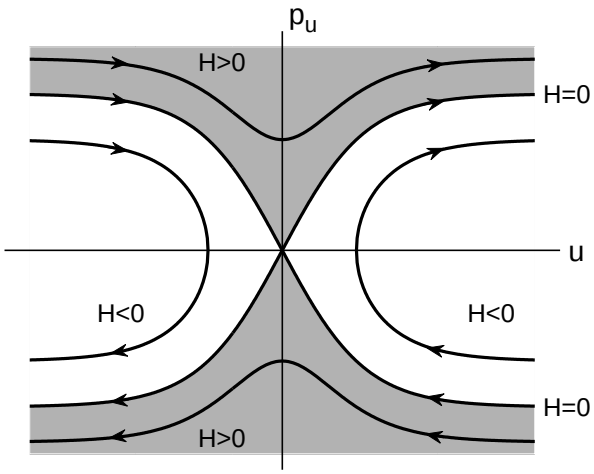

Figure 3.12: Phase portrait of the Hamiltonian system (3.31) which governs the boundary value problem (3.28). The region of positive energy is shaded.

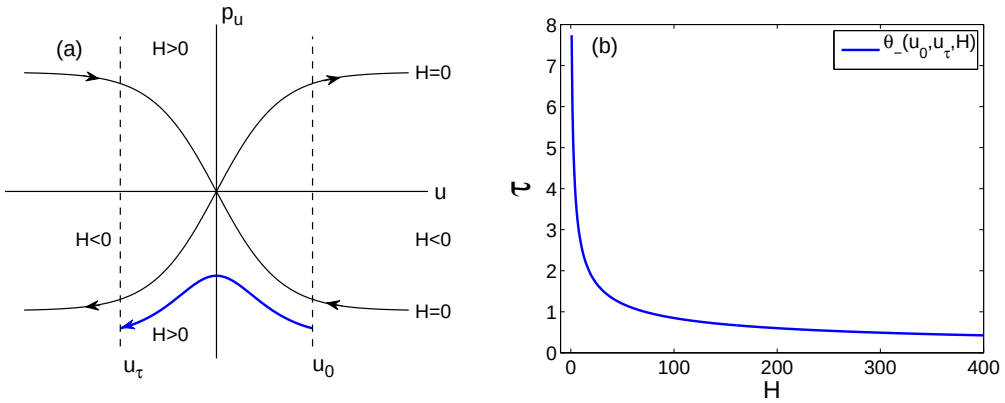

Figure 3.13: (a) Phase portrait of the Hamiltonian (3.31) with an orbit connecting two boundary points $u_\tau < 0 < u_0$ at a given energy $H > 0$. (b) Energy time relation (3.35) for $u_0 = 10$ and $u_\tau = -2$.

with a minus sign, and the expression relating energy and time, Eq. (3.34), results in

$$\begin{aligned}\tau &= \int_{u_\tau}^{u_0} \frac{du}{\sqrt{\tanh^2(u)+2H}} \\ &= \frac{1}{\sqrt{1+2H}} \int_{u_\tau}^{u_0} \frac{d\sinh(u)}{\sqrt{\sinh^2(u)+2H/(1+2H)}} \\ &= \theta_-(u_0,u_\tau,H),\end{aligned} \tag{3.35}$$

where

$$\theta_-(u_0,u_\tau,H) = \frac{1}{\sqrt{1+2H}} \ln\left(\frac{\sinh(u_0)+\sqrt{2H/(1+2H)+\sinh^2(u_0)}}{\sinh(u_\tau)+\sqrt{2H/(1+2H)+\sinh^2(u_\tau)}}\right). \tag{3.36}$$

It is easy to show that in the range $H > 0$ and $u_\tau < 0 < u_0$, Eq. (3.36) is a monotonically decreasing function of H [see Fig. 3.13(b) and also appendix A.5.1 for the proof], i.e., Eq. (3.35) defines the energy H as an analytic expression of τ and of the boundary points. As for the integral which enters the action (3.33), using the relations (3.32) and (3.35) we obtain

$$\begin{aligned}\int_{u_0,H}^{u_\tau} p_u(s)du(s) &= \int_{u_\tau}^{u_0} \sqrt{\tanh^2(u)+2H}\,du \\ &= \int_{u_\tau}^{u_0} \frac{1+2H-1/\cosh^2(u)}{\sqrt{\tanh^2(u)+2H}}du \\ &= (1+2H)\tau - \sigma_-(u_0,u_\tau,H),\end{aligned} \tag{3.37}$$

where we have introduced the abbreviation

$$\sigma_-(u_0,u_\tau,H) = \ln\left(\frac{\tanh(u_0)+\sqrt{2H+\tanh^2(u_0)}}{\tanh(u_\tau)+\sqrt{2H+\tanh^2(u_\tau)}}\right). \tag{3.38}$$

Therefore the entire action (3.33) finally reads

$$S(u_0,u_\tau,\tau,H) = 2(1+H)\tau + 2\ln\left(\frac{\cosh(u_\tau)}{\cosh(u_0)}\right) - 2\sigma_-(u_0,u_\tau,H). \tag{3.39}$$

Since the inverse of the energy-time relation (3.35) is single valued, the expression for the action defines an analytic expression of time τ and of the boundary points in the

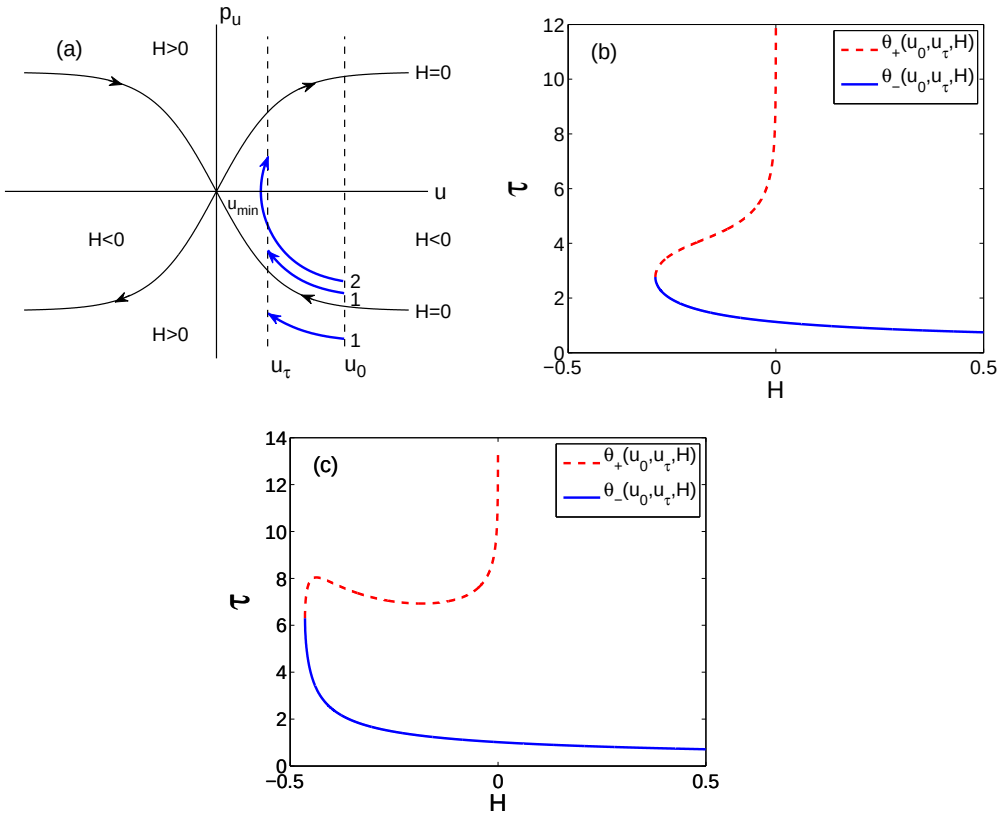

Figure 3.14: (a) Phase portrait of the Hamiltonian (3.31) with direct (1) and indirect (2) paths connecting boundary points $0 < u_\tau < u_0$. (b) Energy time relations (3.35) (solid line) and (3.40) (dashed line) for small values of u_0 ($u_0 = 2$, $u_\tau = 1$) with unique inverse. (c) Energy time relations (3.35) (solid line) and (3.40) (dashed line) for larger values of u_0 ($u_0 = 3$, $u_\tau = 2$) with multivalued inverse in a finite time interval.

region $u_\tau < 0 < u_0$ (see also Fig. 3.11).

Case 2: $0 < u_\tau < u_0$

For boundary points $0 < u_\tau < u_0$ the phase portrait 3.14(a) and Eq. (3.31) show that the connecting path has energy $H > H_{\min} = -\tanh^2(u_\tau)/2$. On the one hand, for energies $H > H_{\min}$, there exists a direct path whose duration is given by Eq. (3.35) and whose action is determined by Eq. (3.39). On the other hand, for $H_{\min} < H < 0$, there exists an indirect path with a turning point at $u_{\min} = \operatorname{artanh}(\sqrt{-2H})$. The duration of this path is obtained from Eq. (3.34) by splitting the path into two parts and using

appropriate signs in Eq. (3.32):

$$\tau = \int_{u_0}^{u_{\min}} \frac{du}{-\sqrt{\tanh^2(u) + 2H}} + \int_{u_{\min}}^{u_\tau} \frac{du}{\sqrt{\tanh^2(u) + 2H}} = \theta_+(u_0, u_\tau, H), \tag{3.40}$$

where

$$\begin{aligned}\theta_+(u_0, u_\tau, H) = &\frac{\ln\left[\sinh(u_0) + \sqrt{2H/(1+2H) + \sinh^2(u_0)}\right]}{\sqrt{1+2H}} \\ &+ \frac{\ln\left[\sinh(u_\tau) + \sqrt{2H/(1+2H) + \sinh^2(u_\tau)}\right]}{\sqrt{1+2H}} \\ &+ \frac{\ln\left[(1+2H)/(-2H)\right]}{\sqrt{1+2H}}.\end{aligned} \tag{3.41}$$

Similarly, the integral appearing in the action (3.33) can be evaluated as [see Eq. (3.37)]

$$\begin{aligned}\int_{u_0,H}^{u_\tau} p_u(s)du(s) &= -\int_{u_0}^{u_{\min}} \sqrt{\tanh^2(u) + 2H}du + \int_{u_{\min}}^{u_\tau} \sqrt{\tanh^2(u) + 2H}du \\ &= (1+2H)\tau - \sigma_+(u_0, u_\tau, H),\end{aligned} \tag{3.42}$$

where we have introduced the abbreviation

$$\begin{aligned}\sigma_+(u_0, u_\tau, H) = &\ln\left[\tanh(u_0) + \sqrt{2H + \tanh^2(u_0)}\right] \\ &+ \ln\left[\tanh(u_\tau) + \sqrt{2H + \tanh^2(u_\tau)}\right] - \ln(-2H).\end{aligned} \tag{3.43}$$

Thus, for the action (3.33) of this path we obtain

$$S(u_0, u_\tau, \tau, H) = 2(1+H)\tau + 2\ln\left(\frac{\cosh(u_\tau)}{\cosh(u_0)}\right) - 2\sigma_+(u_0, u_\tau, H). \tag{3.44}$$

To find the minimising path, we have to take a closer look at the energy-time relation. This relation consists of two branches [see Figs. 3.14(b) and 3.14(c)]. The branch determined by Eq. (3.35) is defined for all energies $H > H_{\min}$ and is a monotonically decreasing function for $0 < u_\tau < u_0$ (see appendix A.5.1). The second branch, defined for negative energies $H_{\min} < H < 0$ only, is given by Eq. (3.40). This branch is monotonically increasing for small values of u_0 and develops an inflection point if the boundary points exceed a critical value (see appendix A.5.2), which implies that, for small values

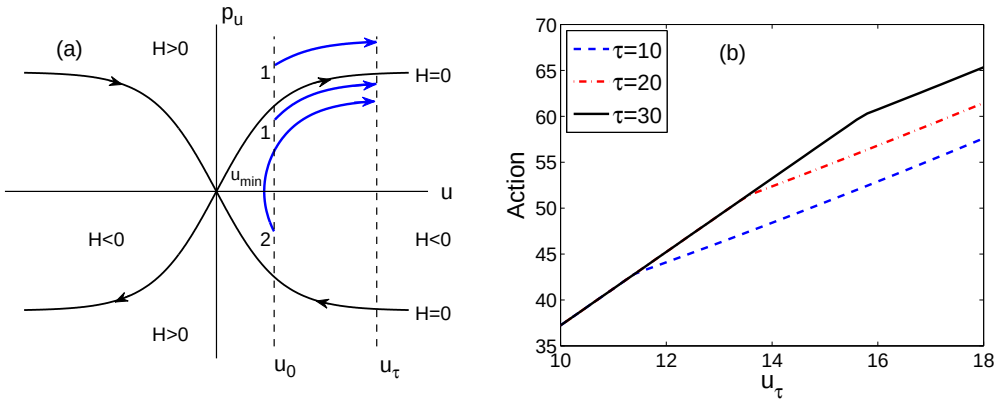

Figure 3.15: (a) Phase portrait of the Hamiltonian (3.31) with direct (1) and indirect (2) orbits connecting boundary points $0 < u_0 < u_\tau$. (b) Minimal action (3.33) as a function of u_τ in the interval $u_\tau > u_0 = 10$ for different values of the time τ, showing a kink moving to the right.

of u_0, the relation determines the energy in terms of time and boundary points uniquely. However, if the initial condition is beyond the critical regime, the energy time relation has a multivalued inverse within a finite time interval [see Fig. 3.14(c)]. The value of the action entering the propagator is then the minimum among the three possible inverse values. The data show that for fixed values of u_0 and u_τ the minimum is given by the low energy solution, i.e., by the direct path, up to a critical value of τ while the minimum for larger values of τ is given by the high energy solution, i.e., the indirect path. The intermediate path, i.e., the solution with energy in between, is always of saddle type. As a consequence, the action, considered as a function of u_τ, switches the analytical branch and develops a kink [see Figs. 3.11(b) and 3.11(c) and 3.15(b)].

Case 3: $0 < u_0 < u_\tau$

As in the previous case there are two types of paths to consider: in the energy range $H > H_{\min} = -\tanh^2(u_0)/2$, there exists a direct path connecting the two boundary points, while for negative energies $H_{\min} < H < 0$, there exist in addition indirect paths with a turning point at $u_{\min} = \operatorname{artanh}(\sqrt{-2H})$. This is similar to the previous case and the relevant integrals can be dealt with by applying the symmetry of the phase portrait [see Fig. 3.15(a)]. To find the duration of the direct path (3.34), we just observe that by swapping the boundary points and reversing the direction of the path we obtain a corresponding mirror orbit with the same duration, which we have dealt with in the

previous case. Thus, Eq. (3.35) tells us that

$$\tau = \int_{u_0}^{u_\tau} \frac{du}{\sqrt{\tanh^2(u) + 2H}} = \theta_-(u_\tau, u_0, H). \tag{3.45}$$

Since the integral entering the action (3.33) has the same symmetry, we obtain the result stated in Eq. (3.37) by swapping u_0 and u_τ on the right-hand side. Thus the action (3.33) finally reads

$$S(u_0, u_\tau, \tau, H) = 2(1+H)\tau + 2\ln\left(\frac{\cosh(u_\tau)}{\cosh(u_0)}\right) - 2\sigma_-(u_\tau, u_0, H). \tag{3.46}$$

The action itself does not share the aforementioned symmetry because of the additional terms appearing in Eq. (3.33).

For the indirect path the same reasoning applies. The duration of the path, given by Eq. (3.40), applies since the right hand side is symmetric in u_0 and u_τ and swapping both arguments does not have any effect. In fact, the same argument is valid for the integral which enters the action. Therefore, Eq. (3.42) holds, since the right hand side is a symmetric expression in the boundary points, and the corresponding action is indeed given by Eq. (3.44).

Overall, we see that the energy-time relationship is at the heart of understanding the structure of the optimal paths, the minimised action, and finally the propagator of the SDE. As in the previous case, the relation consists of two branches [see Figs. 3.14(b) and 3.14(c)]. The lower branch is given by the direct path (3.45), which is a monotonically decreasing function on its domain $H > H_{\min}$. The second branch for negative energies $H_{\min} < H < 0$ is determined by Eq. (3.40) and thus largely the discussion of the previous section applies. If the initial condition is small, so that no cubic singularity appears for $0 < u_\tau < u_0$ (case 2), then such a singularity will finally develop for sufficiently large value of u_τ resulting in a non-analytic minimised action. If, on the contrary, u_0 is so large that the occurrence of the kink has already happened in the domain $0 < u_\tau < u_0$, then the kink just propagates to larger values of u_τ [see Fig. 3.15(b)].

3.3.2 Asymptotics of the action

The analytic expressions derived in the previous subsection allow us to study in some detail the properties of the propagator shown, e.g., in Fig. 3.11. Of particular relevance

is the approach to the stationary state, the tail behaviour of the distribution, and the emergence and dynamics of non-analyticities of the quasi-potential.

Approach to equilibrium

To study the convergence of the propagator towards the stationary distribution, we consider a fixed value of u_0 and u_τ and take the asymptotic limit $\tau \to \infty$. It is obvious from the phase portrait or from the energy-time relation [see Figs. 3.13(b), 3.14(b) and 3.14(c)] that the asymptotic limit implies $H \to 0$. Hence the energy-time relation is determined by Eq. (3.35) or (3.40), depending on the sign of u_τ. For the convenience of the reader, the details of the following derivations are presented in appendix A.4.1. In both cases $u_\tau < 0$ and $u_\tau > 0$, a straightforward expansion yields [see Eqs. (A.37) and (A.39)]

$$\tau = \ln[2\sinh(u_0)] + \ln[-\sinh(u_\tau)/H] + O(H \ln|H|)\,. \tag{3.47}$$

For the action, either Eq. (3.39) or (3.44) applies, depending on the sign of u_τ, yielding the expansion [see Eqs. (A.38) and (A.40)]

$$\begin{aligned} S(u_0, u_\tau, \tau, H) = 2(1+H)\tau + 2\ln\left(\frac{\cosh(u_\tau)}{\cosh(u_0)}\right) \\ -2\left\{\ln\left[2\tanh(u_0)\right] + \ln\left[-\tanh(u_\tau)/H\right]\right\} + O(H). \end{aligned} \tag{3.48}$$

By solving Eq. (3.47) to leading order for H, i.e.,

$$H = -2\sinh(u_0)\sinh(u_\tau)e^{-\tau}, \tag{3.49}$$

Eq. (3.48) yields, as expected, the potential of the stationary distribution

$$S(u_0, u_\tau, \tau, H) = 4\ln[\cosh(u_\tau)] + O(\tau e^{-\tau}). \tag{3.50}$$

The full action as well as the propagator at finite time depends on the intial condition u_0 and hence does not have a symmetry with respect to u_τ. However, the stationary action and the corresponding stationary distribution is independent of u_0 [see Eq. (3.50)] in the limit $\tau \to \infty$. In that limit the symmetry under the change $u_\tau \to -u_\tau$ is restored [see also Eq. (1.12)]. Above all, the saddle-point approximation preserves all the symmetries of the underlying equations of motion.

Tail behaviour of the propagator

To investigate the action for large values of arguments, we consider the asymptotic limit $|u_\tau| \to \infty$ for fixed values of time τ and initial condition u_0, which implies, from the phase portraits of Figs. 3.13(a) and 3.15(a), $H \to +\infty$. The energy-time relation is determined by Eq. (3.35) or (3.45), depending on the sign of u_τ, and a direct expansion results in the expression (see appendix A.4.2)

$$\tau = \frac{1}{\sqrt{1+2H}} \left[|u_\tau - u_0| + O(H^{-1}) \right], \tag{3.51}$$

which is valid irrespective of the sign of u_τ. This expression is easily inverted to obtain

$$1 + 2H = (u_\tau - u_0)^2/\tau^2 + O(u_\tau^{-1}). \tag{3.52}$$

For the action Eq. (3.39) or (3.46) apply, depending on the sign of u_τ. Expansion in terms of H yields σ_- to be of order $O(H^{-1/2})$ (see appendix A.4.2) so that

$$S(u_0, u_\tau, \tau, H) = 2(1+H)\tau + 2\ln\left(\frac{\cosh(u_\tau)}{\cosh(u_0)}\right) + O(H^{-1/2}). \tag{3.53}$$

Hence, using Eq. (3.52) we end up with

$$S(u_0, u_\tau, \tau, H) = \frac{(u_\tau - u_0)^2}{\tau} + \tau + 2\ln\left(\frac{\cosh(u_\tau)}{\cosh(u_0)}\right) + O(u_\tau^{-1}). \tag{3.54}$$

To leading order, the tails of the propagator have a Gaussian shape, as expected, while the subleading terms indicate a transition from the Gaussian shape to the exponential shape of the stationary distribution.

Emergence and propagation of the kink

As mentioned before, a kink in the minimised action appears when the energy-time relation has multivalued inverse. Since $\theta_-(u_0, u_\tau, \tau, H)$ is a monotonically decreasing function of H (see appendix A.5.1), the kink appears when $\theta_+(u_0, u_\tau, \tau, H)$ develops a crossover from a monotonically increasing shape into a cubic shape [see Figs. 3.14(b) and 3.14(c)]. Hence, the time τ_c when the kink appears and its position u_τ as functions

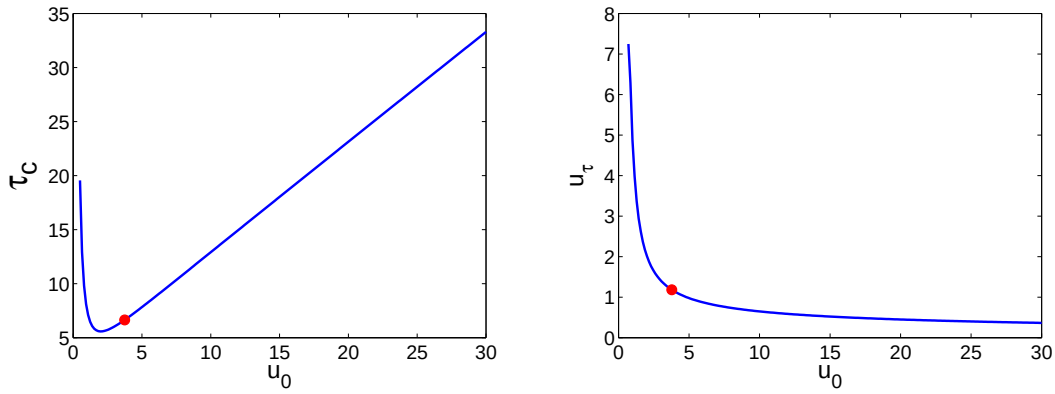

Figure 3.16: Time τ_c and position u_τ for the emergence of the kink in the minimised action as a function of the initial condition u_0 [see Eq. (3.55)]. The closed circle indicates the starting point of the kink for $u_0 = 4$, as in Fig. 3.11(c).

of initial position u_0 are determined by

$$\tau = \theta_+(u_0, u_\tau, H), \qquad \frac{\partial \theta_+}{\partial H} = 0, \qquad \frac{\partial^2 \theta_+}{\partial H^2} = 0. \tag{3.55}$$

Figure 3.16 shows the solution of these equations obtained numerically. For small values of u_0, both the time and the position for the emergence of the kink become large. For large values of u_0, the time becomes large again but the kink appears close to the origin. At an intermediate scale of the size of the regularisation length the time for the occurrence of the kink becomes minimal, and the kink appears close to the initial condition.

After its appearance the kink starts to move with positive velocity [see Fig. 3.15(b) and Fig. 3.11(c)]. We can quantify such a dynamical feature in terms of an asymptotic expansion for large τ and large u_τ, keeping the ratio $c = u_\tau/\tau$ of order $O(1)$. The key to the analysis is the shape of the energy-time relation in such a limit (see Fig. 3.17).

The relation consists of the monotonic lower branch (3.45) determined by θ_- and a cubic shaped upper branch (3.40) determined by θ_+. Depending on the value of τ the action takes its minimum either on the lower branch at an energy H_- which stays of order $O(1)$ or on the upper branch at an energy H_+ which tends to zero in the

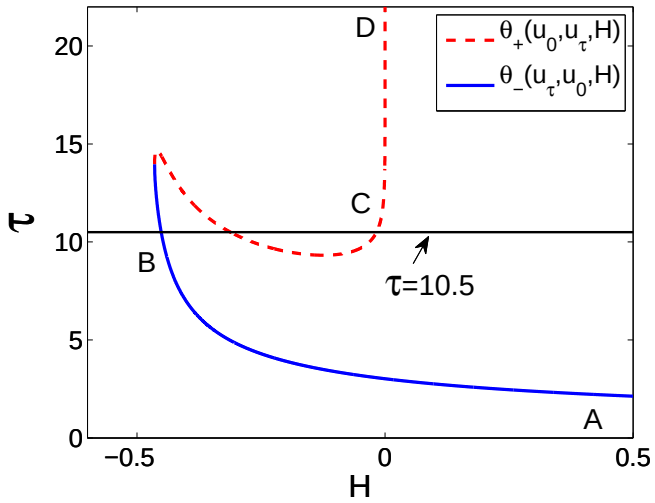

Figure 3.17: Energy time relation, Eqs. (3.45) and (3.40) for $u_0 = 2$ and $u_\tau = 5$. The action takes its minimum on the lower branch AB if $\tau < 10.5$ and on the upper branch CD if $\tau > 10.5$.

asymptotic limit considered here. Hence, Eqs. (3.45) and (3.40) yield

$$\tau = \theta_-(u_\tau, u_0, H_-) = \frac{u_\tau}{\sqrt{1+2H_-}} + O(1), \tag{3.56}$$

$$\tau = \theta_+(u_\tau, u_0, H_+) = \frac{u_\tau - \ln(-2H_+)}{\sqrt{1+2H_+}} + O(1). \tag{3.57}$$

The expression of Eq. (3.56) is easily inverted to obtain

$$1 + 2H_- = (u_\tau/\tau)^2 + O(\tau^{-1}). \tag{3.58}$$

Since we are concerned with $c = u_\tau/\tau = O(1)$, it can be derived from Eq. (3.57) that τH_+ tends to zero in the limit considered here. Hence from Eq. (3.57) we have

$$\ln(-2H_+) = u_\tau - \tau + O(1). \tag{3.59}$$

As for the value of the action along the lower branch Eq. (3.46) yields, if we observe that σ_- [see Eq. (3.38)] is of $O(1)$,

$$S_- = 2(1+H_-)\tau + 2u_\tau + O(1) = \tau\left(\frac{u_\tau}{\tau} + 1\right)^2 + O(1), \tag{3.60}$$

where we have also used the result of Eq. (3.58). For the action along the upper branch (3.44) we have to take into account that σ_+ [see Eq. (3.43)] can be expressed as $-\ln(-2H_+) + O(1)$ so that

$$S_+ = 2\tau + 2u_\tau + 2\ln(-2H_+) + O(1) = 4u_\tau + O(1), \tag{3.61}$$

where we have employed Eq. (3.59) and used the fact that τH_+ tends to zero in the limit considered here. The kink's position is then determined by equating the leading terms of the expressions (3.60) and (3.61), resulting in $u_\tau = \tau$, so that the kink moves with unit speed. Finally, the minimised action to the lowest order reads

$$S = \begin{cases} 4u_\tau & \text{for } u_\tau < \tau, \\ \tau(u_\tau/\tau + 1)^2 & \text{for } u_\tau > \tau, \end{cases} \tag{3.62}$$

which indeed describes the numerical findings shown in Fig. 3.11.

3.4 Summary of chapter

We have studied in this chapter the pure dry friction model (1.8) in order to understand to what extent saddle-point approximations of the path integral representation of the propagator, which is the basis of weak-noise approximations, can be carried out. The advantage of the model that we have considered is that its propagator is known exactly, so that any saddle-point approximations can be compared to the exact result.

For the model (1.8), we have seen that the lowest-order saddle-point approximation yields the correct approximation of the exact propagator in the noise power, and is able to reproduce some features of the propagator for moderate noise power, such as its tail behaviour and its convergence towards the stationary distribution, but not the bimodality of the exact propagator appearing at intermediate times. This bimodality can be recovered by the higher-order approximation. However, the construction of higher-order approximation is plagued by a fundamental singularity of the Jacobian term of the path integral.

To remove this singularity, we have regularised the discontinuity of the SDE with a smooth nonlinear drift involving a small parameter controlling the limit to the piecewise-smooth drift. The price paid for introducing this regularisation is that the two limits, small diffusion and small regularisation, do not commute and that the propagator of

the regularised SDE is no longer known exactly. Nevertheless, we have shown with simulation results that the weak-noise limit of the regularised SDE captures the main features of the piecewise-smooth SDE. In particular, the optimal path structure of the regularised SDE in terms of direct, indirect and intermediate paths is similar to the optimal path structure inferred heuristically for the piecewise-smooth SDE. In addition, the analysis of the regularised SDE justifies the heuristic principles that we have defined and used to perform the saddle-point approximation of the piecewise-smooth SDE. For the regularised SDE considered here, we have finally been able to study the quasi-potential associated with the propagator in a largely analytical way.

Chapter 4

First-passage time of Brownian motion with dry friction

In this chapter, we intend to study the interrelation between noise and discontinuities with respect to FPT problems. The study of FPT problems has a very long tradition with its roots in the first half of the last century by the seminal study of Kramers on chemical kinetics [57] (see also Ref. [47] for an excellent review). Renewed interest in FPT problems has been triggered by studies to characterise large deviation properties, extreme events, and nonequilibrium processes in many particle systems (see, e.g., Refs. [74, 17]). FPT problems are normally non-trivial to solve and a deeper analytical understanding of FPT properties, e.g., the dependence on parameters of the system is often hampered by the lack of analytically tractable model systems. There exists a vast literature about this topic, whereby applications often require the application of numerical tools. Various simple model systems can be handled by analytical means. Among those are the pure diffusion process [61], the Brownian motion with constant drift [54], to some extent the Ornstein-Uhlenbeck process [81, 4] and Bessel processes [39, 31]. We aim at an analytic investigation of the model of Brownian motion with dry friction. In our investigation, we consider the exit from a semi-infinite escape interval (a, ∞) with $a < 0$ as stated in Sec. 2.2 (other interval problems can be analysed analogously). We address the FPT problem for Eq. (1.2) by solving a corresponding Fokker-Planck equation via a spectral decomposition method on the one hand (see Sec. 2.2.1), and by solving a corresponding backward Kolmogorov equation on the other (see Sec. 2.2.2). In Sec. 4.1, we apply these methods to solve the pure dry friction case. This simple example already shows a phase transition phenomenon in the spectrum which is related

to the position of the exit point. Thereafter, in Sec. 4.2 the FPT distribution is derived for the model including viscous friction and external force. There the focus will be on the stick-slip transition and a transition to ballistic exit. Results are summarised in Sec. 4.3.

4.1 Pure dry friction case

Let us first consider the pure dry friction model (1.8). We consider this simplest case as it already shows, somehow counterintuitively, the main phase transition behaviour in the FPT distribution. As a by-product we can also illustrate all the analytical tools in a very transparent setup.

For the pure dry friction case (1.8), we choose $\mu = D = 1$ without loss of generality. Other non-vanishing values are covered by the appropriate rescaling (see appendix A.3.2)

$$u = \mu v/D, \qquad \tau = \mu^2 t/D. \tag{4.1}$$

Hence, in this case Eq. (1.8) can be written in the form (2.12) with

$$\Phi(v) = |v|. \tag{4.2}$$

4.1.1 Analysis of spectrum

We first solve the FPT problem of the model (1.8) by using the spectral decomposition method presented in Sec 2.2.1. The corresponding eigenvalue problem (2.18) consists of a discrete eigenvalue for $\Lambda < 1/4$ and a continuous spectrum for $\Lambda > 1/4$. The details of the derivation are summarised in appendix A.6 for the convenience of the reader.

Case 1: $\Lambda < 1/4$

For $\Lambda < 1/4$, the sole eigenfunction is given by [see Eqs. (A.53) and (A.55)]

$$u_\Lambda(v) = \begin{cases} 2\lambda e^{-(\lambda+1/2)v} & \text{for } v > 0, \\ e^{(\lambda+1/2)v} + (2\lambda - 1)e^{-(\lambda-1/2)v} & \text{for } a < v < 0, \end{cases} \tag{4.3}$$

where $\lambda = \sqrt{1/4 - \Lambda} > 0$. The discrete eigenvalue is determined by the absorbing boundary condition (2.19), which results in

$$e^{2\lambda a} = 1 - 2\lambda \qquad \text{for } \lambda > 0. \tag{4.4}$$

It is obvious that Eq. (4.4) has no real solution for λ in the region $[1/2, \infty)$. Hence, we have $\Lambda > 0$. The solution of Eq. (4.4) for λ is only possible in the region $(0, 1/2)$. Since $e^{2\lambda a}$ is convex as a function of λ and the right hand side of Eq. (4.4) is a straight line, it is easy to verify [see Fig. 4.1(a)] that Eq. (4.4) has no real solution in $(0, 1/2)$ when $a \geqslant -1$ and admits a unique solution, denoted by λ_0, when $a < -1$. The unique eigenvalue $\Lambda_0 = 1/4 - \lambda_0^2$ can be obtained numerically from Eq. (4.4), being a monotonic function of the parameter a [see Fig. 4.1(b)]. As an aside we remark that the solution of Eq. (4.4) can be expressed in terms of the main branch of the Lambert W function [27]. In fact, Eq. (4.4) can be rearranged to be

$$a(1 - 2\lambda)e^{a(1-2\lambda)} = ae^a \qquad \text{for } \lambda > 0. \tag{4.5}$$

Hence, the solution of Eq. (4.4) in terms of the Lambert W function can be expressed as

$$\lambda_0 = 1/2 - W(ae^a)/(2a), \tag{4.6}$$

where $W(z)$ is the main branch of the Lambert W function satisfying $z = W(z)e^{W(z)}$. The other quantities which enter the FPT distribution [see Eq. (2.24)] are easily computed. For the normalisation factor, Eqs. (2.22) and (4.3) yield

$$Z_{\Lambda_0} = \int_a^\infty u_{\Lambda_0}^2(v)e^{|v|}dv = \left[(1/2 - \lambda_0)^2 e^{-2a\lambda_0} - e^{2a\lambda_0}\right]/\lambda_0 - 4\lambda_0 + 2(1 + a). \tag{4.7}$$

The integral of the eigenfunction which enters the FPT distribution [see Eqs. (2.13) and (2.24)] is evaluated as

$$\int_a^\infty u_{\Lambda_0}(v)dv = 2e^{(1/2-\lambda_0)a} - e^{(1/2+\lambda_0)a}/(1/2 + \lambda_0). \tag{4.8}$$

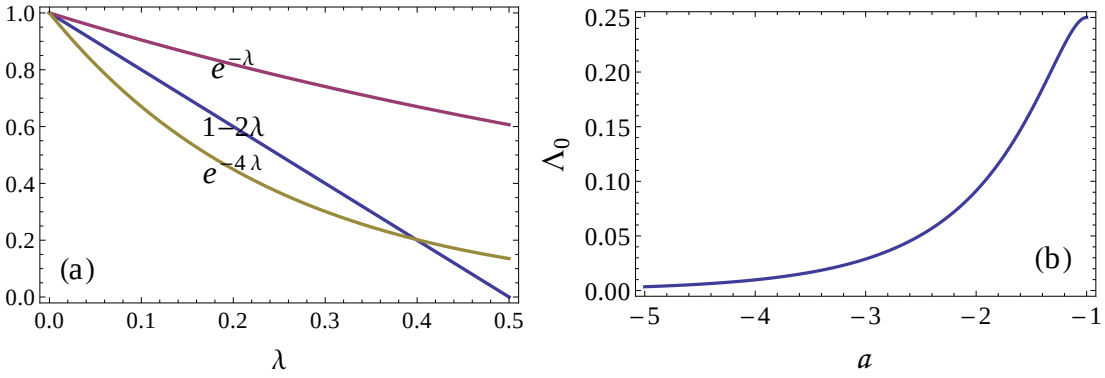

Figure 4.1: (a) Graphical solution of Eq. (4.4) in terms of the convex function $\exp(2a\lambda)$ and the straight line $1-2\lambda$. As examples, $a=-0.5$ and $a=-2$ are used here to illustrate the shapes of the function $\exp(2a\lambda)$ for the two phases $a>-1$ and $a<-1$, respectively. (b) The discrete eigenvalue Λ_0 for $a<-1$. When $a=-1$, the discrete eigenvalue merges with the continuous spectrum $\Lambda \geqslant 1/4$.

Case 2: $\Lambda > 1/4$

For $\Lambda > 1/4$, the eigenfunction can be obtained explicitly as [see Eqs. (A.53) and (A.57)]

$$u_\Lambda(v) = \begin{cases} \sin(\kappa a)\sin(\kappa v)e^{-v/2} + \kappa \sin[\kappa(v-a)]e^{-v/2} & \text{for } v>0, \\ \kappa \sin[\kappa(v-a)]e^{v/2} & \text{for } a<v<0, \end{cases} \tag{4.9}$$

where $\kappa = \sqrt{\Lambda - 1/4} > 0$. Moreover, the normalisation factor in Eq. (2.23) is given by [see Eq. (A.59)]

$$Z_\Lambda = \pi[\kappa^2 + \kappa \sin(2a\kappa) + \sin^2(a\kappa)]/2, \tag{4.10}$$

and the integral over the eigenfunction which enters the FPT distribution [see Eqs. (2.13) and (2.24)] is evaluated as

$$\int_a^\infty u_\Lambda(v)dv = \kappa^2 e^{a/2}/(1/4+\kappa^2). \tag{4.11}$$

Thus, the spectrum consists of a continuous part $\Lambda > 1/4$ and an additional discrete lowest eigenvalue Λ_0 for $a<-1$ which merges with the continuous spectrum at $a=-1$ [see Fig. 4.1(b)]. Hence we expect qualitative changes to appear at such a critical value.

4.1.2 FPT distribution

By using Eqs. (2.13) and (2.24) we obtain the FPT distribution as follows

$$f(T,v_0) = \chi_{\{a\leqslant -1\}}\Lambda_0 u_{\Lambda_0}(v_0)e^{|v_0|-\Lambda_0 T}\int_a^\infty u_{\Lambda_0}(v)dv/Z_{\Lambda_0} \\ +\frac{2}{\pi}e^{|v_0|-T/4+a/2}\int_0^\infty \kappa^2 u_\Lambda(v_0)e^{-\kappa^2 T}/[\kappa^2+\kappa\sin(2a\kappa)+\sin^2(a\kappa)]d\kappa, \quad (4.12)$$

where $\chi_{\{a\leqslant -1\}}$ denotes the indicator function of the set $\{a\leqslant -1\}$, $u_{\Lambda_0}(v_0)$ the eigenfunction of the discrete eigenvalue (4.3), and $u_\Lambda(v_0)$ the eigenfunction of the continuous part of the spectrum (4.9). The normalisation Z_{Λ_0} and the integral $\int_a^\infty u_{\Lambda_0}(v)dv$ are given by Eqs. (4.7) and (4.8), respectively. In the trivial case $a=0$ the discontinuity does not enter the FPT problem and the pure dry friction model is equivalent to that of the one-dimensional Brownian motion with a constant drift [54]. In such a case, the first term in Eq. (4.12) does not contribute and the integral can be evaluated in closed analytic form to yield

$$f(T,v_0) = \frac{2}{\pi}e^{v_0/2-T/4}\int_0^\infty \kappa\sin(\kappa v_0)e^{-\kappa^2 T}d\kappa \\ = \frac{1}{2\sqrt{\pi}}\frac{v_0}{T^{3/2}}e^{-(T-v_0)^2/(4T)} \qquad \text{for } v_0>0, \quad (4.13)$$

a result which is consistent with Refs. [54, 62]. Apart from this trivial case it seems to be difficult to obtain a closed analytic expression from the representation (4.12).

Certainly the FPT distribution changes qualitatively at $a=-1$ when the contribution in Eq. (4.12) coming from the discrete eigenvalue comes into play. That can be demonstrated by focussing on the tail behaviour of the distribution which in itself is of interest when rare events are of interest. First of all it is obvious that for $a<-1$ the first term in Eq. (4.12) determines the decay which is plainly exponential $\exp(-\Lambda_0 T)$. For $a\geqslant -1$, the first term in Eq. (4.12) vanishes, as the coefficient of the characteristic function vanishes at $a=-1$, and the tail is determined by evaluating the Laplace-type integral in the second term. If we have a closer look at the kernel entering the Laplace-type integral:

$$\rho(\kappa,a) = \kappa^2 u_\Lambda(v_0)/[\kappa^2+\kappa\sin(2a\kappa)+\sin^2(a\kappa)], \quad (4.14)$$

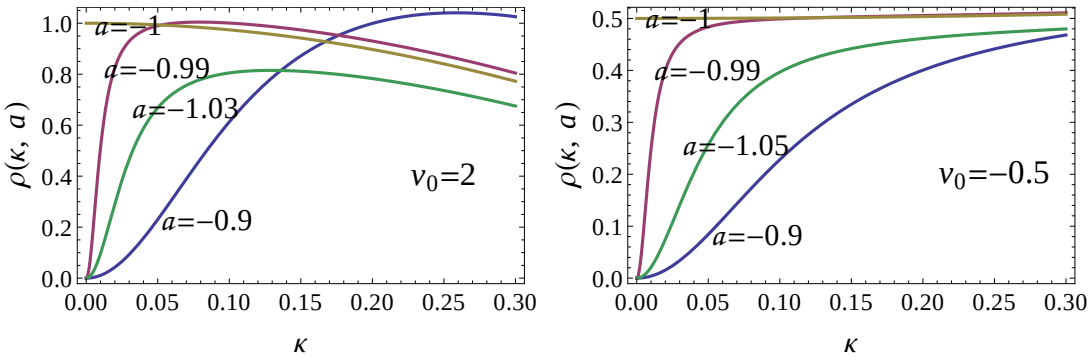

Figure 4.2: Kernel $\rho(\kappa, a)$ [see Eq. (4.14)] appearing in the spectral decomposition (4.12) for two different values of v_0 and various values of the exit point a. Here $u_\Lambda(v_0)$ is given by Eq. (4.9).

it is evident that for $a > -1$ the properties

$$\lim_{\kappa\to 0} \rho(\kappa, a) = 0, \qquad \lim_{\kappa\to 0} \partial_\kappa \rho(\kappa, a) = 0, \qquad \lim_{\kappa\to 0} \partial_\kappa^2 \rho(\kappa, a) \neq 0 \tag{4.15}$$

hold (see Fig. 4.2). Hence, it is straightforward to evaluate the Laplace-type integral to obtain a decay as $T^{-3/2}\exp(-T/4)$ for $a > -1$. For the critical value $a = -1$ the situation differs as

$$\lim_{\kappa\to 0} \rho(\kappa, -1) = \begin{cases} 1 & \text{for } v_0 > 0, \\ 1 + v_0 & \text{for } -1 < v_0 < 0 \end{cases} \tag{4.16}$$

holds. Here the Laplace method yields $T^{-1/2}e^{-T/4}$ for $a = -1$. To summarise, in the long time limit we have

$$f(T, v_0) \sim \begin{cases} e^{-\Lambda_0 T} & \text{for } a < -1, \\ T^{-1/2}e^{-T/4} & \text{for } a = -1, \\ T^{-3/2}e^{-T/4} & \text{for } a > -1. \end{cases} \tag{4.17}$$

To obtain closed analytic expressions for FPT distributions we alternatively can resort to the Laplace transform of the backward Kolmogorov equation (see subsection 2.2.2). In this pure dry friction case Eq. (2.33) reads [see Eq. (4.2)]

$$\frac{\partial^2}{\partial v_0^2}\tilde{f}(s, v_0) - \sigma(v_0)\frac{\partial}{\partial v_0}\tilde{f}(s, v_0) - s\tilde{f}(s, v_0) = 0, \tag{4.18}$$

where the solution has to satisfy the boundary conditions (2.34) and (2.35) as well as the matching condition (2.36) at $v_0 = 0$. It is in fact rather straightforward to compute the solution of this second order problem and we end up with

$$\tilde{f}(s, v_0) = \begin{cases} \exp\left\{[\sqrt{1+4s}(a - v_0) + a + v_0]/2\right\} \sqrt{1+4s}/\theta(s, a) & \text{for } v_0 > 0, \\ \exp\left[(1 + \sqrt{1+4s})(a - v_0)/2\right] \theta(s, v_0)/\theta(s, a) & \text{for } a < v_0 < 0, \end{cases} \tag{4.19}$$

where we have introduced the abbreviation

$$\theta(s, a) = e^{a\sqrt{1+4s}} + \sqrt{1+4s} - 1 \tag{4.20}$$

for the contribution appearing mainly in the denominator. Clearly Eq. (4.19) has a branch cut for $s < -1/4$ which relates to the continuous spectrum found previously. In addition the condition $\theta(s, a) = 0$, which is equivalent to Eq. (4.4), determines a pole for $a < -1$. Hence, when $a < -1$, the simple pole dominates the FPT distribution in the tail to yield an exponential decay [93]. Overall, the analytical structure of the Laplace transform reflects the spectral properties mentioned previously.

In general the inverse Laplace transform of Eq. (4.19) does not seem to be available in closed analytic form. Only in the trivial case $a = 0$, Eq. (4.19) with a simple form

$$\tilde{f}(s, v_0) = e^{(1-\sqrt{1+4s})v_0/2} \qquad \text{for } v_0 > 0, \tag{4.21}$$

as before can be handled with ease resulting in Eq. (4.13) (e.g., using the table of Laplace transforms in Ref. [3]). For the other cases we resort to the so-called Talbot method [84, 1, 2] to compute the distribution of the FPT in the time domain[1]. Figure 4.3 shows that the expressions (4.12) and (4.19) give identical results, as expected. In addition, evaluations of those expressions confirm as well the asymptotic decay given by Eq. (4.17) (see Fig. 4.4).

The closed form of the characteristic function (4.19) allows us to obtain easily the moments of FPT via Eq. (2.37). For the first moment, i.e., for the mean first-passage time (MFPT) we have

$$\langle T \rangle = \begin{cases} 2e^{-a} + a + v_0 - 2 & \text{for } v_0 > 0, \\ 2e^{-a} + a - v_0 - 2e^{-v_0} & \text{for } a < v_0 < 0. \end{cases} \tag{4.22}$$

[1] A Mathematica implementation of this method is available at http://library.wolfram.com/infocenter/MathSource/5026/.

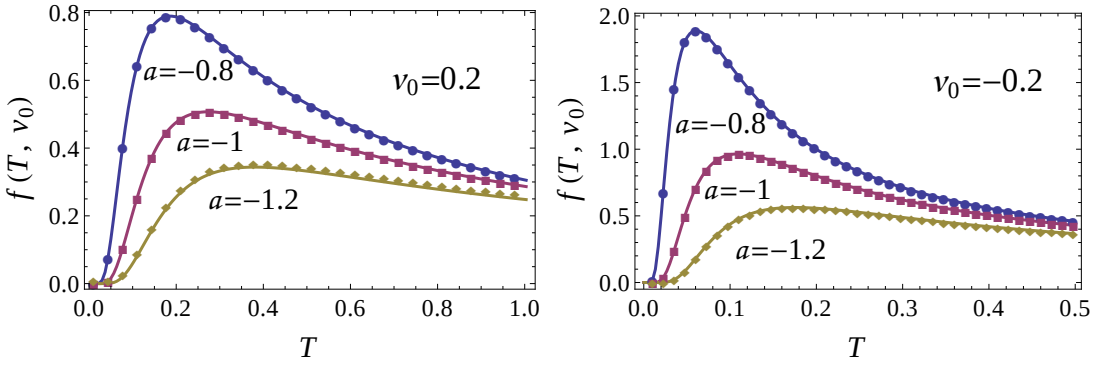

Figure 4.3: FPT distribution of the pure dry friction case [see Eq. (4.2)] for two values of initial velocity, $v_0 = 2$ and $v_0 = -0.2$, and different escape ranges. Lines correspond to a numerical inversion of Eq. (4.19), and points to the evaluation of Eq. (4.12).

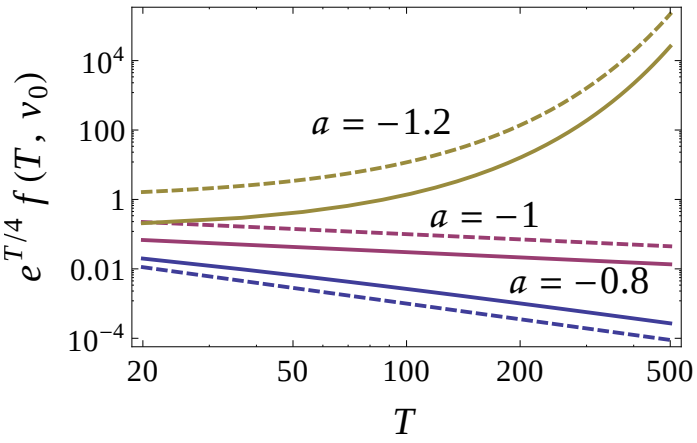

Figure 4.4: Comparison of the FPT distribution obtained from Eq. (4.12) (solid) with the asymptotic result (4.17) (dashed) for the initial velocity $v_0 = -0.2$ and different escape ranges. Data are plotted on a doubly logarithmic scale to uncover the power-law corrections to the leading exponential behaviour.

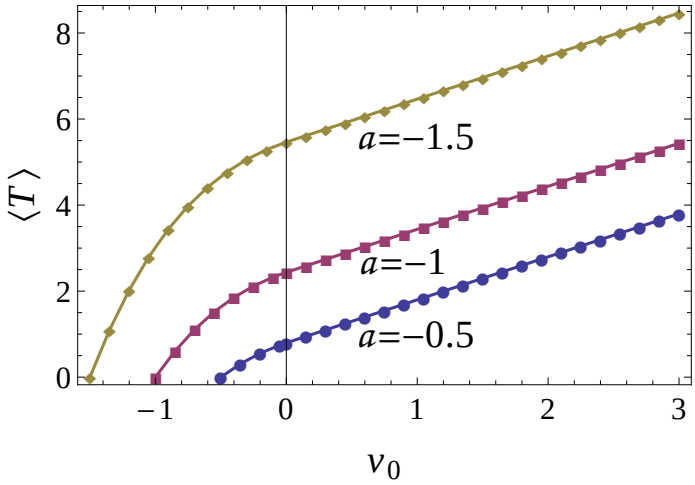

Figure 4.5: MFPT $\langle T \rangle$ for different escape ranges. Lines correspond to the analytical result (4.22), and points to a numerical evaluation of the first moment by using the spectral representation (4.12).

The first moment clearly displays a transition when the initial condition changes sign (see also Fig. 4.5). For $v_0 > 0$ the MFPT depends linearly on the initial velocity. No particular feature is visible at the transition at $a = -1$, as a change in the tail behaviour has no impact on the low-order moments of the distribution.

4.2 Full model

In this section, we consider the full model (1.2) and set $\gamma = D = 1$ without loss of generality. Other cases can be covered by using the appropriate rescaling (see appendix A.3.3)

$$u = \sqrt{\gamma/D}\, v, \qquad \tau = \gamma t. \tag{4.23}$$

Thus, the model (1.2) can be written as Eq. (2.12) with

$$\Phi(v) = (|v| + \mu)^2/2 - bv. \tag{4.24}$$

4.2.1 Analysis of spectrum

In the spectral decomposition method (see Sec. 2.2.1), the corresponding eigenvalue problem (2.18) with potential (4.24) can be solved by using parabolic cylinder functions

(see appendix A.9), which are denoted by $D_\nu(z)$. For the convenience of the reader we summarise the details of the derivation in appendix A.7.

In this case, the eigenvalues are discrete and are determined by the characteristic equation [see Eq. (A.69)]

$$\begin{aligned}\bar{\theta}(\Lambda,a,\mu,b) &= \Gamma(1-\Lambda)\{[D_\Lambda(\mu+b)D_{\Lambda-1}(\mu-b)+D_\Lambda(\mu-b)D_{\Lambda-1}(\mu+b)]D_\Lambda(a-\mu-b)\\ &\quad -[D_\Lambda(-\mu-b)D_{\Lambda-1}(\mu-b)-D_\Lambda(\mu-b)D_{\Lambda-1}(-\mu-b)]D_\Lambda(-a+\mu+b)\}\\ &= 0. \end{aligned} \tag{4.25}$$

In particular, for $\mu = 0$ the model considered here reduces to the Ornstein-Uhlenbeck process and if one uses the property (A.85) the characteristic equation (4.25) can be simplified as

$$D_\Lambda(a-b) = 0, \tag{4.26}$$

which agrees with the standard result of the Ornstein-Uhlenbeck process (see, e.g., Ref. [81]).

To link the current result with the previous section let us first consider the special case without bias ($b = 0$). Intuitively, we expect that if the dry friction term dominates the viscous friction force then the particle will behave like the one subjected to dry friction only. Hence the spectrum obtained from Eq. (4.25) for large values of μ should resemble the spectrum described in the previous section [see, e.g., Fig. 4.1(b)]. In particular, it means that a large gap should develop between the lowest eigenvalue and a quasi-continuous part for small negative values of a. For comparison of the models with and without viscous friction [see Eqs. (4.2) and (4.24)] we observe that the rescaling

$$u = \mu v, \qquad \tau = \mu^2 t \tag{4.27}$$

transforms the SDE with dry and viscous friction to the model with dry friction and a small viscous part of $O(1/\mu^2)$ which vanishes in the limit $\mu \to \infty$ (see appendix A.3.3), i.e.,

$$\dot{u}(\tau) = -\sigma(u(\tau)) - u(\tau)/\mu^2 + \xi(\tau). \tag{4.28}$$

Thus, to compare the eigenvalues obtained from the characteristic equation (4.25) with the spectrum computed in the previous section we rescale velocities by μ and eigenvalues by $1/\mu^2$. Then, indeed numerical evaluation of Eq. (4.25) confirms what one expects intuitively (see Fig. 4.6). The eigenvalues as a function of the exit position a develop

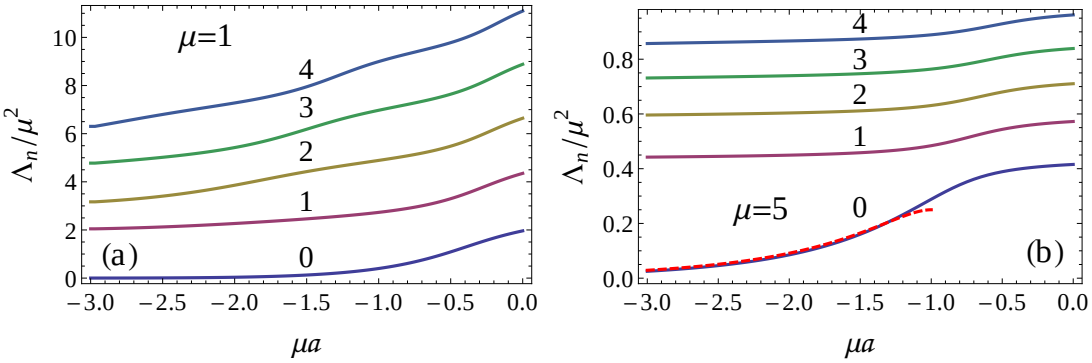

Figure 4.6: First five rescaled eigenvalues Λ_n/μ^2 for the full model without bias ($b = 0$) as a function of the rescaled exit point μa for two different values of the dry friction μ, according to Eq. (4.25). The dashed line in (b) depicts the discrete branch of the model with dry friction only [see Fig. 4.1(b)]

.

a gap if μ is sufficiently large, even though the transition is smoothened by the finite viscous friction. If dry and viscous friction become comparable, i.e., if μ becomes too small such a feature is going to disappear.

If we impose a force on the particle the finite bias will cause a stick-slip transition at $|b| = \mu$ where the minimum of the potential (4.24), i.e., the deterministic stationary state, changes from vanishing to finite velocity [see Eq. (4.24) and Fig. 4.7]. The characteristics of such a transition are also reflected by the eigenvalue spectrum (see Fig. 4.8). For small value of the bias, i.e., $|b| < \mu$, a case which we will call for brevity the dry phase, a substantial spectral gap appears between the lowest and the subleading eigenvalues. This gap shrinks when the transition at $|b| = \mu$ is approached. The spectral gap corresponds to a fast decay of velocity correlations in the system with small bias (see Ref. [88]). If the bias is sufficiently negative, i.e., $b < -\mu$, a case which we will call the wet phase, the potential (4.24) develops a quadratic minimum (see Fig. 4.7) and the spectrum resembles that of the Ornstein-Uhlenbeck process. As with regards to the exit time problem a second transition will occur when on decreasing the force further the quadratic minimum of the potential moves beyond the exit point at $b = -\mu + a$ (Fig. 4.7). Then the exit of the region occurs in a purely ballistic way which decreases the exit time considerably. Hence that transition is related to an increase of the lowest eigenvalue (see Fig. 4.8). These two transitions are clearly visible if the diffusion is sufficiently small, i.e., μ sufficiently large. But they become obscured by noise for large diffusion, i.e., if μ becomes too small.

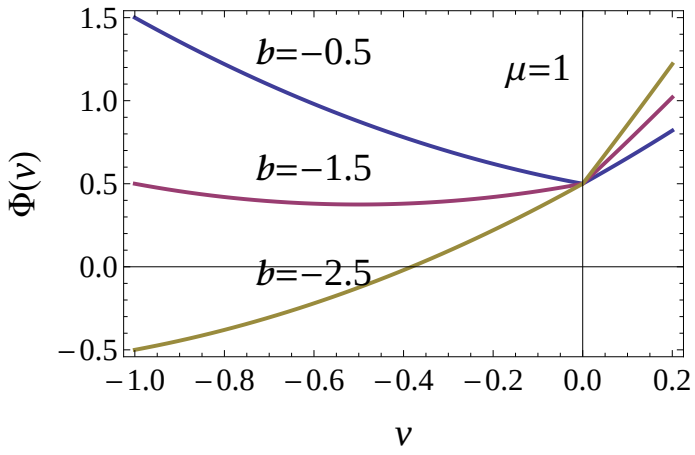

Figure 4.7: Potential (4.24) for $\mu = 1$ and three different values of the bias b.

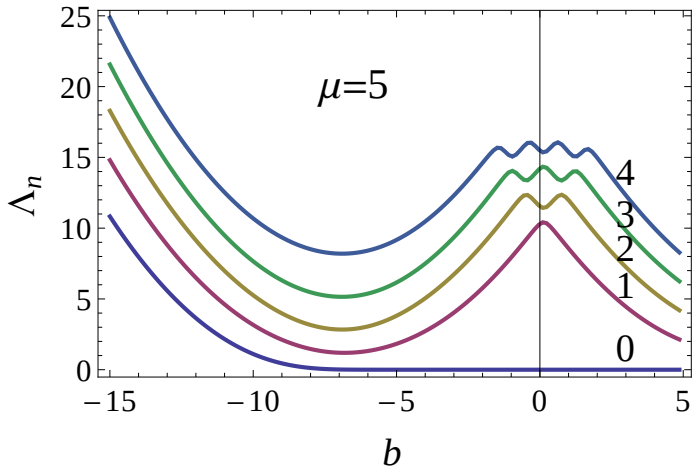

Figure 4.8: First five eigenvalues of the full model as a function of the bias b for exit point at $a = -5$ and dry friction coefficient $\mu = 5$, obtained from Eq. (4.25). The stick-slip transition, i.e., the narrowing of the spectral gap at $b = \pm\mu = \pm 5$, and the transition to a ballistic exit at $b = -\mu + a = -10$ are clearly visible.

4.2.2 FPT distribution

As we have access to the entire spectrum we can derive from Eqs. (2.13) and (2.24) the FPT distribution

$$f(T,v_0) = e^{\Phi(v_0)} \sum_{\Lambda} \Lambda u_\Lambda(v_0) e^{-\Lambda T} \int_a^\infty u_\Lambda(v) dv / Z_\Lambda, \tag{4.29}$$

where the sum is taken over all the discrete eigenvalues [see Eq. (4.25)], $u_\Lambda(v_0)$ refers to the eigenfunction given by Eq. (A.63), the integral $\int_a^\infty u_\Lambda(v)dv$ is stated in Eq. (A.70) and the normalisation factor Z_Λ is given by Eq. (A.72). When $\mu = 0$, the problem considered here reduces to the Ornstein-Uhlenbeck case. In this case, the FPT distribution simplifies considerably and reads

$$f(T,v_0) = \sum_{\Lambda} \Lambda e^{-\Lambda T} \frac{e^{(v_0-b)^2/4} D_\Lambda(v_0-b) D_{\Lambda-1}(a-b)}{e^{(a-b)^2/4} D_{\Lambda+1}(a-b) \partial_\Lambda D_\Lambda(a-b)}, \tag{4.30}$$

where the sum is taken over the discrete eigenvalues that satisfy Eq. (4.26). From Eq. (4.29), it is straightforward to evaluate the shape of the distribution function (see, e.g., Fig. 4.9). While it seems to be difficult to obtain a closed analytic expression for this distribution we may pursue the approach used in the previous section and focus on the Laplace transform. In fact, Eq. (2.33) tells us that [see also Eq. (4.24)]

$$\frac{\partial^2}{\partial v_0^2} \tilde{f}(s,v_0) - [v_0 + \mu\sigma(v_0) - b] \frac{\partial}{\partial v_0} \tilde{f}(s,v_0) - s\tilde{f}(s,v_0) = 0, \tag{4.31}$$

where the Laplace transform $\tilde{f}(s,v_0)$ has to obey the boundary conditions (2.34) and (2.35) as well as the matching condition (2.36). Solving Eq. (4.31) is rather straightforward, as the boundary value problem for the Laplace transform is the formally adjoint of the eigenvalue problem [see Eqs. (A.61) and (A.62)]. It is well known and easy to confirm that the solution of the adjoint problem can be written in terms of the analytic expression for the eigenfunction (see Ref. [36]) if we multiply the eigenfunction with an exponential factor $\exp[\Phi(v_0)]$ containing the potential (4.24). Thus, the solution of Eq. (4.31) can be written down directly as

$$\tilde{f}(s,v_0) = \frac{e^{(a-\mu-b)^2/4 - \Phi(a)}}{\bar{\theta}(-s,a,\mu,b)} e^{\Phi(v_0)} u_{-s}(v_0) \qquad \text{for } v_0 > a, \tag{4.32}$$

where $u_{-s}(v_0)$ refers to Eq. (A.63), and the additional normalisation factor containing the characteristic function $\bar{\theta}$ [see Eq. (4.25)] is obtained by using the boundary condition (2.34). Obviously the poles of the Laplace transform are determined by the characteristic equation (4.25) and thus reflect the spectral structure discussed previously. In addition, the largest simple pole determines the exponential tail of the FPT distribution $f(T, v_0)$.

As stated before, for $\mu = 0$ the model investigated here corresponds to the exit time problem of the Ornstein-Uhlenbeck process, which has been paid much attention to in the past (see, e.g., Refs. [4, 91, 81, 29, 14, 58]). In this case Eq. (4.32) simplifies considerably and reads [see Eqs. (4.25) and (A.63)]

$$\tilde{f}(s, v_0) = \frac{e^{(v_0-b)^2/4} D_{-s}(v_0 - b)}{e^{(a-b)^2/4} D_{-s}(a - b)} \qquad \text{for } v_0 > a, \tag{4.33}$$

which is consistent with the standard result stated, e.g., in Ref. [81].

The analytic expression (4.29) or (4.32) now allows us to discuss the dependence of the exit time problem on the initial velocity v_0. Both expressions, if properly evaluated, give of course identical results (see Fig. 4.9). Here we are going to pay particular attention to the impact of the discontinuity appearing at the origin. Depending on the sign of the initial velocity the particle has to pass the discontinuity at $v = 0$ before exiting at $a < 0$. Thus, a qualitative change of the FPT distribution is expected depending on the sign of v_0. In fact, such a feature is already visible from Eq. (4.32), as different analytical branches of the eigenfunction (A.63) come into play if v_0 changes sign. The dependence on v_0 is still smooth but not differentiable of higher order. The FPT distribution for small positive and small negative values of v_0 look distinctively different, as shown in Fig. 4.9. For $v_0 > 0$, the particle has to pass through $v = 0$ before exiting and thus sticks at the origin at least if the bias is small, causing larger exit times. Thus, the distribution overall is shifted to the right, compared to the case $v_0 < 0$.

The just mentioned phenomenon can be better illustrated by looking at the MFPT which can be obtained in closed analytic form via Eqs. (2.37) and (4.32). While the analytic expression can be written down we just refer to the graphical evaluation of the expressions (see Fig. 4.10). For small bias, $|b| < \mu$, i.e., in the dry phase, there is a possibility that the particle sticks at the origin which will impact on the MFPT. If the particle starts at $v_0 < 0$ it has less chance to stick at the origin when v_0 becomes smaller, and the change of the MFPT with regards to v_0 becomes fairly large. On the contrary, if we choose a positive initial velocity $v_0 > 0$, the particle has always to

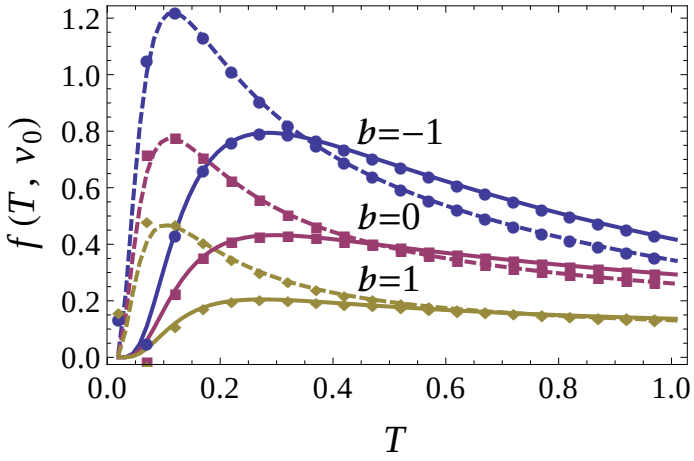

Figure 4.9: Distribution of the FPT for $\mu = 1$, $a = -1$, two values of initial velocity, $v_0 = 0.2$ (solid) and $v_0 = -0.2$ (dashed), and different values of the bias b. Lines correspond to a numerical inversion of the Laplace transform (4.32), and points to the evaluation of Eq. (4.29) taking the first 20 modes into account. A larger number of modes would be required to reproduce the exact result for very small values of t.

pass $v = 0$ before exiting at $a < 0$. Thus, no huge variation of the MFPT with v_0 is detected. If we decrease the bias and enter the wet phase $b < -\mu$, the particle does not stick any more and the just mentioned feature almost disappears. This scenario is much more pronounced if we look at the first derivative $\partial_{v_0}\langle T\rangle$ [see Fig. 4.10(b)]. Like the distribution function itself the MFPT is continuously differentiable, but loses analyticity due to the discontinuity at $v_0 = 0$. A kink can be seen clearly at the origin for small bias $|b| < \mu$, which separates the two different regions of the MFPT for negative and positive initial velocities. This feature is suppressed if we decrease the bias and finally enter the wet phase with $b < -\mu$, where the kink almost disappears.

4.3 Summary of chapter

In this chapter we have studied the FPT problem of Brownian motion with dry and viscous friction, which can be largely solved by analytical means. This is one of the few models for which the FPT distribution can be obtained analytically either by solving the Fokker-Planck equation via a spectral decomposition method or by solving the backward Kolmogorov equation in the Laplace space. While the first method gives more insight into the underlying dynamical mechanisms through the additional spectral information,

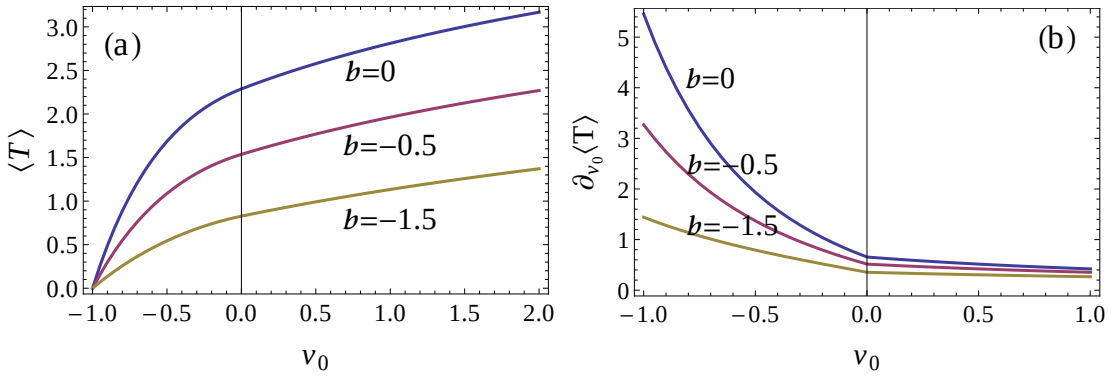

Figure 4.10: (a) MFPT $\langle T \rangle$ as a function of the initial value v_0 for $\mu = 1$, exit condition $a = -1$, and different values of the bias, covering the dry phase $|b| < \mu$ as well as the wet phase $b < -\mu$. (b) First derivative of the MFPT with respect to the initial value for the same data.

the second is able to deliver closed analytic expressions for the MFPT.

The simplest case, where only dry friction acts on the particle, already shows one of the main features, a phase transition phenomenon in the spectrum which is related to the position of the exit point. A unique discrete eigenvalue links up with the continuous part of the spectrum at a critical size of the exit region. Such a transition translates into different asymptotic properties of the FPT distribution. The signature of this transition persists if the viscous friction and the external bias are taken into account, even though the transition is blurred by the finite diffusion. In the full model two new features occur, i.e., a stick-slip transition and a transition to a ballistic exit of the particle. All three transitions are clearly visible in the discrete spectrum of the full model, especially at low diffusion, signalling the different rates of asymptotic decay of the FPT distribution. As an aside, the analysis of the full model covers as special cases the Ornstein-Uhlenbeck process on the one hand, and the previously discussed dry friction case on the other.

Chapter 5

Maximum velocity till the first-passage time

In this chapter, we aim to derive the exact solution of the distribution of the maximum velocity (MVD) till the FPT (see Sec. 2.3) for the dry friction model (1.2). The maximum velocity problem till the FPT is one of the extreme value problems that have many applications, such as in queueing theory [61], fluctuating interfaces [64, 64] and networks [45]. Here the exit range of the FPT problem is chosen to be (a, ∞) with $a < 0$, which is the same as that in chapter 4. This chapter is arranged as follows. In Sec. 5.1, we present the exact solution of the MVD of the pure dry friction case to illustrate all the techniques encountered in the piecewise-smooth systems. Then in Sec. 5.2, we solve the corresponding problem for the full model. Finally, we summarise this chapter in Sec. 5.3.

5.1 Pure dry friction case

For the pure dry friction model (1.8), as stated in Sec. 4.1 we can specialise to consider $\mu = D = 1$, i.e., Eq. (2.12) with the potential $\Phi(v) = |v|$ without loss of generality (see also appendix A.3.2). In this case, Eq. (2.45) reads

$$\frac{\partial^2}{\partial v_0^2} Pr(v < v_m | v_0) - \sigma(v_0) \frac{\partial}{\partial v_0} Pr(v < v_m | v_0) = 0 \qquad \text{for } v_m > a. \tag{5.1}$$

Solving this equation separately for $v_0 > 0$ and $v_0 < 0$ results in

$$Pr(v < v_m|v_0) = \begin{cases} Ae^{v_0} + B & \text{for } v_0 > 0, \\ \bar{A}e^{-v_0} + \bar{B} & \text{for } v_0 < 0. \end{cases} \tag{5.2}$$

Here the four coefficients A, B, $\bar{A}$ and $\bar{B}$ are determined by the boundary conditions (2.46) and (2.47), and the matching conditions (2.48) and (2.49). In this case, Eqs. (2.46), (2.48) and (2.49) yield

$$\bar{A}e^{-a} + \bar{B} = 1, \tag{5.3}$$
$$A + B = \bar{A} + \bar{B}, \tag{5.4}$$
$$A = -\bar{A}. \tag{5.5}$$

For the condition (2.47) we have to distinguish the sign of v_m and obtain

$$Ae^{v_m} + B = 0 \qquad \text{for } v_m > 0, \tag{5.6}$$
$$\bar{A}e^{-v_m} + \bar{B} = 0 \qquad \text{for } v_m < 0. \tag{5.7}$$

Therefore, for $v_m > 0$ the coefficients in Eq. (5.2) are determined by Eqs. (5.3)–(5.6) and are easily evaluated as

$$A = \frac{1}{2 - e^{v_m} - e^{-a}}, \tag{5.8}$$
$$B = \frac{e^{v_m}}{e^{v_m} + e^{-a} - 2}, \tag{5.9}$$
$$\bar{A} = \frac{1}{e^{v_m} + e^{-a} - 2}, \tag{5.10}$$
$$\bar{B} = \frac{e^{v_m} - 2}{e^{v_m} + e^{-a} - 2}. \tag{5.11}$$

For $v_m < 0$ the coefficients are determined by Eqs. (5.3)–(5.5) and (5.7) yielding

$$A = \frac{e^{v_m}}{1 - e^{v_m - a}}, \tag{5.12}$$
$$B = \frac{2e^{v_m} - 1}{e^{v_m - a} - 1}, \tag{5.13}$$
$$\bar{A} = \frac{e^{v_m}}{e^{v_m - a} - 1}, \tag{5.14}$$
$$\bar{B} = \frac{1}{1 - e^{v_m - a}}. \tag{5.15}$$

In summary, since the solution (5.2) depends on the sign of v_0 and the boundary condition (2.47) depends on the sign of v_m, we have first to distinguish the two cases $v_0 > 0$ and $v_0 < 0$. For the case $v_0 > 0$ we have $v_m > 0$ as $v_m \geqslant v_0$, whereas for the case $v_0 < 0$ we have further to distinguish the two domains $v_m > 0$ and $v_m < 0$.

5.1.1 Case 1: $v_0 > 0$

In this case, v_m can only be positive. So it follows from Eqs. (5.2), (5.8) and (5.9) that

$$Pr(v < v_m|v_0) = \frac{e^{v_m} - e^{v_0}}{e^{v_m} + e^{-a} - 2} \qquad \text{for } v_m > v_0. \tag{5.16}$$

Then differentiating Eq. (5.16) with respect to v_m yields the distribution of the maximum velocity

$$p(v_m|v_0) = \frac{e^{v_m}(e^{v_0} + e^{-a} - 2)}{(e^{v_m} + e^{-a} - 2)^2} \qquad \text{for } v_m > v_0. \tag{5.17}$$

Since

$$\frac{\partial}{\partial v_m} p(v_m|v_0) = \frac{e^{v_m}(e^{v_0} + e^{-a} - 2)(e^{-a} - 2 - e^{v_m})}{(e^{v_m} + e^{-a} - 2)^3} \qquad \text{for } v_m > v_0, \tag{5.18}$$

it is easy to check that the distribution $p(v_m|v_0)$ is monotonically decreasing for $a_0 < a < 0$ and has a quadratic maximum for $a < a_0$ in the defined region $v_m > v_0$ (see Fig. 5.1), where

$$a_0 = -\ln(e^{v_0} + 2) < 0. \tag{5.19}$$

This quadratic maximum is attained at the point $v_m = \ln(e^{-a} - 2)$ with the value

$$p(\ln(e^{-a} - 2)|v_0) = \frac{e^{v_0} + e^{-a} - 2}{4(e^{-a} - 2)} \qquad \text{for } a < a_0. \tag{5.20}$$

Since for fixed v_0, on average the particle has to spend more time in the region (a, ∞) for smaller a and hence has more chance to have large velocities before exit (see Fig. 5.1). In addition, in the asymptotic limit $v_m \to \infty$, we have

$$p(v_m|v_0) = e^{-v_m}(e^{v_0} + e^{-a} - 2) + O(e^{-2v_m}), \tag{5.21}$$

which indicates that the MVD decays exponentially.

Finally, we remark that in the trivial case $a = 0$ the problem considered here reduces

to that of the Brownian motion with constant drift [54] as the discontinuity does not enter the FPT problem (see also Sec. 4.1).

5.1.2 Case 2: $a < v_0 < 0$

In this case, v_m can be negative or positive. For negative v_m, the coefficients $\bar{A}$ and $\bar{B}$ are determined by Eqs. (5.14) and (5.15), whereas for positive v_m the coefficients are determined by Eqs. (5.10) and (5.11). Hence from Eq. (5.2) we have the probability

$$Pr(v < v_m|v_0) = \begin{cases} (e^{v_m - v_0} - 1)/(e^{v_m - a} - 1) & \text{for } v_0 < v_m < 0, \\ (e^{v_m} + e^{-v_0} - 2)/(e^{v_m} + e^{-a} - 2) & \text{for } v_m > 0. \end{cases} \tag{5.22}$$

Then differentiating Eq. (5.22) with respect to v_m yields the distribution of the maximum velocity

$$p(v_m|v_0) = \begin{cases} e^{v_m}(e^{-a} - e^{-v_0})/(e^{v_m} - e^{a})^2 & \text{for } v_0 < v_m < 0, \\ e^{v_m}(e^{-a} - e^{-v_0})/(e^{v_m} + e^{-a} - 2)^2 & \text{for } v_m > 0. \end{cases} \tag{5.23}$$

Since

$$\frac{\partial p(v_m|v_0)}{\partial v_m} = \begin{cases} e^{v_m - a}(1 - e^{v_0 - a})(e^{v_m - a} + 1)/(e^{v_m - a} - 1)^3 & \text{for } v_0 < v_m < 0, \\ e^{v_m - v_0}(e^{v_0 - a} - 1)(e^{-a} - 2 - e^{v_m})/(e^{v_m} + e^{-a} - 2)^3 & \text{for } v_m > 0, \end{cases} \tag{5.24}$$

it is easy to see that the distribution $p(v_m|v_0)$ in this case is a monotonically decreasing function of v_m in the region $v_0 < v_m < 0$. Whereas in the region $v_m > 0$, the distribution $p(v_m|v_0)$ is monotonically decreasing for $a > -\ln(3)$ and has a quadratic maximum for $a < -\ln(3)$ (see Fig. 5.2). This maximum is attained at $v_m = \ln(e^{-a} - 2)$ with the value

$$p(\ln(e^{-a} - 2)|v_0) = \frac{e^{-a} - e^{-v_0}}{4(e^{-a} - 2)} \qquad \text{for } a < -\ln(3). \tag{5.25}$$

As shown in Fig. 5.2, the distribution (5.23) is non-smooth at $v_m = 0$. As we know, the non-smooth point at $v_m = 0$ is caused by the dry friction, which leads to different solutions of Eq. (5.1) when v_0 changes sign and finally results in different solutions of the distribution for different signs of v_m due to the boundary condition (2.47). In addition, for fixed value of v_0, the Brownian particle has more chance to attain large maximum velocities for smaller a, as explained in the case $v_0 > 0$ after Eq. (5.20).

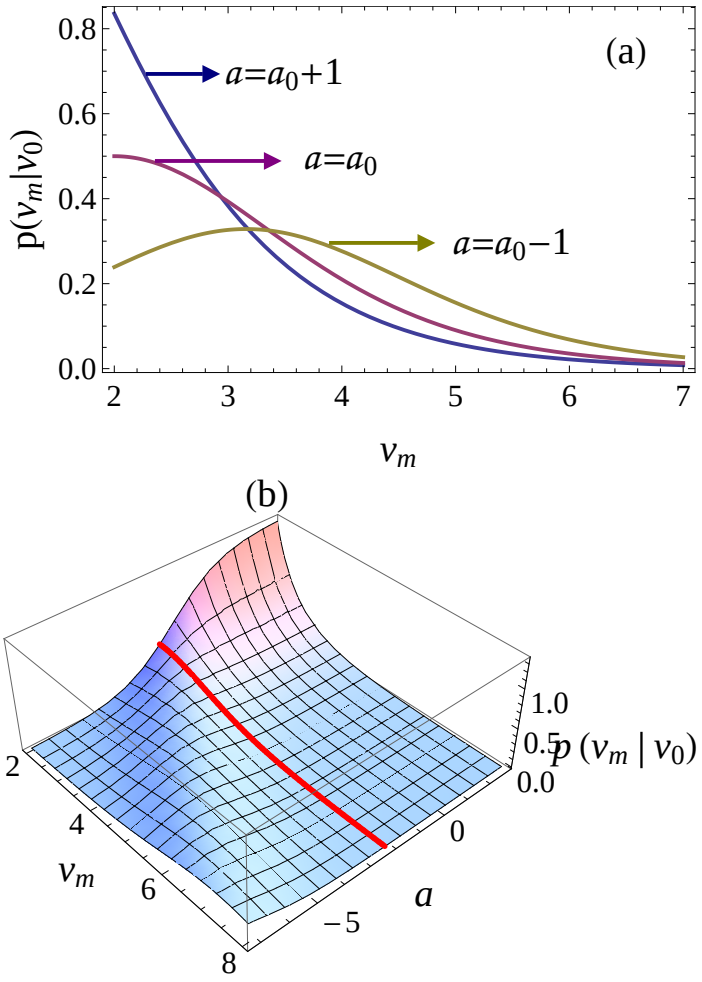

Figure 5.1: MVD till the FPT ($v_m > v_0$) of the pure dry friction case for $v_0 = 2$. (a) MVD till the FPT for three values of a [see Eq. (5.17)]. Here $a_0 = -\ln(e^2+2) \approx -2.24$ denotes the critical value as shown in Eq. (5.19). (b) MVD till the FPT as a function of v_m and a. The red curve indicates the distribution for $a = a_0$.

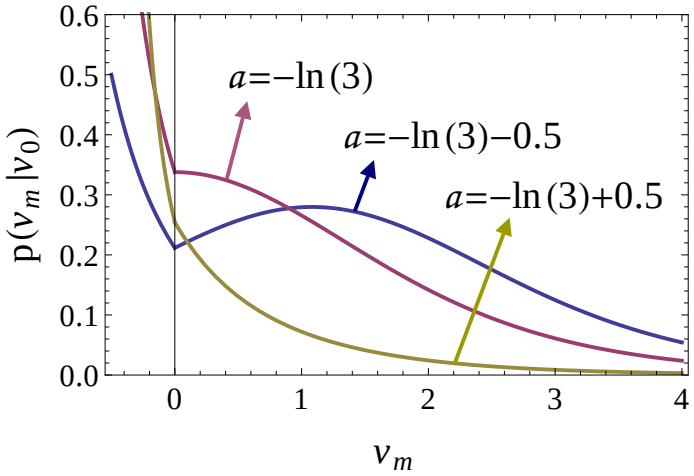

Figure 5.2: MVD till the FPT ($v_m > v_0$) of the pure dry friction case [see Eq. (5.23)] for negative initial velocity $v_0 = -0.5$ and three different values of a.

In this case, the distribution (5.23) also decays exponentially as we have

$$p(v_m|v_0) = e^{-v_m}(e^{-a} - e^{-v_0}) + O(e^{-2v_m}) \tag{5.26}$$

in the asymptotic limit $v_m \to \infty$.

5.2 Full model

For the full model (1.2), as discussed in Sec. 4.2 we can consider $\gamma = D = 1$ without loss of generality (see also appendix A.3.3), i.e., Eq. (2.12) with the potential $\Phi(v) = (|v| + \mu)^2/2 - bv$. In this case, Eq. (2.45) reads

$$\frac{\partial^2}{\partial v_0^2} Pr(v < v_m|v_0) - [\mu\sigma(v_0) + v_0 - b]\frac{\partial}{\partial v_0} Pr(v < v_m|v_0) = 0 \qquad \text{for } v_m > a. \tag{5.27}$$

This equation can be solved separately for positive and negative v_0 to yield

$$Pr(v < v_m|v_0) = \begin{cases} A\,\mathrm{erfi}\left(\dfrac{v_0 + \mu - b}{\sqrt{2}}\right) + B & \text{for } v_0 > 0, \\ \bar{A}\,\mathrm{erfi}\left(\dfrac{v_0 - \mu - b}{\sqrt{2}}\right) + \bar{B} & \text{for } v_0 < 0, \end{cases} \tag{5.28}$$

where erfi(z) is the imaginary error function defined by the error function (1.11) via

$$\operatorname{erfi}(z) = -i \operatorname{erf}(iz) = \frac{2}{\sqrt{\pi}} \int_0^z e^{t^2} dt. \tag{5.29}$$

Here i denoting the complex image number. Hence we have the following properties:

$$\operatorname{erfi}(-z) = -\operatorname{erfi}(z), \qquad \frac{d}{dz}\operatorname{erfi}(z) = \frac{2}{\sqrt{\pi}} e^{z^2}. \tag{5.30}$$

Moreover, we have in the leading order that

$$\operatorname{erfi}(z) \simeq \frac{1}{\sqrt{\pi} z} e^{z^2} \tag{5.31}$$

in the asymptotic limit $z \to \infty$.

As for the pure dry friction case, the coefficients in Eq. (5.28) are determined by the boundary conditions (2.46) and (2.47), and the matching conditions (2.48) and (2.49). Eqs. (2.46), (2.48) and (2.49) give

$$\bar{A} \operatorname{erfi}\left(\frac{a - \mu - b}{\sqrt{2}}\right) + \bar{B} = 1, \tag{5.32}$$

$$A \operatorname{erfi}\left(\frac{\mu - b}{\sqrt{2}}\right) + B = \bar{A} \operatorname{erfi}\left(\frac{-\mu - b}{\sqrt{2}}\right) + \bar{B}, \tag{5.33}$$

$$A e^{(\mu - b)^2/2} = \bar{A} e^{(\mu + b)^2/2}, \tag{5.34}$$

and the boundary condition (2.47), which depends on the sign of v_m, results in

$$A \operatorname{erfi}\left(\frac{v_m + \mu - b}{\sqrt{2}}\right) + B = 0 \qquad \text{for } v_m > 0, \tag{5.35}$$

$$\bar{A} \operatorname{erfi}\left(\frac{v_m - \mu - b}{\sqrt{2}}\right) + \bar{B} = 0 \qquad \text{for } v_m < 0. \tag{5.36}$$

Here we have used the differential property in Eq. (5.30) to derive Eq. (5.34). Therefore,

for $v_m > 0$ we can solve Eqs. (5.32)–(5.35) to obtain

$$A = e^{2b\mu}/C_+, \tag{5.37}$$
$$B = \operatorname{erfi}\left(\frac{\mu - b + v_m}{\sqrt{2}}\right) e^{2b\mu}/C_+, \tag{5.38}$$
$$\bar{A} = 1/C_+, \tag{5.39}$$
$$\bar{B} = 1 - \operatorname{erfi}\left(\frac{a - b - \mu}{\sqrt{2}}\right)/C_+, \tag{5.40}$$

where

$$C_+ = \operatorname{erfi}\left(\frac{a - b - \mu}{\sqrt{2}}\right) + \operatorname{erfi}\left(\frac{b + \mu}{\sqrt{2}}\right) + \left[\operatorname{erfi}\left(\frac{b - \mu - v_m}{\sqrt{2}}\right) + \operatorname{erfi}\left(\frac{\mu - b}{\sqrt{2}}\right)\right] e^{2b\mu}. \tag{5.41}$$

For $v_m < 0$ we have to solve Eqs. (5.32)–(5.34) and (5.36) resulting in

$$A = e^{2\mu b}/C_-, \tag{5.42}$$
$$B = \left[\operatorname{erfi}\left(\frac{b + \mu - v_m}{\sqrt{2}}\right) - \operatorname{erfi}\left(\frac{b + \mu}{\sqrt{2}}\right) - e^{2b\mu}\operatorname{erfi}\left(\frac{\mu - b}{\sqrt{2}}\right)\right]/C_-, \tag{5.43}$$
$$\bar{A} = 1/C_-, \tag{5.44}$$
$$\bar{B} = \operatorname{erfi}\left(\frac{b + \mu - v_m}{\sqrt{2}}\right)/C_-, \tag{5.45}$$

where

$$C_- = \operatorname{erfi}\left(\frac{a - \mu - b}{\sqrt{2}}\right) + \operatorname{erfi}\left(\frac{b - \mu - v_m}{\sqrt{2}}\right). \tag{5.46}$$

Similarly to the dry friction case, we can now write down the MVD till the FPT explicitly in the two cases $v_0 > 0$ and $v_0 < 0$.

5.2.1 Case 1: $v_0 > 0$

In this case, v_m can only be positive. So it follows from Eqs. (5.28), (5.37) and (5.38) that the probability

$$Pr(v < v_m | v_0) = \frac{\left[\operatorname{erfi}\left(\frac{b-\mu-v_m}{\sqrt{2}}\right) - \operatorname{erfi}\left(\frac{b-\mu-v_0}{\sqrt{2}}\right)\right] e^{2b\mu}}{\operatorname{erfi}\left(\frac{a-b-\mu}{\sqrt{2}}\right) + \operatorname{erfi}\left(\frac{b+\mu}{\sqrt{2}}\right) + \left[\operatorname{erfi}\left(\frac{b-\mu-v_m}{\sqrt{2}}\right) - \operatorname{erfi}\left(\frac{b-\mu}{\sqrt{2}}\right)\right] e^{2b\mu}} \tag{5.47}$$

for $v_m > v_0$. Hence differentiating Eq. (5.47) with respect to v_m we obtain the MVD

$$p(v_m|v_0) = \sqrt{\frac{2}{\pi}} e^{(v_m+\mu-b)^2/2+2\mu b} \Bigg\{ \operatorname{erfi}\left(\frac{b+\mu-a}{\sqrt{2}}\right) - \operatorname{erfi}\left(\frac{b+\mu}{\sqrt{2}}\right) + \left[\operatorname{erfi}\left(\frac{b-\mu}{\sqrt{2}}\right) - \operatorname{erfi}\left(\frac{b-\mu-v_0}{\sqrt{2}}\right)\right] e^{2b\mu} \Bigg\} \Big/ C_+^2 \qquad \text{for } v_m > v_0, \quad (5.48)$$

where C_+ is defined in Eq. (5.41). As shown in Fig. 5.3, when the bias b becomes larger the Brownian particle has more chance to attain large maximum velocities, as expected. From numerical results, we observe that depending on the values of v_0 and the parameters μ, a and b, the distribution $p(v_m|v_0)$ is monotonically decreasing or has a quadratic maximum in the domain $v_m > v_0$. In addition, by using the asymptotic property (5.31) it is easy to evaluate Eq. (5.48) to obtain that in the leading order the distribution (5.48) decays as

$$p(v_m|v_0) \sim (v_m + \mu - b) e^{-(v_m+\mu-b)^2/2}. \quad (5.49)$$

Intuitively, for the full model without bias ($b = 0$) we expect that if the dry friction dominates the viscous friction the tail behaviour of the corresponding distribution $p(v_m|v_0)$ should resemble that of the pure dry friction case. In order to compare the tail behaviour of the models with and without viscous friction, we consider the full model (1.2) with $\mu = D = 1$ and $b = 0$, i.e.,

$$\dot{v}(t) = -\sigma(v(t)) - \gamma v(t) + \xi(t). \quad (5.50)$$

From appendix A.3.3 we know that we can obtain the MVD of Eq. (5.50) from Eq. (5.48) by using the transformation

$$v_m \to \sqrt{\gamma} v_m, \qquad \mu \to \mu/\sqrt{\gamma} \quad (5.51)$$

and then letting $\mu = 1$. As shown in Fig. 5.4, the MVD of Eq. (5.50) approaches the decay rate of the dry friction case when the viscous coefficient γ becomes small, as expected.

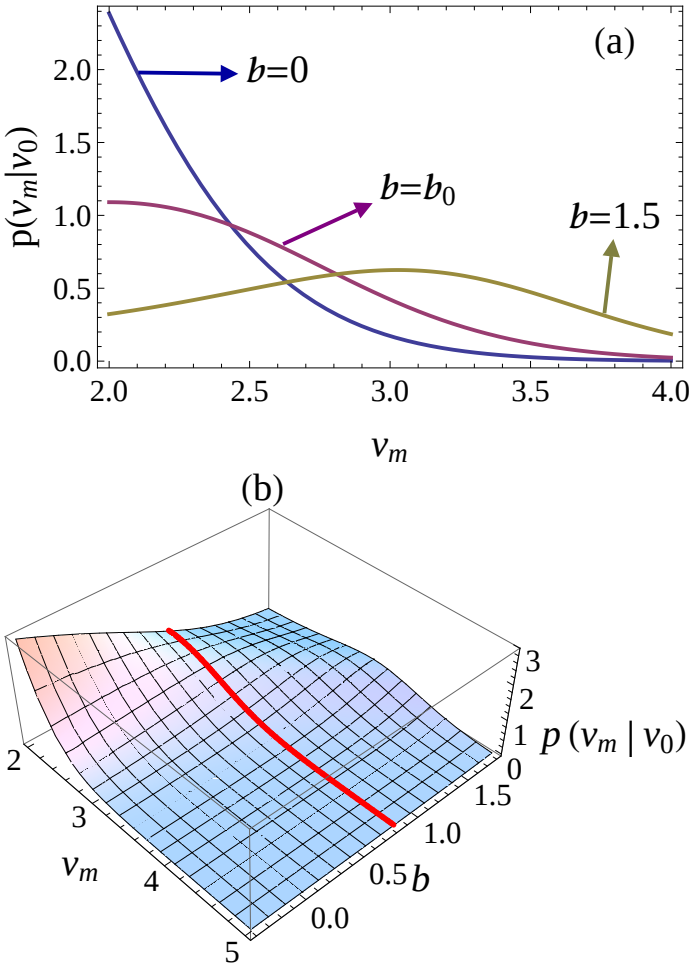

Figure 5.3: MVD till the FPT ($v_m > v_0$) of the full model [see Eq. (5.48)] for positive initial velocity $v_0 = 2$, $\mu = 1$, $a = -1$. (a) MVD till the FPT for three different values of b. Here $b_0 \approx 0.819$. When $b > b_0$, a quadratic maximum appears in the distribution. (b) MVD till the FPT as a function of v_m and b. The red curve indicates the distribution for $b = b_0$.

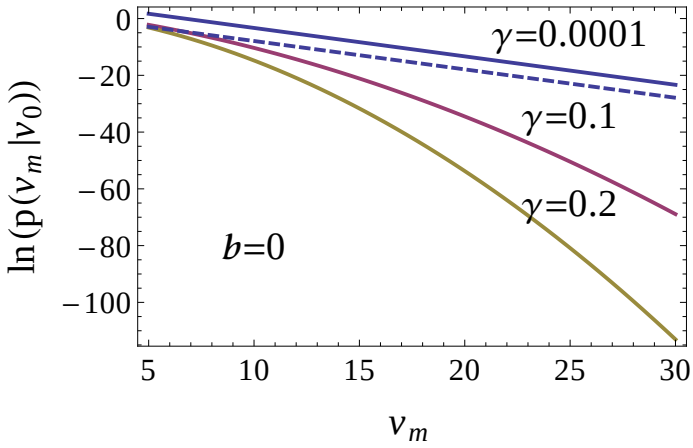

Figure 5.4: Tail behaviour of the MVD till the FPT of the model (5.50) (full) for $\mu = D = 1$ and three different values of γ. The dashed line shows the result of the pure dry friction model (1.8) with the same arguments [see Eq. (5.17)].

5.2.2 Case 2: $a < v_0 < 0$

In this case, v_m can be negative or positive. It follows from Eqs. (5.28), (5.44) and (5.45) that the probability

$$Pr(v < v_m|v_0) = \frac{\operatorname{erfi}\left(\frac{v_0-b-\mu}{\sqrt{2}}\right) + \operatorname{erfi}\left(\frac{b+\mu-v_m}{\sqrt{2}}\right)}{\operatorname{erfi}\left(\frac{a-b-\mu}{\sqrt{2}}\right) + \operatorname{erfi}\left(\frac{b+\mu-v_m}{\sqrt{2}}\right)} \tag{5.52}$$

for $v_0 < v_m < 0$, and from Eqs. (5.28), (5.39) and (5.40) that

$$Pr(v < v_m|v_0) = \frac{\operatorname{erfi}\left(\frac{b+\mu}{\sqrt{2}}\right) + \operatorname{erfi}\left(\frac{v_0-b-\mu}{\sqrt{2}}\right) + \left[\operatorname{erfi}\left(\frac{b-\mu-v_m}{\sqrt{2}}\right) + \operatorname{erfi}\left(\frac{\mu-b}{\sqrt{2}}\right)\right] e^{2b\mu}}{\operatorname{erfi}\left(\frac{b+\mu}{\sqrt{2}}\right) + \operatorname{erfi}\left(\frac{a-b-\mu}{\sqrt{2}}\right) + \left[\operatorname{erfi}\left(\frac{b-\mu-v_m}{\sqrt{2}}\right) + \operatorname{erfi}\left(\frac{\mu-b}{\sqrt{2}}\right)\right] e^{2b\mu}} \tag{5.53}$$

for $v_m > 0$. Hence differentiating Eqs. (5.52) and (5.53) with respect to v_m yields the MVD till the FPT:

$$p(v_m|v_0) = \frac{\sqrt{\frac{2}{\pi}}\left[\operatorname{erfi}\left(\frac{\mu+b-a}{\sqrt{2}}\right) + \operatorname{erfi}\left(\frac{v_0-\mu-b}{\sqrt{2}}\right)\right] e^{(b+\mu-v_m)^2/2}}{\left[\operatorname{erfi}\left(\frac{a-b-\mu}{\sqrt{2}}\right) + \operatorname{erfi}\left(\frac{b+\mu-v_m}{\sqrt{2}}\right)\right]^2} \tag{5.54}$$

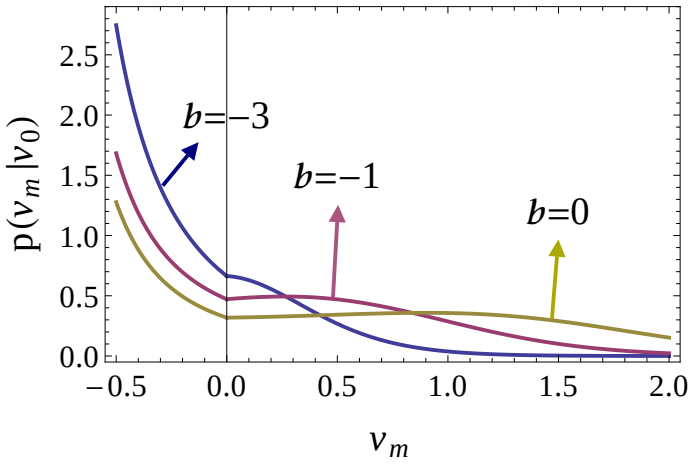

Figure 5.5: MVD till the FPT ($v_m > v_0$) of the full model (1.2) [see Eqs. (5.54) and (5.55)] for negative initial velocity $v_0 = -0.5$, $\mu = 1$, $a = -1$ and three different values of b.

for $v_0 < v_m < 0$, and

$$p(v_m|v_0) = \frac{\sqrt{\frac{2}{\pi}}\left[\text{erfi}\left(\frac{\mu+b-a}{\sqrt{2}}\right) + \text{erfi}\left(\frac{v_0-\mu-b}{\sqrt{2}}\right)\right] e^{(v_m+\mu-b)^2/2+2\mu b}}{\left\{\text{erfi}\left(\frac{a-\mu-b}{\sqrt{2}}\right) + \text{erfi}\left(\frac{b+\mu}{\sqrt{2}}\right) + \left[\text{erfi}\left(\frac{b-\mu-v_m}{\sqrt{2}}\right) - \text{erfi}\left(\frac{b-\mu}{\sqrt{2}}\right)\right] e^{2b\mu}\right\}^2} \tag{5.55}$$

for $v_m > 0$. As shown in Fig. 5.5, a non-smooth point is observed at $v_m = 0$, which indicates the effect of the dry friction in the MVD problem. As the bias b becomes larger, the distribution has smaller value for small v_m and has larger value for large v_m, as expected. It is easy to check that the distribution (5.55) decays like Eq. (5.49) in the asymptotic limit $v_m \to \infty$. In addition, as the case $v_0 > 0$ we can use the transformation (5.51) to obtain the distribution $p(v_m|v_0)$ of the model (5.50). Finally, we find that in this case the decay rate of the MVD also approaches that of the dry friction case when the viscous coefficient γ becomes small, in consistence with the results shown in Fig. 5.4.

In the trivial case $\mu = 0$, the problem considered here reduces to that of the Ornstein-Uhlenbeck process. It is easy to check that in this case Eqs. (5.48), (5.54) and (5.55) agree with each other and result in the same expression

$$p(v_m|v_0) = \frac{\sqrt{\frac{2}{\pi}}\left[\text{erfi}\left(\frac{b-a}{\sqrt{2}}\right) + \text{erfi}\left(\frac{v_0-b}{\sqrt{2}}\right)\right] e^{(b-v_m)^2/2}}{\left[\text{erfi}\left(\frac{a-b}{\sqrt{2}}\right) + \text{erfi}\left(\frac{b-v_m}{\sqrt{2}}\right)\right]^2} \qquad \text{for } v_m > v_0. \tag{5.56}$$

5.3 Summary of chapter

In this chapter, we have shown that the MVD till the FPT can be solved analytically for the pure dry friction case and the full model, respectively. In both cases, we have to distinguish the two cases $v_0 > 0$ and $v_0 < 0$. For $v_0 > 0$, the maximum velocity is positive and only one branch of the solution enters the distribution, which is smooth in the defined region $v_m > v_0$. However, for $v_0 < 0$ the maximum velocity can be negative or positive, and we have to solve the corresponding problem on the two domains $v_m > 0$ and $v_m < 0$, respectively. Since the distribution functions are different for positive and negative v_m, a non-smooth point is observed at $v_m = 0$, which as we know is caused by the dry friction and is a ubiquitous feature of piecewise-smooth stochastic systems.

Chapter 6

Functionals of Brownian motion with dry friction

Functionals of a process $v(t)$ have been investigated intensively in the past and have found numerous applications in physics [61]. For instance, two of the popular functionals are the local time $\int_0^t \delta(v(\tau))d\tau$ and the occupation time $\int_0^t \theta(v(\tau))d\tau$ (see, e.g., Ref. [77]), which describe how much time the process $v(t)$ has visited the origin and how long it has spent on the upper half plane in the time window $[0, t]$, respectively. Here $\delta(v)$ is the Dirac delta function and $\theta(v)$ is the step function with $\theta(v) = 1$ for $v > 0$ and $\theta(v) = 0$ for $v \leqslant 0$. In addition, the area under the process, i.e., $\int_0^t v(\tau)d\tau$, which is referred to as displacement if $v(t)$ denotes the velocity of an object, is of particular importance due to its physical meaning.

However, to find statistical properties of functionals is usually non-trivial even for some of the simplest functionals, such as the local time and the occupation time. For the displacement, which is equivalent to solve a stochastic differential equation with inertial term, one often restricts the study to the overdamped case, in which limit the inertial term can be neglected [76]. To the best of my knowledge, the distributions of the displacement are only available in closed analytic form for the cases of the pure diffusion process and the Ornstein-Uhlenbeck process [57]. To compute the distribution of a functional, there are two significant achievements, i.e., the celebrated Feynman-Kac formula developed by Kac [50] and the so-called backward Fokker-Planck technique proposed by Majumdar and Comtet [63] (see also Sec. 2.4), both of which tackle positive support functionals. The former enables one to obtain a corresponding Schrödinger

equation for the distribution of a functional and the later results in a backward Fokker-Planck equation for the distribution. The advantage of the later over the former is that the later depends only on the initial condition of the process, no extra integral over v is required to obtain the distribution of the functional.

In this chapter, we first extend the backward Fokker-Planck technique for a positive support functional (see Sec. 2.4) to an arbitrary support functional $T = \int_0^t U(v(\tau))d\tau$ in Sec. 6.1 by replacing the Laplace transform for T with a Fourier transform. Here $U(v)$ is an arbitrary-prescribed function and the process $v(t)$ obeys the generic Langevin equation (2.12). Rather than solving the backward equation directly, we then derive from this equation a recursive ordinary differential equation (ODE) for the moments of the functional. In Sec. 6.2 we show that the moments of the local time and the occupation time in the Laplace domain are given explicitly by the solution of the corresponding homogeneous ODE. Then we apply the results to consider the pure dry friction model (1.5) in Sec. 6.3 and the full model (1.2) without bias in Sec. 6.4, respectively. For this two models, we show that the moments of the local time, the occupation time and the displacement can be obtained in closed analytic form in the Laplace space. Finally, a summary of this chapter is given in Sec. 6.5.

6.1 Functionals with generic support

For the Langevin equation (2.12) let us first consider the quantity $T = \int_0^t U(v(\tau))d\tau$ (2.50) with an arbitrary-prescribed function $U(v)$. As in Sec. 2.4, let us denote its distribution as $p(T, t, v_0)$. Since T can be negative here, rather than using the Laplace transform (2.51) we apply the following Fourier transform

$$\bar{p}(k, t, v_0) = \int_{-\infty}^{\infty} p(T, t, v_0) e^{-ikT} dT = \left\langle e^{-ik\int_0^t U(v(\tau))d\tau} \right\rangle. \tag{6.1}$$

Then, following the same derivation procedure in Sec. 2.4, we obtain [see also Eq. (2.54)]

$$\frac{\partial}{\partial t}\bar{p}(k, t, v_0) = \frac{\partial^2}{\partial v_0^2}\bar{p}(k, t, v_0) - \Phi'(v_0)\frac{\partial}{\partial v_0}\bar{p}(k, t, v_0) - ikU(v_0)\bar{p}(k, t, v_0). \tag{6.2}$$

If one uses the following Laplace transform in t direction:

$$r(k, s, v_0) = \int_0^{\infty} \bar{p}(k, t, v_0) e^{-st} dt, \tag{6.3}$$

the partial differential equation (6.2) can be reduced to the following ODE:

$$\frac{\partial^2}{\partial v_0^2} r(k,s,v_0) - \Phi'(v_0)\frac{\partial}{\partial v_0} r(k,s,v_0) - [ikU(v_0)+s]r(k,s,v_0) = -1, \tag{6.4}$$

where we have used the condition $p(T,0,v_0) = \delta(T)$, which results in $\bar{p}(k,0,v_0) = 1$ [see Eq. (6.1)]. The appropriate boundary conditions for $r(k,s,v_0 \to \pm\infty)$ are to be derived from the observation that if the particle starts at $v_0 \to \pm\infty$ it will never cross the origin in finite time. In particular, we have

$$p(T_{\rm loc}, t, v_0 \to \pm\infty) = \delta(T_{\rm loc}) \tag{6.5}$$

for the local time, and

$$p(T_{\rm occ}, t, v_0 \to \infty) = \delta(T_{\rm occ} - t), \qquad p(T_{\rm occ}, t, v_0 \to -\infty) = \delta(T_{\rm occ}) \tag{6.6}$$

for the occupation time. Here we have used the notations $T_{\rm loc}$ and $T_{\rm occ}$ to denote the local time and the occupation time, respectively. Later on, we will use the notation $T_{\rm dis}$ for the displacement.

In general, it is difficult to derive the exact expression of the distribution $p(T,t,v_0)$. However, for a stable potential in Eq. (2.12), i.e., $\Phi(v) \to \infty$ when $v \to \pm\infty$, the distribution $p(T,t,v_0)$ is simply Gaussian around its mean in the long time limit, as pointed out in Ref. [77] for the local time and the occupation time. Thus the limiting distribution around mean is characterised only by the first and the second moments, denoted as

$$p_{\rm asym}(T,t,v_0) = \frac{1}{\sqrt{2\pi {\rm Var}(T)}} \exp\left[-\frac{(T - M_1(t,v_0))^2}{2{\rm Var}(T)}\right], \tag{6.7}$$

where

$${\rm Var}(T) = M_2(t,v_0) - M_1^2(t,v_0) \tag{6.8}$$

stands for the variance of T, $M_1(t,v_0)$ and $M_2(t,v_0)$ are the first and the second moments. As stated in Ref. [77], the argument is as follows: at large time t the process $v(t)$ [see Eq. (2.12)] becomes mixing and the corresponding propagator $p(v,t|v_0,0)$ tends to the stationary distribution $\exp[-\Phi(v)]/Z$, where Z is a normalisation factor. Thus, at time increments which exceed the correlation time of the system (2.12), the random

variables $U(v(\tau)) - \langle U(v(\tau))\rangle$ are only weekly correlated. Therefore, using the definition

$$T - \langle T\rangle = \int_0^t \left[U(v(\tau)) - \langle U(v(\tau))\rangle\right] d\tau, \tag{6.9}$$

we expect the central limit theorem to hold in the limit that when t is much larger than the relaxation time and the correlation time of the two aforementioned variables, which yields a Gaussian distribution for the functional T around its mean. Hence, for a stable potential, in order to determine the limiting distribution of T around its mean we only need to know the first and the second moments, which can be obtained by using the results stated in the following subsections. Since the dry friction model (1.2) has a stable potential, we will see later in Secs. 6.3 and 6.4 that the distributions of the local time, the occupation time and the displacement can be given explicitly in the long time limit.

In general, it is difficult to solve the inhomogeneous ODE (2.56) or (6.4) directly. Hence, rather than considering the solutions of these ODEs, we derive an equation for the moments of functionals in the following subsection. This equation will turn out to be much easier to handle than Eq. (2.56) or (6.4).

6.1.1 Moments of the functional

Here we assume the potential $\Phi(v)$ in Eq. (2.12) to be continuous and smooth everywhere apart from a non-smooth point at $v = 0$ for the purpose of considering the dry friction model (1.2). But the result can be of course applied to a smooth potential. Now let us assume that the n-th moment $M_n(t, v_0)$ of T exists. Then its Laplace transform in time direction is simply given by

$$\widetilde{M}_n(s, v_0) = \int_0^\infty M_n(t, v_0) e^{-st} dt = i^n \frac{\partial^n}{\partial k^n} r(k, s, v_0)\bigg|_{k=0} \qquad \text{for } n \geqslant 1, \tag{6.10}$$

where $r(k, s, v_0)$ is defined in Eq. (6.3) and satisfies Eq. (6.4). Thus acting the operator $i^n \frac{\partial^n}{\partial k^n}$ on Eq. (6.4) and setting $k = 0$, we obtain for $\widetilde{M}_n(s, v_0)$ a recursive differential equation

$$\frac{\partial^2}{\partial v_0^2}\widetilde{M}_n(s, v_0) - \Phi'(v_0)\frac{\partial}{\partial v_0}\widetilde{M}_n(s, v_0) - s\widetilde{M}_n(s, v_0) = -nU(v_0)\widetilde{M}_{n-1}(s, v_0). \tag{6.11}$$

The initial iterative value is given by [see Eqs. (6.1) and (6.3)]

$$\widetilde{M}_0(s, v_0) = r(0, s, v_0) = \frac{1}{s}. \tag{6.12}$$

Similarly, it is easy to verify that Eq. (6.11) can be derived from Eq. (2.56) as well. However, Eq. (2.56) is only for functionals with non-negative support. Hence, in order to consider the displacement it is necessary to use the generalised backward Fokker-Planck technique [see Eq. (6.4)].

6.1.2 Boundary conditions

In order to solve Eq. (6.11), it is important to know the corresponding boundary conditions for $v_0 \to \pm\infty$. Using Eq. (6.5) and the uniform convergence of the Laplace transform (6.10) for $\mathrm{Re}(s) > 0$ it follows that the moments of the local time obey

$$\widetilde{M}_n(s, v_0 \to \pm\infty) = 0 \qquad \text{for } \mathrm{Re}(s) > 0 \text{ and } n \geqslant 1, \tag{6.13}$$

whereas a similar argument and Eq. (6.6) yield for the moments of the occupation time that

$$\widetilde{M}_n(s, v_0 \to \infty) = \frac{n!}{s^{n+1}}, \qquad \widetilde{M}_n(s, v_0 \to -\infty) = 0 \qquad \text{for } \mathrm{Re}(s) > 0 \text{ and } n \geqslant 1. \tag{6.14}$$

For the displacement, in general we are not able to find an accurate boundary condition. But we expect that for $|v_0| \gg t$ the velocity of the particle does not change much in the time window $[0, t]$ and the displacement should be at the scale of $v_0 t$. Hence the n-th moment of the displacement as a function of v_0 should be bounded by a polynomial of order n in v_0. We will see later that this condition is sufficient for us to determine the solution of the dry friction model (1.2).

6.1.3 Matching conditions

Since we are here concerned with a piecewise-smooth potential $\Phi(v_0)$, we have to solve Eq. (6.11) for the two domains $v_0 > 0$ and $v_0 < 0$, respectively. Then we have to match the solutions by using the continuity condition at $v_0 = 0$, i.e.,

$$\widetilde{M}_n(s, 0-) = \widetilde{M}_n(s, 0+), \tag{6.15}$$

and the matching condition [depends on $U(v)$] obtained by integrating Eq. (6.11) across $v_0 = 0$, which is

$$\frac{\partial}{\partial v_0}\widetilde{M}_n(s,0+) - \frac{\partial}{\partial v_0}\widetilde{M}_n(s,0-) = -n\widetilde{M}_{n-1}(s,0) \tag{6.16}$$

for the local time, and

$$\frac{\partial}{\partial v_0}\widetilde{M}_n(s,0+) = \frac{\partial}{\partial v_0}\widetilde{M}_n(s,0-) \tag{6.17}$$

for both the occupation time and the displacement. Here we have used the shorthand notation $\frac{\partial}{\partial v_0}\widetilde{M}_n(s,0\pm)$ to denote $\frac{\partial}{\partial v_0}\widetilde{M}_n(s,v_0)|_{v_0\to 0\pm}$.

6.1.4 Structure of the solution

Let us briefly discuss how we are going to approach the analytic solutions of Eq. (6.11) for a general potential $\Phi(v)$ with a discontinuity at $v = 0$. Suppose that the appropriate fundamental piecewise-smooth solution $\varphi(s, v_0)$ of the corresponding homogeneous ODE of Eq. (6.11) is known, which vanishes for $\mathrm{Re}(s) > 0$ when $v_0 \to \pm\infty$. The solution obeys

$$\frac{\partial^2}{\partial v_0^2}\varphi(s,v_0) - \Phi'(v_0)\frac{\partial}{\partial v_0}\varphi(s,v_0) - s\varphi(s,v_0) = 0 \tag{6.18}$$

for $v_0 \neq 0$ and we assume $\varphi(s, v_0)$ to be continuous at $v_0 = 0$. In addition, let us denote one particular piecewise-smooth solution of Eq. (6.11) as $\widetilde{M}_n^p(s, v_0)$ (may be discontinuous at $v_0 = 0$), which satisfies the appropriate boundary conditions of Eq. (6.11) (see subsection 6.1.2) and solves Eq. (6.11) on the two domains $v_0 > 0$ and $v_0 < 0$, respectively. Then the general solutions of Eq. (6.11) can be expressed as

$$\widetilde{M}_n(s,v_0) = \widetilde{M}_n^p(s,v_0) + \begin{cases} C_n^+\varphi(s,v_0) & \text{for } v_0 > 0, \\ C_n^-\varphi(s,v_0) & \text{for } v_0 < 0, \end{cases} \tag{6.19}$$

where the coefficients $C_n^\pm$ are determined by the matching conditions at $v_0 = 0$ (see subsection 6.1.3). In general, we may not be able to do the inverse inverse Laplace transform analytically to obtain $M_n(t, v_0)$. However, in the long time limit the behaviour of the moments is dominated by the singular terms of the Laplace transform and those are often not too difficult to evaluate. We can also resort to numerical Laplace inversion, such as the so-called Talbot method [1] (see the footnote on page 66), which usually gives accurate results even at a very short time.

6.2 Local time, occupation time and displacement

In this section, we will demonstrate that for the cases of the local time and the occupation time the formula (6.19) can be simplified considerably and that the Laplace transforms of the moments can be expressed in terms of the solution $\varphi(s, v_0)$. The situation for the displacement is slightly more involved and we will discuss this case at the end of this section.

6.2.1 Local time

In this case, we only need to solve the corresponding homogeneous ODE of Eq. (6.11) as $\widetilde{M}_n^p(s, v_0)$ vanishes in the solution (6.19). Hence, by using the matching conditions at $v_0 = 0$ [see Eqs. (6.15) and (6.16)] it can be easily derived from Eq. (6.11) that the moments of the local time satisfy the following recursive relation

$$\widetilde{M}_n(s, v_0) = \frac{n\varphi(s, v_0)\widetilde{M}_{n-1}(s, 0)}{\frac{\partial}{\partial v_0}\varphi(s, 0-) - \frac{\partial}{\partial v_0}\varphi(s, 0+)} \qquad \text{for } n \geqslant 1. \tag{6.20}$$

Therefore, using the condition (6.12) we can check that the higher moments are determined by the first moment via

$$\widetilde{M}_n(s, v_0) = n!\big[s\widetilde{M}_1(s, 0)\big]^{n-1}\widetilde{M}_1(s, v_0), \tag{6.21}$$

where

$$\widetilde{M}_1(s, v_0) = \frac{\varphi(s, v_0)/s}{\frac{\partial}{\partial v_0}\varphi(s, 0-) - \frac{\partial}{\partial v_0}\varphi(s, 0+)}. \tag{6.22}$$

This simple relation enables us to obtain the distribution of the local time explicitly in the Fourier-Laplace space, which reads [see Eq. (6.3)]

$$r(k, s, v_0) = \sum_{n=0}^{\infty} \frac{(-ik)^n}{n!}\widetilde{M}_n(s, v_0) = \frac{\widetilde{M}_1(s, v_0)}{s\widetilde{M}_1(s, 0)}\frac{1}{1 + iks\widetilde{M}_1(s, 0)}. \tag{6.23}$$

Then the Laplace transform of the local time distribution with respect to time t can be obtained by inverting the Fourier transform with respect to k:

$$u(T_{\mathrm{loc}}, s, v_0) = \frac{\widetilde{M}_1(s, v_0)}{s^2\widetilde{M}_1^2(s, 0)} \exp\left(-\frac{T_{\mathrm{loc}}}{s\widetilde{M}_1(s, 0)}\right) \qquad \text{for } T_{\mathrm{loc}} \geqslant 0, \tag{6.24}$$

which indicates that the distribution of the local time is fully determined by the Laplace transform of its first moment. The result (6.24) extends that obtained in Ref. [77] to be valid for arbitrary v_0 [see Eq. (30) therein]. In general, we may not be able to do the inverse Laplace transform for Eq. (6.24) analytically. However, we can resort to numerical inversion (e.g., the Talbot method [1]) to produce the distribution $p(T_{\rm loc}, t, v_0)$ numerically, especially for short time t.

6.2.2 Occupation time

Since in this case $U(v_0) = \theta(v_0)$ is piecewise-constant in Eq. (6.11), it is possible to obtain particular solutions $\widetilde{M}_n^p(s, v_0)$ in Eq. (6.19) explicitly in terms of the solution $\varphi(s, v_0)$. For this purpose, let us first introduce the operator

$$L_s = \frac{\partial^2}{\partial v_0^2} - \Phi'(v_0)\frac{\partial}{\partial v_0} - s. \tag{6.25}$$

Then differentiating the following equation [see Eq. (6.18)]

$$L_s \varphi(s, v_0) = 0 \tag{6.26}$$

m times with respect to s results in

$$L_s \frac{\partial^m}{\partial s^m}\varphi(s, v_0) = m\frac{\partial^{m-1}}{\partial s^{m-1}}\varphi(s, v_0). \tag{6.27}$$

Now we can start to derive the solution of Eq. (6.11) for $n = 1$ by noting that in this case a particular solution of Eq. (6.19) is

$$\widetilde{M}_1^p(s, v_0) = \begin{cases} 1/s^2 & \text{for } v_0 > 0, \\ 0 & \text{for } v_0 < 0. \end{cases} \tag{6.28}$$

Using the property (6.27) and the inductive method (see appendix A.8 for the details), we end up with the following formula for the moments of the occupation time from Eqs. (6.11) and (6.19),

$$\widetilde{M}_n(s, v_0) = \begin{cases} n!/s^{n+1} + \sum_{m=0}^{n-1}(-1)^m \binom{n}{m} C_{n-m}^{+} \frac{\partial^m}{\partial s^m}\varphi(s, v_0) & \text{for } v_0 > 0, \\ C_n^{-}\varphi(s, v_0) & \text{for } v_0 < 0, \end{cases} \tag{6.29}$$

where $\binom{n}{m} = n!/[m!(n-m)!]$ is the binomial coefficient. The coefficients C_n^+ and C_n^- are determined by the first-order smooth matching condition at $v_0 = 0$ [see Eqs. (6.15) and (6.17)]. Thus, we obtain the explicit formulae

$$C_1^{\pm} = \frac{\frac{\partial}{\partial v_0}\varphi(s,0\mp)}{s^2\varphi(s,0)\left[\frac{\partial}{\partial v_0}\varphi(s,0+) - \frac{\partial}{\partial v_0}\varphi(s,0-)\right]}, \tag{6.30}$$

and for $n > 1$

$$C_n^{\pm} = \left\{ \sum_{m=1}^{n-1} (-1)^m \binom{n}{m} C_{n-m}^+ \left[\frac{\partial}{\partial v_0}\varphi(s,0\mp)\frac{\partial^m}{\partial s^m}\varphi(s,0) - \varphi(s,0)\frac{\partial^m}{\partial s^m}\frac{\partial}{\partial v_0}\varphi(s,0+) \right] \right.$$
$$\left. + n!\frac{\partial}{\partial v_0}\varphi(s,0\mp)/s^{n+1} \right\} \Big/ \left\{ \varphi(s,0)\left[\frac{\partial}{\partial v_0}\varphi(s,0+) - \frac{\partial}{\partial v_0}\varphi(s,0-)\right] \right\}. \tag{6.31}$$

While such expressions are certainly more involved than those for the local time problem we can still express the entire moment problem in terms of the fundamental solution of the homogeneous equation.

6.2.3 Displacement

For the displacement, by using the first-order smooth matching condition [see Eqs. (6.15) and (6.17)] the coefficients in Eq. (6.19) are determined to be

$$C_n^{\pm} = \left\{ \varphi(s,0)\left[\frac{\partial}{\partial v_0}\widetilde{M}_n^p(s,0+) - \frac{\partial}{\partial v_0}\widetilde{M}_n^p(s,0-)\right] - \frac{\partial}{\partial v_0}\varphi(s,0\mp)\left[\widetilde{M}_n^p(s,0+) \right.\right.$$
$$\left.\left. - \widetilde{M}_n^p(s,0-)\right] \right\} \Big/ \left\{ \varphi(s,0)\left[\frac{\partial}{\partial v_0}\varphi(s,0+) - \frac{\partial}{\partial v_0}\varphi(s,0-)\right] \right\}. \tag{6.32}$$

However, in this case particular solutions $\widetilde{M}_n^p(s,v_0)$ of the corresponding inhomogeneous ODE (6.11) are not simple to write down in general. So a general formula as Eq. (6.21) or (6.29) is not available. Fortunately, for the dry friction model (1.2) we will see in the following sections that particular solutions can be constructed straightforwardly.

In the next two sections, we first consider the simplest dry friction case, i.e., the pure dry friction case, in order to show the effectiveness of our method and then consider the dry and viscous friction case, both of which have a symmetric potential. Since the full model with bias does not have a symmetric potential, the formulae are much longer compared to these two symmetric cases. Hence the corresponding formulae will not be

presented here. However, it is straightforward to generalise the formulae of the dry and viscous friction case to the full model with bias. As the computations in the following two sections are difficult to handle by hand, we have used Mathematica to do most of the symbolic computations.

6.3 Pure dry friction case

Firstly, let us consider the model (1.2) with only dry friction, i.e., $\gamma = b = 0$. This simplest stochastic model with dry friction is an ideal model to show the effectiveness of our method. It is worth to notice that the local time and the occupation time of this simple case have been investigated in Refs. [63, 77] even though the authors did not attempt to study dry friction effect in a stochastic setting. An integral representation of the occupation time distribution of this piecewise-constant stochastic model has also been derived in Ref. [82]. But the recursive relations for the moments of the local time and the occupation time have not been given explicitly. To the best of my knowledge analytic results of the displacement for the pure dry friction model are not available in the literature.

In this case, we let $\mu = D = 1$ without loss of generality (see Sec. 4.1 and also appendix A.3.2). Hence the pure dry friction case can be written in the form (2.12) with a stable potential $\Phi(v) = |v|$. The appropriate fundamental solution of the homogeneous ODE (6.18) is

$$\varphi(s, v_0) = e^{(1-\sqrt{1+4s})|v_0|/2}, \tag{6.33}$$

which vanishes for $\mathrm{Re}(s) > 0$ in the limit $v_0 \to \pm\infty$.

Then, from Eqs. (6.24) and (6.22) we obtain the local time distribution in the Laplace space with respect to time t:

$$u(T_{\mathrm{loc}}, s, v_0) = \frac{\sqrt{1+4s}-1}{s} e^{-(\sqrt{1+4s}-1)(T_{\mathrm{loc}}+|v_0|/2)} \qquad \text{for } T_{\mathrm{loc}} \geqslant 0. \tag{6.34}$$

Using the substitution $s = \alpha - 1/4$, Eq. (6.34) reads

$$u(T_{\mathrm{loc}}, \alpha - 1/4, v_0) = 2e^{T_{\mathrm{loc}}+|v_0|/2} \frac{e^{-\sqrt{\alpha}(2T_{\mathrm{loc}}+|v_0|)}}{\sqrt{\alpha}+1/2}. \tag{6.35}$$

From the table of Laplace transforms in Ref. [3] we have the following inverse Laplace

transform

$$\mathcal{L}^{-1}\left(\frac{e^{-k\sqrt{\alpha}}}{b+\sqrt{\alpha}}\right)=\frac{e^{-k^2/(4t)}}{\sqrt{\pi t}}-be^{bk+b^2t}\mathrm{erfc}\left(b\sqrt{t}+\frac{k}{2\sqrt{t}}\right)=F(t,b,k), \tag{6.36}$$

where $\mathcal{L}^{-1}$ denotes the operator of the inverse Laplace transform with respect to α and $\mathrm{erfc}(z)=1-\mathrm{erf}(z)=2\int_z^\infty e^{-t^2}dt/\sqrt{\pi}$ is the complementary error function. Hence, using the shifting property of Laplace transform, we obtain from Eq. (6.35) the inverse Laplace transform of $u(T_{\rm loc},s,v_0)$, i.e, the local time distribution

$$\begin{aligned}p(T_{\rm loc},t,v_0)&=2e^{T_{\rm loc}+|v_0|/2-t/4}F(t,1/2,2T_{\rm loc}+|v_0|)\\&=\frac{2}{\sqrt{\pi t}}e^{-(2T_{\rm loc}+|v_0|-t)^2/(4t)}-e^{2T_{\rm loc}+|v_0|}\mathrm{erfc}\left(\frac{\sqrt{t}}{2}+\frac{2T_{\rm loc}+|v_0|}{2\sqrt{t}}\right)\end{aligned} \tag{6.37}$$

for $T_{\rm loc}\geqslant 0$, which generalises the result in Ref. [77] to be valid for any v_0 [see Eq. (A4) therein].

The moments of the local time are given explicitly by [see Eqs. (6.21) and (6.22)]

$$\widetilde{M}_n(s,v_0)=\frac{n!}{4^n s^{n+1}}(\sqrt{1+4s}+1)^n e^{(1-\sqrt{1+4s})|v_0|/2}, \tag{6.38}$$

which have a single pole at $s=0$ and a branch cut for $s<-1/4$. Using the integral path as shown in Fig. 6.1 with $s_0=-1/4$, $R\to\infty$ and $\varepsilon\to 0$, and the residue theory for the $(n+1)$-th order pole at $s=0$, we can evaluate the inverse Laplace transform of $\widetilde{M}_n(s,v_0)$ to obtain in the long time limit that (see Ref. [71])[1]

$$M_n(t,v_0)=4^{-n}\,\frac{\partial^n}{\partial s^n}\left[(\sqrt{1+4s}+1)^n e^{(1-\sqrt{1+4s})|v_0|/2+st}\right]\Big|_{s=0}+O(e^{-(1/4-o)t}). \tag{6.39}$$

In particular, the first two moments read

$$M_1(t,v_0)=\frac{t}{2}+\frac{1-|v_0|}{2}+O(e^{-(1/4-o)t}), \tag{6.40}$$

$$M_2(t,v_0)=\frac{t^2}{4}+\frac{(2-|v_0|)t}{2}+\frac{v_0^2-2|v_0|-2}{4}+O(e^{-(1/4-o)t}), \tag{6.41}$$

[1] In Eq. (6.39) the notation o stands for an arbitrary small positive correction to 1/4. This correction is due to a power-law correction to the leading exponential behaviour. The same notation will be used in the rest of this chapter.

which result in the variance

$$\mathrm{Var}(T_{\mathrm{loc}}) = \frac{t}{2} - \frac{3}{4} + O(e^{-(1/4-o)t}). \tag{6.42}$$

Finally the limiting distribution (6.7) reads

$$p_{\mathrm{asym}}(T_{\mathrm{loc}}, t, v_0) = \frac{1}{\sqrt{\pi(t-3/2)}} \exp\left[-\frac{(2T_{\mathrm{loc}} - t + |v_0| - 1)^2}{4t-6}\right] + O(e^{-(1/4-o)t}). \tag{6.43}$$

Figure 6.2 shows the comparison of the limiting distribution (6.43) in leading order and the analytic expression (6.37). As we can see, the small deviations visible for short times disappear at large times. In the long time limit, from Eq. (6.39) we can evaluate the third and the fourth cumulants as (see Ref. [76])

$$K_3 = M_3(t,v_0) - 3M_1(t,v_0)M_2(t,v_0) + 2M_1^3(t,v_0) = 7/4 + O(e^{-(1/4-o)t}), \tag{6.44}$$

$$\begin{aligned} K_4 &= M_4(t,v_0) - 3M_2^2(t,v_0) - 4M_1(t,v_0)M_3(t,v_0) + 12M_1^2(t,v_0)M_2(t,v_0) - 6M_1^4(t,v_0) \\ &= -45/8 + O(e^{-(1/4-o)t}), \end{aligned} \tag{6.45}$$

which are both negligible compared to the first two moments [see Eqs. (6.40) and (6.41)] and thus are consistent with the limiting Gaussian distribution (6.43).

For the occupation time, it is straightforward to obtain the moments in the Laplace space by using the formula (6.29). The first two moments are given explicitly by

$$\widetilde{M}_1(s,v_0) = \frac{1}{2s^2}\begin{cases} 2 - e^{-(\sqrt{1+4s}-1)v_0/2} & \text{for } v_0 > 0, \\ e^{(\sqrt{1+4s}-1)v_0/2} & \text{for } v_0 < 0, \end{cases} \tag{6.46}$$

$$\widetilde{M}_2(s,v_0) = \frac{1}{4s^3}\begin{cases} 8 - \dfrac{5\sqrt{4s+1}+4v_0 s+1}{\sqrt{4s+1}} e^{-(\sqrt{4s+1}-1)v_0/2} & \text{for } v_0 > 0, \\ \dfrac{3\sqrt{4s+1}-1}{\sqrt{4s+1}} e^{(\sqrt{4s+1}-1)v_0/2} & \text{for } v_0 < 0. \end{cases} \tag{6.47}$$

As for the local time, one can evaluate the moments in the time domain by using the integral path as shown in Fig. 6.1 to obtain (see Ref. [71])

$$M_1(t,v_0) = \frac{t}{2} + \frac{v_0}{2} + O(e^{-(1/4-o)t}), \tag{6.48}$$

$$M_2(t,v_0) = \frac{t^2}{4} + \frac{1+v_0}{2}t + \frac{v_0^2-6}{4} + O(e^{-(1/4-o)t}). \tag{6.49}$$

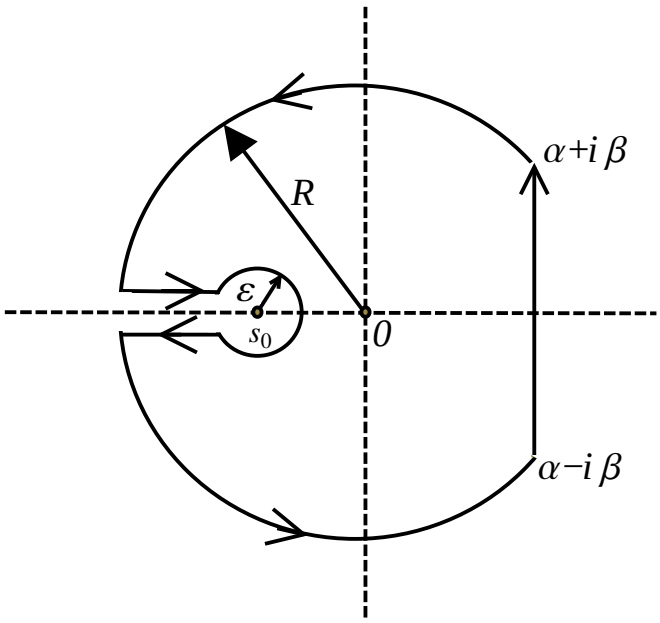

Figure 6.1: Integral path used to evaluate the inversion of Eq. (6.38). s_0 is the maximal singularity on the negative real axis.

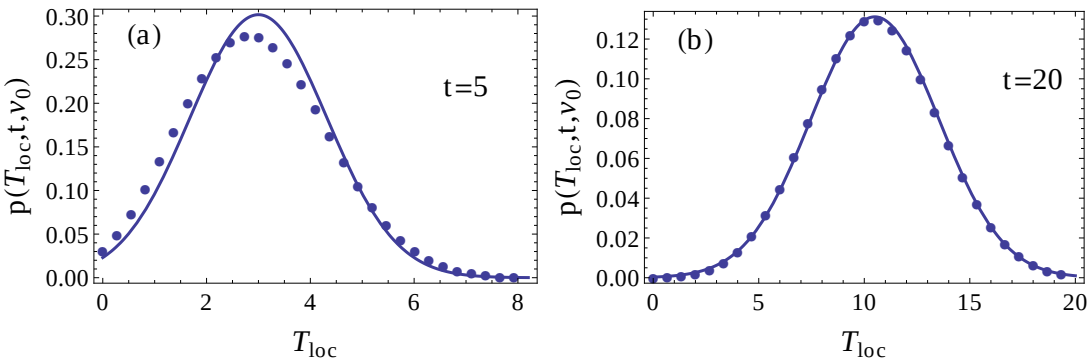

Figure 6.2: Local time distribution of the pure dry friction case for $v_0 = 0$ and two different times: (a) $t = 5$ and (b) $t = 20$. Lines correspond to the leading order limiting distribution (6.43), and points to the analytic expression (6.37).

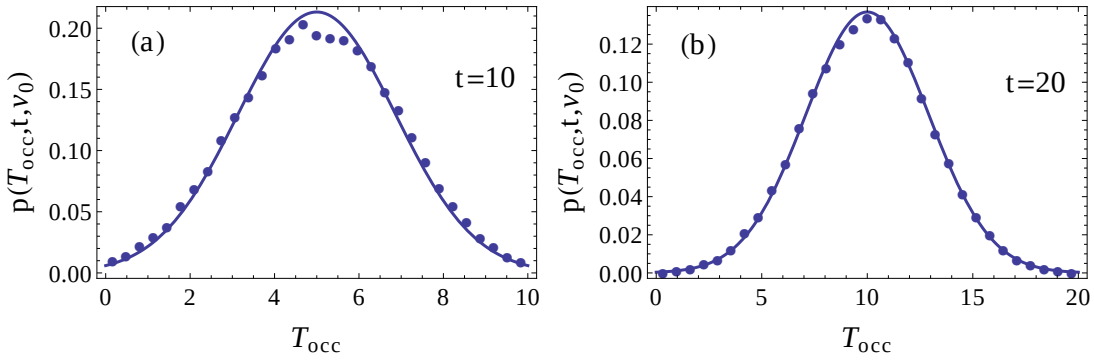

Figure 6.3: Occupation time distribution of the pure dry friction case for $v_0 = 0$ and two different times: (a) $t = 5$ and (b) $t = 20$. Lines correspond to the leading-order asymptotic distribution (6.51), and points to the Monte Carlo simulation of the Langevin equation (1.8) by using the Euler-Maruyama scheme with time-step $\Delta t = 0.0001$ and an ensemble of 10^6 realisations.

Thus the variance is

$$\mathrm{Var}(T_{\mathrm{occ}}) = \frac{t}{2} - \frac{3}{2} + O(e^{-(1/4-o)t}), \tag{6.50}$$

and the limiting distribution (6.7) reads

$$p_{\mathrm{asym}}(T_{\mathrm{occ}}, t, v_0) = \frac{1}{\sqrt{\pi(t-3)}} \exp\left[-\frac{(2T_{\mathrm{occ}} - t - v_0)^2}{4t-12}\right] + O(e^{-(1/4-o)t}). \tag{6.51}$$

As shown in Fig. 6.3, at large time this limiting distribution in leading order matches well with the Monte Carlo simulation of the corresponding Langevin equation by using the Euler-Maruyama scheme (see appendix A.2.1). In addition, using the formula (6.29) and the integral path as shown in Fig. 6.1, we can obtain in the long time limit that the third and the fourth cumulants in this case are

$$K_3 = O(e^{-(1/4-o)t}), \qquad K_4 = -45/4 + O(e^{-(1/4-o)t}), \tag{6.52}$$

which are both very small and are again in line with the limiting Gaussian distribution.

For the displacement, i.e., $U(v_0) = v_0$, it is obvious that a particular polynomial solution of Eq. (6.11) for $n = 1$ is

$$\widetilde{M}_1^p(s, v_0) = \frac{sv_0 - \sigma(v_0)}{s^3}. \tag{6.53}$$

Hence, the first moment can be obtained from Eqs. (6.19) and (6.20) to yield

$$\widetilde{M}_1(s,v_0) = \frac{sv_0 - \sigma(v_0)}{s^3} + \frac{\sigma(v_0)}{s^3} e^{(1-\sqrt{1+4s})|v_0|/2}. \tag{6.54}$$

Since

$$|v_0| e^{(1-\sqrt{1+4s})|v_0|/2} = -\sqrt{4s+1}\frac{\partial}{\partial s} e^{(1-\sqrt{1+4s})|v_0|/2}, \tag{6.55}$$

we can use the property (6.27) for $m = 1$ to construct a particular solution of Eq. (6.11) for $n = 2$ as

$$\widetilde{M}_2^p(s,v_0) = \frac{(2s|v_0| - 3)^2 + 8s + 3}{2s^5} + \frac{\sqrt{1+4s}v_0^2 + 2|v_0|}{s^3(1+4s)} e^{(1-\sqrt{1+4s})|v_0|/2}, \tag{6.56}$$

where the first term is the polynomial solution due to Eq. (6.53) and the second term is caused by the second term of Eq. (6.54). Then the second moment is determined by Eqs. (6.19) and (6.32), yielding

$$\widetilde{M}_2(s,v_0) = \widetilde{M}_2^p(s,v_0) - \frac{(11s+3)\left(\sqrt{4s+1}+1\right)}{s^5(4s+1)} e^{(1-\sqrt{1+4s})|v_0|/2}. \tag{6.57}$$

Therefore, using the integral path as shown in Fig. 6.1 we obtain in the long time limit that (see Ref. [71])

$$M_1(t,v_0) = v_0(1 + |v_0|/2) + O(e^{-(1/4-o)t}), \tag{6.58}$$

$$M_2(t,v_0) = 10t + v_0^4/4 + 5|v_0|^3/3 + 5v_0^2 - 54 + O(e^{-(1/4-o)t}). \tag{6.59}$$

Thus the variance is given by

$$\mathrm{Var}(T_{\mathrm{dis}}) = 10t + 2|v_0|^3/3 + 4v_0^2 - 54 + O(e^{-(1/4-o)t}), \tag{6.60}$$

and the limiting distribution reads

$$p_{\mathrm{asym}}(T_{\mathrm{dis}},t,v_0) = \frac{1}{\sqrt{2\pi\sigma^2}} \exp\left[-\frac{(T_{\mathrm{dis}} - v_0 - v_0|v_0|/2)^2}{2\sigma^2}\right] + O(e^{-(1/4-o)t}), \tag{6.61}$$

where

$$\sigma^2 = 10t + 2|v_0|^3/3 + 4v_0^2 - 54. \tag{6.62}$$

As shown in Fig. 6.4, at large time this limiting distribution in leading order matches well with the Monte Carlo simulation of the corresponding Langevin equation. In this case, the higher moments can be obtained as well if one uses the properties (6.55) and

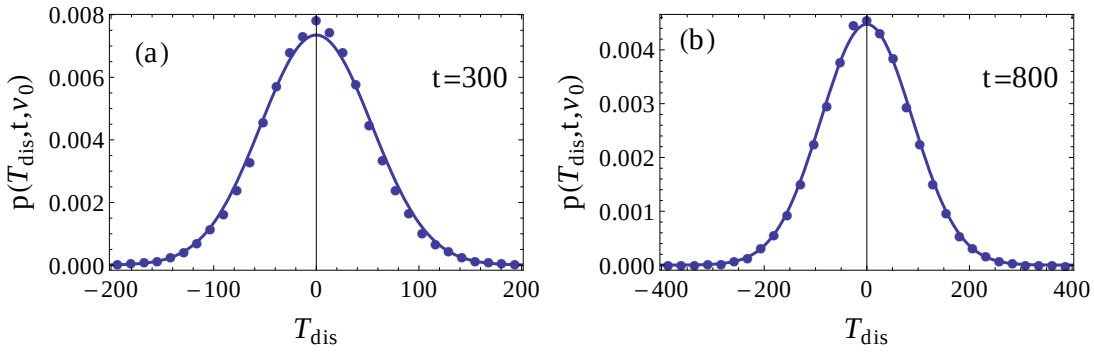

Figure 6.4: Displacement distribution of the pure dry friction case for $v_0 = 0$ and two different times: (a) $t = 300$ and (b) $t = 800$. Lines correspond to the leading-order asymptotic distribution (6.61), and points to the Monte Carlo simulation of the Langevin equation (1.8) by using the Euler-Maruyama scheme with time-step $\Delta t = 0.001$ and an ensemble of 10^6 realisations (see appendix A.2.1).

(6.27)[2]. A quite tedious but straightforward computation (using Mathematica) finally results in that the third and the fourth cumulants in the long time limit read

$$K_3 = \begin{cases} O(1) & \text{for } v_0 \neq 0, \\ 0 & \text{for } v_0 = 0, \end{cases} \qquad K_4 = 21120t + O(1), \tag{6.63}$$

which show that the fourth cumulant depends linearly on time. Hence, even though the displacement around mean is Gaussian in the long time limit the entire distribution is not strictly Gaussian.

6.4 Dry and viscous friction case

For the full model (1.2) without bias ($b = 0$), i.e., the dry and viscous friction case, we set $\gamma = D = 1$ without loss of generality (see Sec. 4.2 and also appendix A.3.3). Hence the dry and viscous friction case can be written as the form (2.12) with a stable potential

$$\Phi(v) = (|v| + \mu)^2/2. \tag{6.64}$$

[2]The main idea is to use the property (6.55) to express the right hand side of Eq. (6.11) only in terms of a polynomial in v_0 and the sum of derivatives of $\varphi(s, v_0)$ with coefficients that are independent of v_0. Then it is easy to find separately a particular solution for the polynomial by matching coefficients and a particular solution for the term including derivatives of $\varphi(s, v_0)$ by using the property (6.27).

The fundamental solution of the homogeneous ODE (6.18) is

$$\varphi(s, v_0) = e^{(|v_0|+\mu)^2/4} D_{-s}(|v_0| + \mu), \tag{6.65}$$

which vanishes for $\mathrm{Re}(s) > 0$ when $v_0 \to \pm\infty$. Here the function $D_\nu(z)$ denotes the parabolic cylinder function (see appendix A.9).

For the local time, we have from Eqs. (6.21) and (6.22) that

$$\widetilde{M}_n(s, v_0) = \frac{n!}{2^n s^{n+1}} \left(\frac{D_{-s}(\mu)}{D_{-s-1}(\mu)} \right)^{n-1} \frac{e^{(|v_0|+\mu)^2/4} D_{-s}(|v_0| + \mu)}{e^{\mu^2/4} D_{-s-1}(\mu)}. \tag{6.66}$$

For real argument z the parabolic cylinder function fulfills $D_\nu(z) \neq 0$ for any ν with nonvanishing imaginary part and $D_\nu(z) > 0$ for any negative real values of ν (see appendix A.9). Hence, we conclude that all the singularities of Eq. (6.66) lie on the non-positive real axis as $\mu > 0$. In addition, all these singularities are poles. The largest negative pole which determines the asymptotic properties of the moments is given by

$$s_0 = \max\{s : D_{-s-1}(\mu) = 0\} < -1. \tag{6.67}$$

The dependence of this value on the dry friction coefficient μ is displayed in Fig. 6.5 and turns out to be a monotonically decreasing function. Thus it is straightforward to evaluate Eq. (6.66) to obtain

$$M_n(t, v_0) = \frac{e^{(|v_0|+\mu)^2/4}}{2^n e^{\mu^2/4}} \frac{\partial^n}{\partial s^n} \left[\left(\frac{D_{-s}(\mu)}{D_{-s-1}(\mu)} \right)^{n-1} \frac{D_{-s}(|v_0| + \mu)}{D_{-s-1}(\mu)} e^{st} \right] \Bigg|_{s=0} + O(e^{(s_0+o)t}), \tag{6.68}$$

where $s_0 + o < 0$. In particular, the first two moments in the long time limit are given explicitly as follows:

$$M_1(t, v_0) = \frac{D_0(\mu) t}{2D_{-1}(\mu)} + \frac{D_0(\mu)}{2D_{-1}(\mu)} \left(\frac{D_{-1}^{(1,0)}(\mu)}{D_{-1}(\mu)} - \frac{D_0^{(1,0)}(|v_0| + \mu)}{D_0(|v_0| + \mu)} \right) + O(e^{(s_0+o)t}), \tag{6.69}$$

$$M_2(t, v_0) = \frac{D_0^2(\mu) t^2}{4D_{-1}^2(\mu)} + \frac{D_0^2(\mu)}{2D_{-1}^2(\mu)} \left(2\frac{D_{-1}^{(1,0)}(\mu)}{D_{-1}(\mu)} - \frac{D_0^{(1,0)}(\mu)}{D_0(\mu)} - \frac{D_0^{(1,0)}(|v_0| + \mu)}{D_0(|v_0| + \mu)} \right) t + O(1), \tag{6.70}$$

where the notation $D_\Lambda^{(1,0)}(z)$ denotes the derivative of the parabolic cylinder function with respect to its index, i.e., $\frac{\partial}{\partial \nu} D_\nu(z)\big|_{\nu=\Lambda}$. Thus we obtain the variance in leading

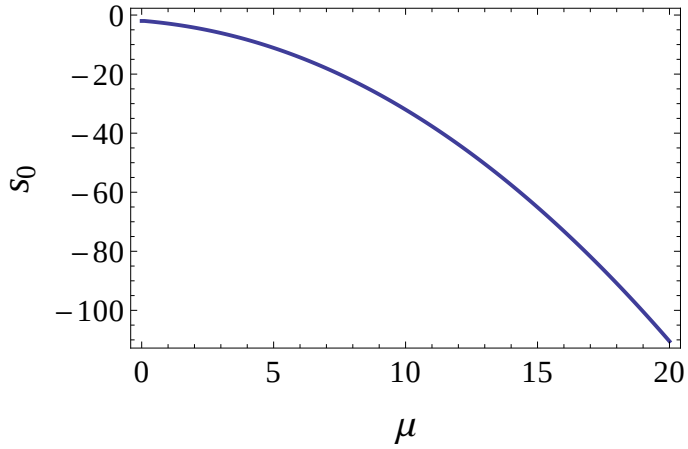

Figure 6.5: Maximal solution $s = s_0$ (6.67) of the equation $D_{-s-1}(\mu) = 0$ as a function of μ.

order that

$$\mathrm{Var}(T_{\mathrm{loc}}) = \frac{D_0^2(\mu)}{2D_{-1}^2(\mu)} \left(\frac{D_{-1}^{(1,0)}(\mu)}{D_{-1}(\mu)} - \frac{D_0^{(1,0)}(\mu)}{D_0(\mu)} \right) t + O(1). \tag{6.71}$$

Here we have stated the results for the second moment and the variance up to $O(1)$ as the constant term is too cumbersome to write down explicitly. Of course, including such a term the expression is correct up to $O(e^{(s_0+o)t})$ as that of the first moment. The same reasoning will apply in the rest of this section. As shown in Fig. 6.6, at large time the corresponding limiting distribution (6.7) in leading order matches well with the numerical evaluation of Eq. (6.24). In the long time limit, we can check from Eq. (6.68) that the third and the fourth cumulants satisfy

$$K_3 = c_3(\mu)t + O(1), \qquad K_4 = c_4(\mu)t + O(1), \tag{6.72}$$

where the coefficients $c_3(\mu)$ and $c_4(\mu)$ are both independent of the initial value v_0 and can be computed explicitly by using Mathematica. Since the expressions are too cumbersome to write down, we only give a graphical discussion here. Intuitively, we expect that if the dry friction term dominates the viscous friction force then the cumulants of the local time in this case will behave like those of the pure dry friction case [see Eqs. (6.44) and (6.45)], i.e., the coefficients $c_3(\mu)$ and $c_4(\mu)$ in Eq. (6.72) tend to zero for large μ. Indeed, numerical evaluation of the coefficients confirms what we expect intuitively (see Fig. 6.7).

For the occupation time, the first two moments in the Laplace space can be obtained

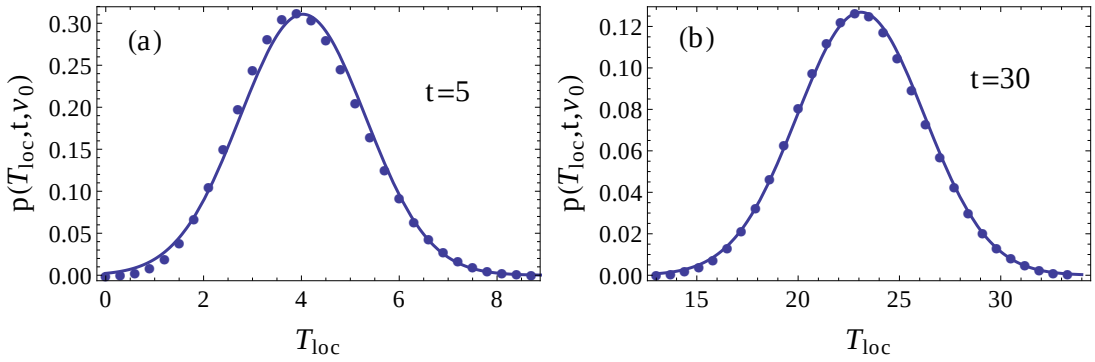

Figure 6.6: Local time distribution of the dry and viscous friction case for $v_0 = 0$ and two different times: (a) $t = 5$ and (b) $t = 30$. Lines corresponds to the leading-order limiting distribution (6.43), and points to the numerical evaluation of Eq. (6.24).

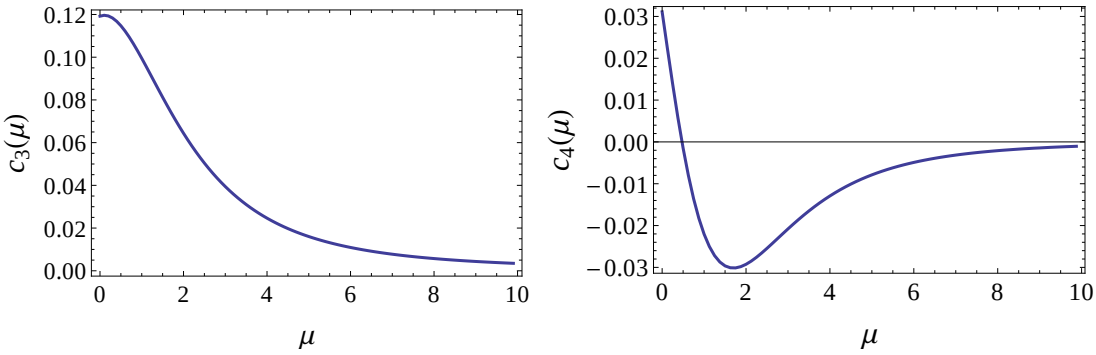

Figure 6.7: Coefficients $c_3(\mu)$ and $c_4(\mu)$ in the third and the fourth cumulants of the local time of the dry and viscous friction case [see Eq. (6.72)].

easily from Eq. (6.29) as follows,

$$\widetilde{M}_1(s,v_0)=\frac{1}{2s^2D_{-s}(\mu)}\begin{cases}2D_{-s}(\mu)-e^{v_0^2/4+\mu v_0/2}D_{-s}(\mu+v_0) & \text{for } v_0>0,\\ e^{v_0^2/4-\mu v_0/2}D_{-s}(\mu-v_0) & \text{for } v_0<0,\end{cases} \tag{6.73}$$

$$\begin{aligned}\widetilde{M}_2(s,v_0)=&\frac{e^{v_0^2/4+\mu v_0/2}D_{-s}(\mu+v_0)}{2s^3D_{-s-1}(\mu)D_{-s}^2(\mu)}\Big\{D_{-s}(\mu)\left[sD_{-s-1}^{(1,0)}(\mu)-2D_{-s-1}(\mu)\right]\\ &+D_{-s-1}(\mu)\left[sD_{-s}^{(1,0)}(\mu)-D_{-s}(\mu)\right]\Big\}+\frac{2}{s^3}\\ &-\frac{e^{v_0^2/4+\mu v_0/2}}{s^2D_{-s}(\mu)}D_{-s}^{(1,0)}(\mu+v_0)\quad\text{for } v_0>0,\end{aligned} \tag{6.74}$$

$$\begin{aligned}\widetilde{M}_2(s,v_0)=&\frac{e^{v_0^2/4-\mu v_0/2}D_{-s}(\mu-v_0)}{2s^3D_{-s-1}(\mu)D_{-s}^2(\mu)}\Big\{D_{-s}(\mu)\Big[sD_{-s-1}^{(1,0)}(\mu)+D_{-s-1}(\mu)\Big]\\ &-sD_{-s-1}(\mu)D_{-s}^{(1,0)}(\mu)\Big\}\quad\text{for } v_0<0.\end{aligned} \tag{6.75}$$

As for the local time, all the singularities of these two moments lie on the non-positive real axis. The maximal negative singularity is s_0+1, where s_0 is defined in Eq. (6.67) (see also Fig. 6.5). Hence, we obtain in the long time limit that

$$M_1(t,v_0)=\frac{t}{2}+\frac{\sigma(v_0)}{2}\left(\frac{D_0^{(1,0)}(|v_0|+\mu)}{D_0(|v_0|+\mu)}-\frac{D_0^{(1,0)}(\mu)}{D_0(\mu)}\right)+O(e^{(s_0+1+o)t}), \tag{6.76}$$

$$\begin{aligned}M_2(t,v_0)=&\frac{t^2}{4}+\frac{\sigma(v_0)}{2}\left(\frac{D_0^{(1,0)}(|v_0|+\mu)}{D_0(|v_0|+\mu)}-\frac{D_0^{(1,0)}(\mu)}{D_0(\mu)}\right)t\\ &+\frac{1}{2}\left(\frac{D_{-1}^{(1,0)}(\mu)}{D_{-1}(\mu)}-\frac{D_0^{(1,0)}(\mu)}{D_0(\mu)}\right)t+O(1).\end{aligned} \tag{6.77}$$

Therefore, the corresponding variance of the occupation time reads

$$\mathrm{Var}(T_{\mathrm{occ}})=\frac{1}{2}\left(\frac{D_{-1}^{(1,0)}(\mu)}{D_{-1}(\mu)}-\frac{D_0^{(1,0)}(\mu)}{D_0(\mu)}\right)t+O(1). \tag{6.78}$$

As shown in Fig. 6.8, at large time the corresponding limiting distribution (6.7) matches well with the Monte Carlo simulation of the corresponding Langevin equation. In the long time limit, we can check from Eq. (6.29) that the third and the fourth cumulants satisfy

$$K_3=O(1),\qquad K_4=c_4(\mu)t+O(1), \tag{6.79}$$

where $c_4(\mu)$ is independent of the initial value v_0. As for the local time, for large μ the cumulants (6.79) in this case should behave like those of the pure dry friction case [see

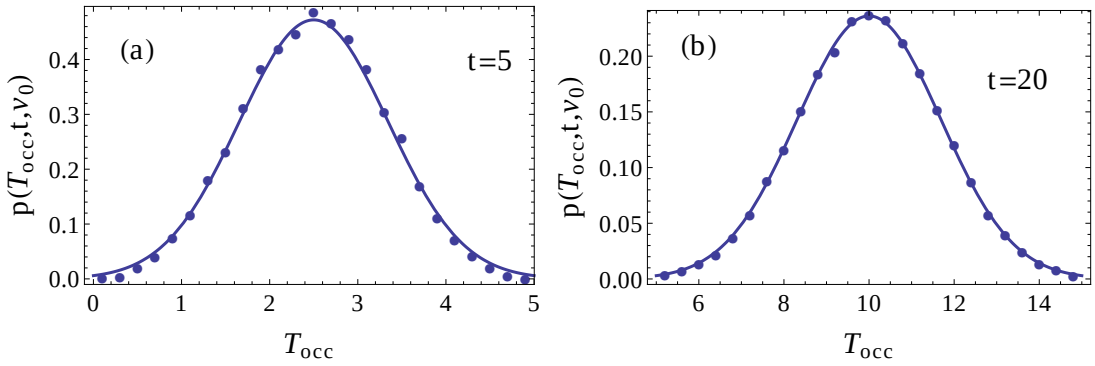

Figure 6.8: Occupation time distribution of the dry and viscous friction case for $v_0 = 0$, $\mu = 1$ and two different times: (a) $t = 5$ and (b) $t = 20$. Lines correspond to the leading-order asymptotic distribution (6.7), and points to the Monte Carlo simulation of the corresponding Langevin equation by using the Euler-Maruyama scheme with time-step $\Delta t = 0.0001$ and an ensemble of 10^6 realisations (see appendix A.2.1).

Eq. (6.52), i.e., the coefficient $c_4(\mu)$ in Eq. (6.79) decays to zero]. Indeed, numerical evaluation of this coefficient confirms our expectation (see Fig. 6.9).

For the displacement, one particular polynomial solution of Eq. (6.11) for $n = 1$ is

$$\widetilde{M}_1^p(s, v_0) = \frac{sv_0 - \mu\sigma(v_0)}{s^2(s+1)}. \tag{6.80}$$

Hence the first moment is given by Eqs. (6.19) and (6.32):

$$\widetilde{M}_1(s, v_0) = \frac{sv_0 - \mu\sigma(v_0)}{s^2(s+1)} + \mu\sigma(v_0)\frac{e^{(|v_0|+\mu)^2/4} D_{-s}(|v_0|+\mu)}{s^2(s+1)e^{\mu^2/4} D_{-s}(\mu)}. \tag{6.81}$$

Using the recurrence relation of the parabolic cylinder function [see Eq. (A.80)], we have

$$\begin{aligned} |v_0| e^{(|v_0|+\mu)^2/4} D_{-s}(|v_0|+\mu) &= e^{(|v_0|+\mu)^2/4}\big[D_{-s+1}(|v_0|+\mu) - sD_{-s-1}(|v_0|+\mu) \\ &\quad -\mu D_{-s}(|v_0|+\mu)\big] \\ &= \varphi(s-1, v_0) - s\varphi(s+1, v_0) - \mu\varphi(s, v_0). \end{aligned} \tag{6.82}$$

Then using the property (6.27) and the following properties of the operator L_s [see Eqs. (6.25) and (6.26)],

$$L_s\varphi(s+m, v_0) = m\varphi(s+m, v_0) \qquad \text{for any } m, \tag{6.83}$$

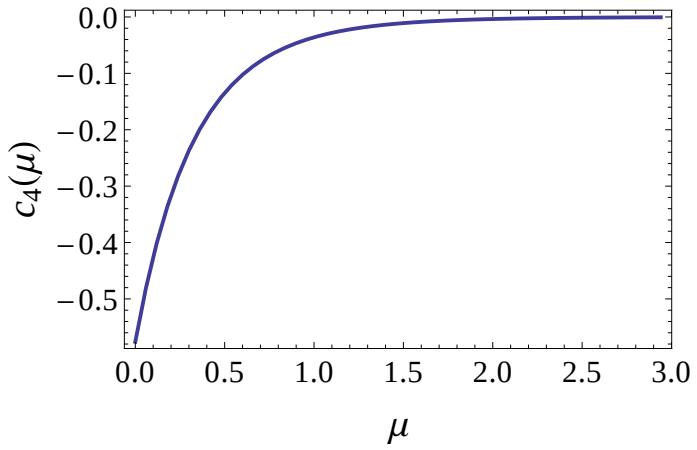

Figure 6.9: Coefficient $c_4(\mu)$ in the fourth cumulant of the occupation time of the dry and viscous friction case [see Eq. (6.79)].

we can construct a particular solution of Eq. (6.11) for $n = 2$ as

$$\begin{aligned}\widetilde{M}_2^p(s,v_0) = \frac{2\mu e^{(|v_0|+\mu)^2/4}}{s^2(s+1)e^{\mu^2/4}D_{-s}(\mu)}\Big[&D_{-s+1}(|v_0|+\mu)+sD_{-s-1}(|v_0|+\mu)\\ &+\mu\frac{\partial}{\partial s}D_{-s}(|v_0|+\mu)\Big]+\frac{2v_0^2}{s(s+1)(s+2)}-\frac{2\mu(3s+2)|v_0|}{s^2(s+1)^2(s+2)}\\ &+\frac{4(s+\mu^2)(s+1)+2\mu^2 s}{s^3(s+1)^2(s+2)},\end{aligned} \tag{6.84}$$

where the first term is caused by the second term of Eq. (6.81) and the last three terms are the polynomial solution due to Eq. (6.80). Thus the second moment is determined by Eqs. (6.19) and (6.32):

$$\begin{aligned}\widetilde{M}_2(s,v_0) = \widetilde{M}_2^p(s,v_0) - &\frac{2\mu e^{(|v_0|+\mu)^2/4}D_{-s}(|v_0|+\mu)}{s^3(s+1)^2(s+2)e^{\mu^2/4}D_{-s}(\mu)D_{-s-1}(\mu)}\\ &\times\Big\{\mu(s+1)(s+2)\Big[D_{-s-1}(\mu)-sD^{(1,0)}_{-s-1}(\mu)\Big]\\ &+s(s^2+2s+2)D_{-s}(\mu)+s(s+1)^2(s+2)D_{-s-2}(\mu)\Big\}.\end{aligned} \tag{6.85}$$

In this case, by expansion we can check that $s = -1$ and $s = -2$ are removable singularities for the first two moments and the maximal negative singularity is still given by $s_0 + 1$, where s_0 has been introduce in Eq. (6.67) (see also Fig. 6.5). Hence, we can evaluate the corresponding inverse Laplace transforms to obtain in the long time limit

that

$$M_1(t,v_0) = v_0 + \mu\sigma(v_0)\left(\frac{D_0^{(1,0)}(\mu)}{D_0(\mu)} - \frac{D_0^{(1,0)}(|v_0|+\mu)}{D_0(|v_0|+\mu)}\right) + O(e^{(s_0+1+o)t}), \quad (6.86)$$

$$M_2(t,v_0) = 2\left[1+\mu^2\left(\frac{D_{-1}^{(1,0)}(\mu)}{D_{-1}(\mu)} - \frac{D_0^{(1,0)}(\mu)}{D_0(\mu)}\right) - 2\mu\frac{D_{-2}(\mu)}{D_{-1}(\mu)}\right]t + O(1). \quad (6.87)$$

Therefore the variance is

$$\mathrm{Var}(T_{\mathrm{dis}}) = 2\left[1+\mu^2\left(\frac{D_{-1}^{(1,0)}(\mu)}{D_{-1}(\mu)} - \frac{D_0^{(1,0)}(\mu)}{D_0(\mu)}\right) - 2\mu\frac{D_{-2}(\mu)}{D_{-1}(\mu)}\right]t + O(1). \quad (6.88)$$

As shown in Fig. 6.11, at large time the corresponding limiting distribution (6.7) in leading order matches well with the Monte Carlo simulation of the corresponding Langevin equation. In this case, the higher moments can also be obtained if one uses the properties (6.27) and (6.83) of the operator L_s as well as the recurrence relation of the parabolic cylinder function (6.82) (see also the footnote on page 104). But we should resort to software to do the corresponding symbolic calculations. Finally, we confirm that the third and the fourth cumulants satisfy

$$K_3 = \begin{cases} O(1) & \text{for } v_0 \neq 0, \\ 0 & \text{for } v_0 = 0, \end{cases} \qquad K_4 = c_4(\mu)t + O(1), \quad (6.89)$$

which are consistent with those of the pure dry friction case [see Eq. (6.63)]. Here the coefficient $c_4(\mu)$, which is shown in Fig. 6.10 as a function of μ, does not depend on the initial value v_0. Again, the entire distribution in the long time limit is not strictly Gaussian as the fourth cumulant depends linearly on time.

In addition, to compare our analytical results with that obtained in Ref. [70] by solving the corresponding Fokker-Planck equation numerically, we need to specialise our general expressions to the case $v_0 = 0$ and translate our expressions, given in non-dimensional units, to the original scale (1.2) via [see appendix A.3.3]

$$\mu \to \mu/\sqrt{D\gamma}, \qquad M_2(t,v_0) \to DM_2(\gamma t, \sqrt{\gamma/D}v_0)/\gamma. \quad (6.90)$$

As shown in Fig. 6.12, one can see that the figures of the second moment and the distribution recover the numerical results presented in Ref. [70] (see Figs. 5 and 9 therein).

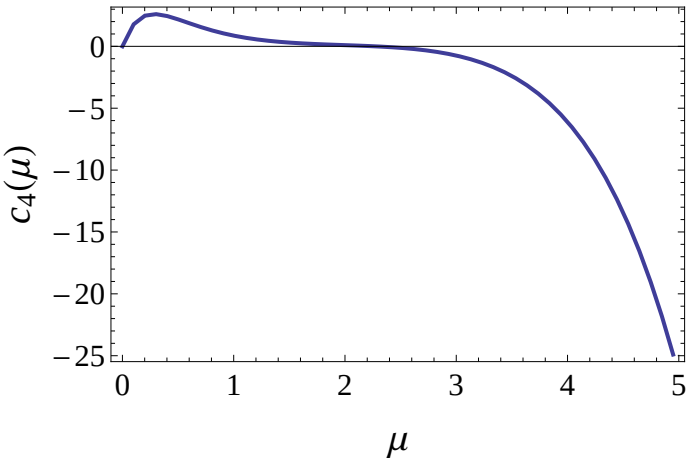

Figure 6.10: Coefficient $c_4(\mu)$ in the fourth cumulant of the displacement of the dry and viscous friction case [see Eq. (6.89)].

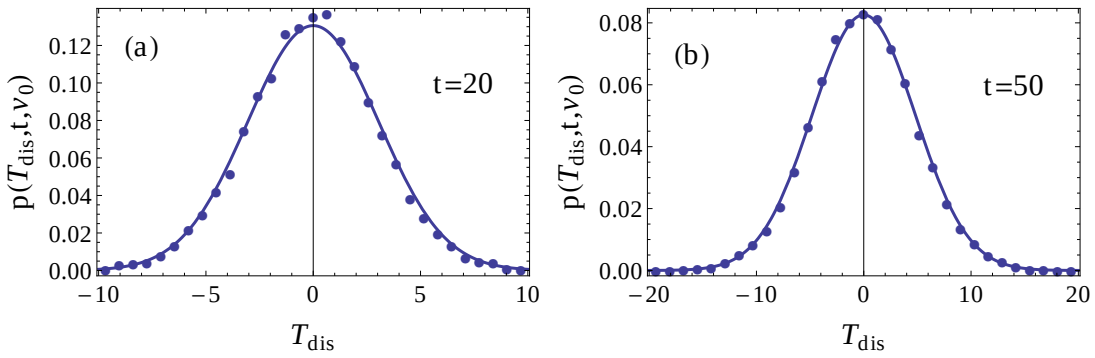

Figure 6.11: Displacement distribution of the dry and viscous friction case for $v_0 = 0$, $\mu = 1$ and two different times: (a) $t = 20$ and (b) $t = 50$. Lines correspond to the leading-order asymptotic distribution of Eq. (6.7), and points to the Monte Carlo simulation of the corresponding Langevin equation by using the Euler-Maruyama scheme with time-step $\Delta t = 0.001$ and an ensemble of 10^6 realisations (see appendix A.2.1).

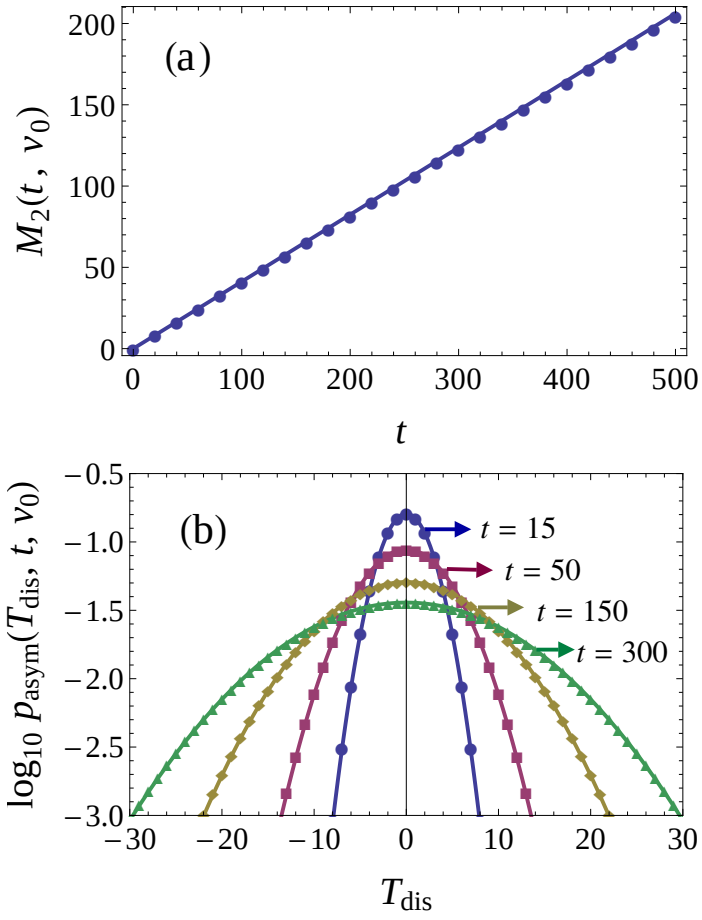

Figure 6.12: Analytic results of the full model without bias in the original scaling system (1.2) for $\gamma = 1$ and $v_0 = 0$. (a) The second moment in leading order obtained from Eq. (6.87) via the transforms (6.90); (b) the limiting displacement distribution in leading order obtained from Eqs. (6.7), (6.86) and (6.88) via the transforms (6.90). Lines correspond to the results of $\mu = 6$ and $D = 5.4$, and points to $\mu = 1.1$ and $D = 1$. These two sets of arguments are properly chosen according to a fluctuation dissipation relation presented in [70], ensuring that the numerical results coincide with each other.

6.5 Summary of chapter

In this chapter, we have extended the backward Fokker-Planck technique developed in Ref. [63] to compute stochastic properties of a general support functional. For a generic Langevin equation, the recursive differential equation for the moments of functionals has been derived and solutions have been provided for the local time and the occupation time in terms of the solution of the corresponding homogeneous equation. In addition, the distribution of the local time in the Laplace space has been shown to be fully determined by the Laplace transform of the first moment.

The developed results have been applied to consider functionals of the dry friction model. In particular, three of the simplest functionals have been considered, i.e., the local time, the occupation time and the displacement, which allow us to obtain some analytic results. The moments of these three functionals have been shown explicitly in the Laplace space for the pure dry friction case and the dry and viscous friction case, respectively. It is interesting to observe that in the long time limit the first two moments satisfy $M_1(t, v_0) \sim t$ and $M_2(t, v_0) \sim t^2$ identically for the local time and the occupation time, and $M_1(t, v_0) = O(1)$ and $M_2(t, v_0) \sim t$ for the displacement. Intuitively, the difference between them should not come as a surprise as the local time and occupation time are nonnegative while the displacement can be negative. However, in the dry friction case all the variances for the three functionals satisfy $\mathrm{Var}(T) \sim t$ in the long time limit.

Since the dry friction model has a stable potential, the distributions of the three functionals around means are simply Gaussian distributions in the long time limit, which are determined by the first two corresponding moments. In addition, these limiting distributions have been shown to match well with the analytic results of the local time and the results of Monte Carlo simulations of the occupation time and the displacement, respectively. The results obtained here for the dry and viscous friction case can be extended straightforwardly to the full model (1.2) with bias term, in which case we may analyse stick-slip transitions depending on the bias.

Chapter 7

Concluding remarks and outlook

Conclusions of this thesis

In this thesis, we have investigated dynamical properties of piecewise-smooth stochastic systems with respect to weak-noise approximations, FPT problems and some simple functionals. In particular, we took the model of Brownian motion with dry friction as an example to illustrate some interesting phenomena of the piecewise-smooth cases. The most important results of this thesis are concluded as follows.

In chapter 3, we have used the pure dry friction model as an example to study the validity and accuracy of weak-noise approximations for piecewise-smooth stochastic systems. Our study shows that the conclusion of the weak-noise approximation is ambivalent. While the weak-noise approximation, if some heuristics are used, is able to reproduce main features of piecewise-smooth systems, its predictive features are limited as one usually does not have a priori control over higher order terms and as one deals with expressions that are not smooth. Nevertheless, the study of the pure dry friction model shows that we can put some confidence in formal expansions if results are considered with some common sense, i.e., if some heuristic principles are applied. To avoid the singularity caused by the dry friction, we have also regularised the discontinuity with a nonlinear smooth drift to obtain a smooth version of SDE. We have shown with simulation results that the weak-noise limit of the regularised SDE captures the main features of the piecewise-smooth SDE, even though the weak-noise limit does not commute with the limit of the regularised model approaching the singular case. For this regularised SDE, which is interesting in itself, we have studied the quasi-potential associated with

the propagator in a largely analytical way.

In chapter 4 we switched our investigation to the impact of discontinuities on FPT problems of piecewise-smooth stochastic systems. In order to obtain some analytic results, we confined our investigation to the model of Brownian motion with dry friction. We have provided analytic solutions to the FPT problem of this dry friction model using two different but closely related approaches which are based on eigenfunction decompositions on the one hand and on the backward Kolmogorov equation on the other. For the pure dry friction case, we have found an unexpected phase transition phenomenon of the spectrum related to the exit point. Depending on the exit point, there exists an isolated eigenvalue or not. This phase transition phenomenon finally results in different tail decay rates of the FPT distribution. For the full model, we have observed in the spectrum two additional phase transitions which are the stick-slip transition and the transition to ballistic exit. As we know, these transitions are induced by the dry friction force. We expect that similar phase transitions can be found in other piecewise-smooth stochastic systems.

Immediately after chapter 4, we investigated in chapter 5 the MVD till the FPT. We have obtained the analytic solution of the maximum velocity till the FPT of the model of Brownian motion with dry friction. For the considered FPT problem, a kink may occur in the MVD depending on the sign of the initial velocity. This kink is induced by the dry friction force, which is discontinuous at the origin. We have used this particular problem as a testbed for piecewise-smooth stochastic systems and to illustrate how to handle discontinuities in a stochastic setup which is often referred to when extreme events, here the maximum velocity, are at stake.

Finally, in chapter 6 we studied a more challenging problem, i.e., functionals of piecewise-smooth stochastic systems. As in the previous chapters, in order to obtain some analytic results we have taken the dry friction model as a starting example to address this problem. For this model, we have considered three of the simplest functionals, i.e., the local time, the occupation time and the displacement. By generalising the backward Fokker-Planck technique, we have developed a recursive differential equation for the moments of arbitrary support functionals of a generic Langevin equation. For the local time and the occupation time, we have derived in the Laplace space the general formulae of the moments, which only depends on the solution of the corresponding homogeneous equation of the recursive moment equation. In addition, the local time distribution in the Laplace space has also been shown to be fully determined by its

first moment. We have applied the results to consider the dry friction model. For this model, we have shown that the moments of the local time, the occupation time and the displacement can be obtained explicitly in the Laplace domain. In the long time limit, the behaviour of the moments has also been analysed asymptotically. For this dry friction model with a stable potential, we have obtained the limiting distributions of the three considered functionals around means, which are all Gaussian. In addition, these limiting distributions are shown to match well with the analytic results of the local time and the results of Monte Carlo simulations of the occupation time and the displacement, respectively.

Some open problems

The availability of analytic results for high dimensional stochastic models is rather limited, contrary to the one-variable case. Even the computation of the stationary distribution is often a challenge if detailed balance is violated, and dynamical quantities, like correlations or exit probabilities, are certainly out of reach. As examples, some interesting problems closely related to this thesis are listed below.

(1) It would be interesting to obtain the exact propagator of the displacement of the dry friction model (1.2) with a piecewise-smooth potential. For this purpose, we can try to solve the two-dimensional Fokker-Planck equation

$$\frac{\partial}{\partial t}p(x,v,t|x_0,v_0,0) = -v\frac{\partial}{\partial x}p(x,v,t|x_0,v_0,0) + \frac{\partial}{\partial v}[\Phi'(v)p(x,v,t|x_0,v_0,0)] + \frac{\partial^2}{\partial v^2}p(x,v,t|x_0,v_0,0), \tag{7.1}$$

where x stands for the displacement and v for the velocity, $\Phi(v)$ is stated in Eq. (1.7) with a non-smooth point at $v = 0$. Here $p(x,v,t|x_0,v_0,0)$ represents the joint probability density that $x(t) = x$ and $v(t) = v$ given the initial conditions $x(0) = x_0$ and $v(0) = v_0$. This problem can be regarded as a simple model to investigate the impact of discontinuities on high dimensional variables in a stochastic setup. However, this two-dimensional problem is much more difficult to solve than the one-dimensional case. Moreover, since the potential $\Phi(v)$ does not depend on x, stationary joint distribution does not exist in this case. Alternatively, we can try to analyse the backward Fokker-Planck equation (6.4) directly, but the solution of which is also difficult to obtain.

(2) To investigate the validity of the weak-noise approximation of the pure dry friction model with inertia term. For this purpose, we can also use the path integral representation of the propagator and the saddle-point approximation. In this case, the propagator in terms of path integral reads

$$p(x_t, v_t, t|x_0, v_0, 0) = \int_{(v_0,0)}^{(v_t,t)} \mathcal{D}[v] J[v] \mathrm{e}^{-\frac{1}{4D}\int_0^t [\dot{v}+\mu\sigma(v)]^2 ds} \delta\left(x_t - x_0 - \int_0^t v(s)ds\right), \tag{7.2}$$

i.e., the path integral (3.2) with the constraint

$$\int_0^t v(s)ds = x_t - x_0. \tag{7.3}$$

Here the Jacobian term

$$J[v] = \exp\left(\mu \int_0^t \delta(v)ds\right) \tag{7.4}$$

comes from the transformation $\xi(t) \to v(t)$. The saddle-point approximation of the path integral (7.2) may be analysed similarly with Eq. (3.2). For the details of how to find the optimal path of Eq. (7.2), we refer to Ref. [22]. For instance, at the lowest order we have to minimise the action

$$S^{(0)}[v] = \int_0^t [\dot{v}(s) + \mu\sigma(v)]^2 ds \tag{7.5}$$

subjected to the boundary conditions

$$v(0) = v_0, \qquad v(t) = v_t \tag{7.6}$$

and the constraint (7.3). This problem can be solved by using the method of Lagrangian multiplier. In a preliminary study of this problem, we found that the optimal paths are not straight but parabolic. The challenge here is that the optimal indirect paths are not available analytically as in this case the t_1 and t_2 like those of the one-dimensional case [see Eq. (3.9)] cannot be determined exactly. In addition, since an analytic solution of the propagator is not available in this case, it is hard to check whether the weak-noise approximation is effective or not for this two-dimensional problem.

(3) To obtain analytic results for the FPT distribution with respect to the displacement. Suppose that we put a small object on an one-dimensional horizontal table with finite length L. And the velocity of the object obeys the dry friction model (1.2) without

bias. Then it would be very interesting to know the mean time when this object falls down the table. In fact, here we have to solve a FPT problem for the displacement. Suppose the table is on the interval $[0, L]$ and the initial displacement of the object is $x(0) = x_0 \in (0, L)$. Then we have to solve the two-dimensional Fokker-Planck equation (7.1) with boundary conditions (see Ref. [76])

$$p(0, v, t|x_0, v_0, 0) = 0 \qquad \text{for } v > 0, \tag{7.7}$$

$$p(L, v, t|x_0, v_0, 0) = 0 \qquad \text{for } v < 0. \tag{7.8}$$

To the best of my knowledge there is no exact analytic solution to the problem (7.1), (7.7) and (7.8) so far [67]. Even for the pure diffusion process, i.e., $\Phi(v) = 0$ in Eq. (7.1), only the mean FPT of the displacement is available in an asymptotic way (see Refs. [67, 68]). While one of course could proceed a numerical solution of this particular problem, the focus here would be the impact of discontinuities on the two-dimensional FPT problem, e.g., transition phenomenon related to the exit point, as in the one-dimensional case. Since this phenomenon is hard to observe numerically, it is desirable to obtain an analytic solution to this two-dimensional FPT problem. In addition, it would be interesting to have some experimental data for this FPT problem with respect to the displacement.

(4) Throughout this thesis, we have only analysed the interrelation between Gaussian white noise and discontinuity. The results of the interrelation of dry friction and other kinds of noise are very limited. As far as I know, some analytic results of this topic are only available for the model with dry friction and Poissonian shot-noise [7, 8]. Thus, it is meaningful to study the impact of discontinuities on other kinds of noise. For instance, we can replace the Gaussian white noise $\xi(t)$ in Eq. (1.2) with an Ornstein-Uhlenbeck noise $\eta(t)$ characterised by

$$\dot{\eta}(t) = -\beta\eta(t) + \sqrt{D}\xi(t), \tag{7.9}$$

where β is a positive constant. Then similarly to the first item for the displacement, we have to solve the following two-dimensional Fokker-Planck equation

$$\begin{aligned}\frac{\partial}{\partial t}p(v, \eta, t|v_0, \eta_0, 0) = \frac{\partial}{\partial v}\left\{\left[\Phi'(v) - \eta\right]p(v, \eta, t|v_0, \eta_0, 0)\right\} + \beta\frac{\partial}{\partial \eta}[\eta p(v, \eta, t|v_0, \eta_0, 0)] \\ + D\frac{\partial^2}{\partial \eta^2}p(v, \eta, t|v_0, \eta_0, 0),\end{aligned} \tag{7.10}$$

where $\Phi(v)$ is stated in Eq. (1.7). Even though we may resort to numerical methods to obtain the solution of Eq. (7.10) numerically, analytic results are desirable, for instance, if we are interested in the weak-noise limit and in the limit of the coloured noise approaching the white noise.

(5) It would be interesting to compare the analytic results derived in this thesis with experimental data. For instance, we may apply the mechanical experiment setups used in Refs. [23, 42, 40, 41] to obtain experimental data. Then comparing these data with the analytic FPT distribution and the MVD till the FPT we may check whether there is a dry friction effect between a solid object and a solid surface. In addition, we can also compare the experimental results with the theoretical results of the occupation time and the displacement with respect to moments and distributions in order to check the usefulness of the dry friction model for an experiment setup.

Appendix A

A.1 Analytic action of Eq. (1.9) in the weak-noise limit

For our purpose, let us first consider in the following the approximation of $\hat{p}(x,\tau|x',\tau)$ (1.10) for $x'>0$ in the limit

$$\frac{|\tau-|x|-x'|}{2\sqrt{\tau}}\to\infty. \tag{A.1}$$

Using the leading-order term of the error function (1.11) in the limit $|z|\to\infty$ (see, e.g., Ref. [3]):

$$\mathrm{erf}(z)=\frac{2}{\sqrt{\pi}}\int_0^z e^{-t^2}dt\simeq\begin{cases}1-e^{-z^2}/(\sqrt{\pi}z) & \text{for } z>0,\\ -1-e^{-z^2}/(\sqrt{\pi}z) & \text{for } z<0,\end{cases} \tag{A.2}$$

it follows from Eq. (1.10) that

$$\hat{p}(x,\tau|x',0)\simeq\frac{e^{-\tau/4}}{2\sqrt{\pi\tau}}e^{-(|x|-x')/2}e^{-(x-x')^2/(4\tau)}-\frac{e^{-(\tau-|x|-x')^2/(4\tau)-|x|}}{2\sqrt{\pi/\tau}(\tau-|x|-x')}+\frac{e^{-|x|}}{2} \tag{A.3}$$

for $\tau>|x|+x'$, and

$$\hat{p}(x,\tau|x',0)\simeq\frac{e^{-\tau/4}}{2\sqrt{\pi\tau}}e^{-(|x|-x')/2}e^{-(x-x')^2/(4\tau)}-\frac{e^{-(\tau-|x|-x')^2/(4\tau)-|x|}}{2\sqrt{\pi/\tau}(\tau-|x|-x')} \tag{A.4}$$

for $\tau<|x|+x'$.

Case 1: $\tau < x'$

In this case, Eq. (A.4) applies. Since the terms that enter the exponentials of Eq. (A.4) satisfy

$$-\tau/4 - (|x| - x')/2 - (x - x')^2/(4\tau) \geqslant -(\tau - |x| - x')^2/(4\tau) - |x| \tag{A.5}$$

for all x, we have in the leading order that

$$\ln \hat{p}(x, \tau|x', 0) \simeq -\tau/4 - (|x| - x')/2 - (x - x')^2/(4\tau). \tag{A.6}$$

Case 2: $\tau > x'$

In this case we have to derive the asymptotic results for $\tau < |x| + x'$ and $\tau > |x| + x'$ separately. On the one hand, for $\tau < |x| + x'$, Eq. (A.4) applies and results in Eq. (A.6). On the other hand, under the condition $\tau > |x| + x'$, it is straightforward to check that

$$-\tau/4 - (|x| - x')/2 - (x - x')^2/(4\tau) \leqslant -|x| \tag{A.7}$$

if and only if $x \leqslant (\sqrt{\tau} - \sqrt{x'})^2$. Therefore, for $\tau > |x| + x'$ we obtain from Eq. (A.3) in the leading order that

$$\ln \hat{p}(x, \tau|x', 0) \simeq -|x| \tag{A.8}$$

for $x \in [x' - \tau, (\sqrt{\tau} - \sqrt{x'})^2]$, and Eq. (A.6) for $x \notin [x' - \tau, (\sqrt{\tau} - \sqrt{x'})^2]$.

Now we apply the above analysis to evaluate the analytic propagator (1.9)

$$p(v_t, t|v_0, 0) = \frac{\mu}{D} \hat{p}\left(\frac{\mu}{D} v_t, \frac{\mu^2}{D} t \middle| \frac{\mu}{D} v_0, 0\right). \tag{A.9}$$

We can use the results of $\hat{p}(x, t|x', 0)$ [see Eqs. (A.6) and (A.8)] directly by letting

$$x = \frac{\mu}{D} v_t, \quad x' = \frac{\mu}{D} v_0, \quad \tau = \frac{\mu^2}{D} t. \tag{A.10}$$

Hence, it is easy to know that the action $I(v_t, t|v_0, 0)$ (3.16) in the limit $D \to 0$ is

$$I(v_t, t|v_0, 0) = (v_t - v_0)^2/t + 2\mu(|v_t| - v_0) + \mu^2 t \tag{A.11}$$

for $t < v_0/\mu$, and

$$I(v_t, t|v_0, 0) = \begin{cases} (v_t - v_0)^2/t + 2\mu(|v_t| - v_0) + \mu^2 t & \text{for } v_t \notin [v_0 - \mu t, (\sqrt{\mu t} - \sqrt{v_0})^2], \\ 4\mu|v_t| & \text{for } v_t \in [v_0 - \mu t, (\sqrt{\mu t} - \sqrt{v_0})^2] \end{cases} \tag{A.12}$$

for $t > v_0/\mu$. These actions are exactly the same as those of the SPA(0) [see Eqs. (3.14) and (3.15)] since

$$(v_t - v_0)^2/t + 2\mu(|v_t| - v_0) + \mu^2 t = \begin{cases} (v_t - v_0 + \mu t)^2/t - 4\mu v_t & \text{for } v_t < 0, \\ (v_t - v_0 + \mu t)^2/t & \text{for } v_t > 0. \end{cases} \tag{A.13}$$

A.2 Some numerical schemes

A.2.1 Euler-Maruyama scheme

We integrate the generic Langevin equation (1.5) on the interval $[0, \Delta t]$ to obtain

$$v(\Delta t) - v(0) = -\int_0^{\Delta t} \Phi'(v(s))ds + \sqrt{D}\int_0^{\Delta t} \xi(s)ds, \tag{A.14}$$

where Δt is a small time-step. Since $\xi(s)$ is Gaussian, the integral $\int_0^{\Delta t} \xi(s)ds$ is also Gaussian. From Eqs. (1.3) and (1.4) we have

$$\left\langle \int_0^{\Delta t} \xi(s)ds \right\rangle = \int_0^{\Delta t} \langle \xi(s) \rangle ds = 0, \tag{A.15}$$

$$\left\langle \left(\int_0^{\Delta t} \xi(s)ds \right)^2 \right\rangle = \int_0^{\Delta t}\int_0^{\Delta t} \langle \xi(s)\xi(s') \rangle dsds' = \int_0^{\Delta t}\int_0^{\Delta t} 2\delta(s - s')dsds' = 2\Delta t. \tag{A.16}$$

Following Eq. (A.14) and the above properties of the integral $\int_0^{\Delta t} \xi(s)ds$, we can obtain for the generic Langevin equation (1.5) the so-called Euler-Maruyama scheme

$$v_{n+1} = v_n - \Phi'(v_n)\Delta t + \sqrt{2D\Delta t}W, \tag{A.17}$$

where v_n stands for the approximation to $v(n\Delta t)$ and W the standard Normal random variable. In chapter 6, we simulate the functional $T = \int_0^t U(v(\tau))d\tau$ by using the scheme

$$T_{n+1} = T_n - U(v_n)\Delta t \tag{A.18}$$

with the initial condition $T_0 = 0$. Here T_n is the approximation to the functional T at time $n\Delta t$.

A.2.2 Symplectic Euler scheme

For the Hamiltonian system

$$\dot{p}(t) = \frac{\partial}{\partial q} H(p, q), \tag{A.19}$$

$$\dot{q}(t) = -\frac{\partial}{\partial p} H(p, q) \tag{A.20}$$

with a separated Hamiltonian [see also Eqs. (2.10) and (2.11)]

$$H(p, q) = U(p) + V(q), \tag{A.21}$$

the so-called symplectic Euler scheme reads

$$p_{n+1} = p_n + \Delta t V'(q_n), \tag{A.22}$$

$$q_{n+1} = q_n - \Delta t U'(p_{n+1}). \tag{A.23}$$

This scheme is called symplectic scheme since it can preserve the discrete symplectic structure of the Hamiltonian system (A.19) and (A.20), i.e., for the above scheme we have $dp_{n+1} \wedge dq_{n+1} = dp_n \wedge dq_n$. This symplectic scheme can preserve the Hamiltonian of the original system better than other non-symplectic scheme in the long time simulation (see, e.g., Ref. [46]).

A.2.3 Numerical scheme for the Fokker-Planck equation

For the Fokker-Planck equation (1.6), in the weak-noise limit we assume the time-dependent solution has the form

$$p(v, t|v_0, 0) = N e^{-\varphi(v,t)/D}, \tag{A.24}$$

where N is a normalisation constant. Then substituting Eq. (A.24) into Eq. (1.6) results in

$$-\frac{\partial \varphi(v,t)}{\partial t} = D\Phi''(v) - \Phi'(v)\frac{\partial \varphi(v,t)}{\partial v} - D\frac{\partial^2 \varphi(v,t)}{\partial v^2} + \left(\frac{\partial \varphi(v,t)}{\partial v}\right)^2. \tag{A.25}$$

We can approximate the above equation by the Euler scheme in time and space directions to obtain

$$\frac{\varphi_k^n - \varphi_k^{n+1}}{\Delta t} = D\Phi''(v_n) - \Phi'(v_n)\frac{\varphi_{k+1}^n - \varphi_k^n}{\Delta v} - D\frac{\varphi_{k+2}^n - 2\varphi_{k+1}^n + \varphi_k^n}{(\Delta v)^2} + \left(\frac{\varphi_{k+1}^n - \varphi_k^n}{\Delta v}\right)^2, \tag{A.26}$$

where φ_k^n is the approximation to $\varphi(v_k, t_n)$, Δt is the time-step and Δv is the space-step. Rearranging Eq. (A.26) yields the final scheme

$$\begin{aligned}\varphi_k^{n+1} = \varphi_k^n - \Delta t\, D\, \Phi''(v_n) + \Delta t\, \Phi'(v_n)\, \frac{\varphi_{k+1}^n - \varphi_k^n}{\Delta v} + \Delta t\, D\, \frac{\varphi_{k+2}^n - 2\varphi_{k+1}^n + \varphi_k^n}{(\Delta v)^2} \\ -\Delta t \left(\frac{\varphi_{k+1}^n - \varphi_k^n}{\Delta v}\right)^2.\end{aligned} \tag{A.27}$$

In practice, we have to truncate the infinite domain into a finite domain, dented as $[-L, L]$. Here we use the following numerical boundary conditions

$$\varphi(-L, t) = \varphi(-L + \Delta v, t) + \Delta v, \qquad \varphi(L, t) = \varphi(L - \Delta v, t) + \Delta v, \tag{A.28}$$

and the initial value condition

$$\varphi(v, \Delta t) = \frac{(v - v_0 + \Phi'(v_0)\Delta t)^2}{4\Delta t}. \tag{A.29}$$

This initial value condition comes from the following derivation. For short time Δt, we can get an approximation to $v(\Delta t)$ from the corresponding Langevin equation [see Eq. (1.5)] of the Fokker-Planck equation (1.6):

$$v(\Delta t) \approx v_0 - \Phi'(v_0)\Delta t + \sqrt{D}\int_0^{\Delta t} \xi(s) ds. \tag{A.30}$$

Hence, we know that $v(\Delta t)$ is an approximately Gaussian random variable [see appendix A.2.2] with mean $v_0 - \Phi'(v_0)\Delta t$ and variance $2D\Delta t$. So the appropriate initial condition for $\varphi(v, \Delta t)$ is derived in Eq. (A.29).

A.3 Rescaling transforms of the Fokker-Planck equation

Even though transformation of variables can be done for the generic Langevin equation (1.5) directly (see Ref. [76]), it is easier to understand the transformation by looking at

the corresponding Fokker-Planck equation (1.6).

Let $\tau = \alpha t$ and $u = \beta v$, and assume $f(u, \tau|u_0, 0) = p(v, t|v_0, 0)/\beta$, denoting the new propagator. Then we have

$$\frac{\partial p}{\partial t} = \alpha\beta \frac{\partial f}{\partial \tau}, \qquad \frac{\partial^2 p}{\partial v^2} = \beta^3 \frac{\partial f}{\partial u^2}, \qquad \frac{\partial}{\partial v}[\Phi'(v)p] = \beta^2 \frac{\partial}{\partial u}\left[\Phi'\left(\frac{u}{\beta}\right) f\right]. \tag{A.31}$$

Substituting the above equations into Eq. (1.6) yields

$$\frac{\partial}{\partial \tau} f(u, \tau|u_0, 0) = \frac{\beta}{\alpha}\frac{\partial}{\partial u}\left[\Phi'\left(\frac{u}{\beta}\right) f(u, \tau|u_0, 0)\right] + \frac{D\beta^2}{\alpha}\frac{\partial^2}{\partial u^2} f(u, \tau|u_0, 0). \tag{A.32}$$

A.3.1 Case 1: $\Phi'(v) = \mu \tanh(v/\varepsilon)$

In this case, Eq. (A.32) reads

$$\frac{\partial}{\partial \tau} f(u, \tau|u_0, 0) = \frac{\beta}{\alpha}\frac{\partial}{\partial u}\left[\mu \tanh\left(\frac{u}{\beta\varepsilon}\right) f(u, \tau|u_0, 0)\right] + \frac{D\beta^2}{\alpha}\frac{\partial^2}{\partial u^2} f(u, \tau|u_0, 0). \tag{A.33}$$

Hence, it is obvious that the choices $\beta\varepsilon = 1$ and $\beta\mu/\alpha = 1$, i.e., $\alpha = \mu/\varepsilon$ and $\beta = 1/\varepsilon$, result in the Fokker-Planck equation corresponding to the Langevin equation (3.26).

A.3.2 Case 2: $\Phi'(v) = \mu\sigma(v)$

In this case, Eq. (A.32) reads

$$\frac{\partial}{\partial \tau} f(u, \tau|u_0, 0) = \frac{\beta}{\alpha}\frac{\partial}{\partial u}\left[\mu\sigma(u) f(u, \tau|u_0, 0)\right] + \frac{D\beta^2}{\alpha}\frac{\partial^2}{\partial u^2} f(u, \tau|u_0, 0) \tag{A.34}$$

for $\beta > 0$. Therefore, the choices $\alpha = \mu^2/D$ and $\beta = \mu/D > 0$ lead to the Fokker-Planck equation corresponding to the pure dry friction case (1.8) with $\mu = D = 1$.

A.3.3 Case 3: $\Phi'(v) = \mu\sigma(v) + \gamma v - b$

In this case, Eq. (A.32) reads

$$\frac{\partial}{\partial \tau} f(u, \tau|u_0, 0) = \frac{\beta}{\alpha}\frac{\partial}{\partial u}\left[\left(\mu\sigma(u) + \gamma\frac{u}{\beta} - b\right) f(u, \tau|u_0, 0)\right] + \frac{D\beta^2}{\alpha}\frac{\partial^2}{\partial u^2} f(u, \tau|u_0, 0) \tag{A.35}$$

for $\beta > 0$. Hence, if one chooses $\gamma/\alpha = 1$ and $D\beta^2/\alpha = 1$, i.e., $\alpha = \gamma$ and $\beta = \sqrt{\gamma/D}$, Eq. (A.35) results in

$$\frac{\partial}{\partial\tau} f(u,\tau|u_0,0) = \frac{\partial}{\partial u}\left[\left(\frac{\mu}{\sqrt{D\gamma}}\sigma(u) + u - \frac{b}{\sqrt{D\gamma}}\right) f(u,\tau|u_0,0)\right] + \frac{\partial^2}{\partial u^2} f(u,\tau|u_0,0). \tag{A.36}$$

Therefore, we can consider the full model (1.2) for $\gamma = D = 1$ without loss of generality.

For the special case with $b = 0$ and $\gamma = D = 1$, the choices $\beta\mu/\alpha = 1$ and $\beta^2/\alpha = 1$, i.e., $\alpha = \mu^2$ and $\beta = \mu$, result in a Fokker-Planck equation corresponding to the the Langevin equation (4.28) in chapter 4.

A.4 Asymptotic analysis

A.4.1 Asymptotic limit $\tau \to \infty$

In this asymptotic limit, H tends to zero. For the case $u_\tau < 0 < u_0$, we have $H > 0$. Then we can derive from Eq. (3.36) that

$$\begin{aligned}\theta_-(u_0,u_\tau,H) &= \ln[2\sinh(u_0)] + O(H) - \frac{1}{\sqrt{1+2H}}\ln\left[-\frac{H}{\sinh(u_\tau)} + O(H^2)\right] \\ &= \ln[2\sinh(u_0)] + O(H) - [1 - H + O(H^2)]\{-\ln[-\sinh(u_\tau)/H] + O(H)\} \\ &= \ln[2\sinh(u_0)] + \ln[-\sinh(u_\tau)/H] + O[H\ln(H)],\end{aligned} \tag{A.37}$$

and from Eq. (3.38) that

$$\begin{aligned}\sigma_-(u_0,u_\tau,H) &= \ln[2\tanh(u_0)] + O(H) - \ln[-H/\tanh(u_\tau) + O(H^2)] \\ &= \ln[2\tanh(u_0)] + \ln[-\tanh(u_\tau)/H] + O(H).\end{aligned} \tag{A.38}$$

For the case $u_0 > 0$ and $u_\tau > 0$, we have $H < 0$. Hence we can derive from Eq. (3.41) that

$$\begin{aligned}\theta_+(u_0,u_\tau,H) &= \ln[2\sinh(u_0)] + \ln[2\sinh(u_\tau)] + O(H) + \frac{\ln(1+2H)}{\sqrt{1+2H}} - \frac{\ln(-2H)}{\sqrt{1+2H}} \\ &= \ln[2\sinh(u_0)] + \ln[2\sinh(u_\tau)] + O(H) - [1 - H + O(H^2)]\ln(-2H) \\ &= \ln[2\sinh(u_0)] + \ln[-\sinh(u_\tau)/H] + O[H\ln(-H)],\end{aligned} \tag{A.39}$$

and from Eq. (3.43) that

$$\begin{aligned}\sigma_+ &= \ln[2\tanh(u_0)] + \ln[2\tanh(u_\tau)] + O(H) - \ln(-2H) \\ &= \ln[2\tanh(u_0)] + \ln[-\tanh(u_\tau)/H] + O(H).\end{aligned} \tag{A.40}$$

Therefore, from Eqs. (A.37) and (A.39) we know both the energy-time relations (3.35) and (3.40) result in Eq. (3.47) in the limit considered here.

A.4.2 Asymptotic limit $|u_\tau| \to \infty$

Let us first consider the case $u_\tau < 0 < u_0$. Since $H \to +\infty$ when $u_\tau \to -\infty$, we have [see Eq. (3.36)]

$$\begin{aligned}\theta_-(u_0, u_\tau, H) &= \frac{1}{\sqrt{1+2H}} \ln\left[\sinh(u_0) + \sqrt{\frac{2}{2+H^{-1}} + \sinh^2(u_0)}\right] \\ &\quad - \frac{1}{\sqrt{1+2H}} \ln\left[\sinh(u_\tau) + \sqrt{\frac{2}{2+H^{-1}} + \sinh^2(u_\tau)}\right] \\ &= \frac{1}{\sqrt{1+2H}} \left\{\ln\left[\sinh(u_0) + \cosh(u_0)\right] + O(H^{-1})\right\} \\ &\quad - \frac{1}{\sqrt{1+2H}} \left\{\ln\left[\sinh(u_\tau) + \cosh(u_\tau)\right] + O(H^{-1})\right\} \\ &= \frac{1}{\sqrt{1+2H}}[u_0 - u_\tau + O(H^{-1})].\end{aligned} \tag{A.41}$$

Similarly, for the case $u_\tau > u_0 > 0$, we have

$$\theta_-(u_\tau, u_0, H) = \frac{1}{\sqrt{1+2H}}[u_\tau - u_0 + O(H^{-1})]. \tag{A.42}$$

Hence, we obtain Eq. (3.51) for $|u_\tau| \to \infty$.

For $H \to +\infty$, we have

$$\begin{aligned}\ln\left[\tanh(u_0) + \sqrt{2H + \tanh^2(u_0)}\right] &= \ln\left[\sqrt{2H}\left(\frac{\tanh(u_0)}{\sqrt{2H}} + \sqrt{1 + \frac{\tanh^2(u_0)}{2H}}\right)\right] \\ &= \ln(\sqrt{2H}) + O(H^{-1/2}).\end{aligned} \tag{A.43}$$

Similarly, we obtain

$$\ln\left[\tanh(u_\tau)+\sqrt{2H+\tanh^2(u_\tau)}\right]=\ln(\sqrt{2H})+O(H^{-1/2}). \tag{A.44}$$

Hence, substituting Eqs. (A.43) and (A.44) into Eq. (3.38) we obtain $\sigma_-(u_0,u_\tau,H)=O(H^{-1/2})$. In addition, the same analysis applies to yield $\sigma_-(u_\tau,u_0,H)=O(H^{-1/2})$.

A.5 Energy-time relation

A.5.1 Monotonicity of θ_-

Consider the expression defined in Eq. (3.36) either for $u_\tau<0<u_0$ and $H>0$, or for $0<u_\tau<u_0$ and $H>H_{\min}=-\tanh^2(u_\tau)/2$. The argument of the logarithm in Eq. (3.36) can be written as

$$g(x)=\frac{a+\sqrt{x+a^2}}{b+\sqrt{x+b^2}}, \tag{A.45}$$

where $a=\sinh(u_0)$, $b=\sinh(u_\tau)$ and $x=2H/(1+2H)$, being a monotonically increasing function of H. It is easy to see that $g(x)>1$ in the given parameter ranges, i.e, either $b<0<a$ and $x>0$, or $0<b<a$ and $x>-b^2$. In addition, it follows by differentiation that $g'(x)<0$, i.e., g is monotonically decreasing. Hence, θ_- considered as a function of H is the product of two positive monotonically decreasing functions so that θ_- itself is monotonically decreasing.

A.5.2 Critical points of θ_+

Since Eq. (3.41) is a symmetric expression in the first two arguments it is sufficient to consider the case $0<u_\tau<u_0$ and $H_{\min}=-\tanh^2(u_\tau)/2<H<0$. The critical points are determined by the vanishing derivative of θ_+. It is more convenient to consider the expression in terms of the new variable $\chi\in[0,u_\tau]$ defined by $H=-\tanh^2(\chi)/2$, where $-\chi$ represents the turning point of the indirect path, introduced in the case 2 of section 3.3.1. Then differentiation gives

$$\frac{\partial\theta_+(u_0,u_\tau,-\tanh^2(\chi)/2)}{\partial\chi}=h(\sinh(u_0),\sinh(\chi))+h(\sinh(u_\tau),\sinh(\chi)), \tag{A.46}$$

where we have introduced

$$h(a,z) = z\ln\left(a/z + \sqrt{(a/z)^2 - 1}\right) - \frac{(1+z^2)a}{z\sqrt{a^2-z^2}}, \quad (0 < z < a). \tag{A.47}$$

The critical points of θ_+ are thus determined by the solutions of the equation

$$h(\sinh(u_0), z) + h(\sinh(u_\tau), z) = 0. \tag{A.48}$$

We now show that the right-hand side of Eq. (A.46) is a concave function of $z = \sinh(\chi)$, so that there exist at most two solutions. To do so, compute the second derivative of Eq. (A.47):

$$\frac{\partial h(a,z)}{\partial z} = \ln\left(a/z + \sqrt{(a/z)^2 - 1}\right) + a\frac{z^4 - 2(a^2+1)z^2 + a^2}{z^2\left(a^2-z^2\right)^{3/2}}, \tag{A.49}$$

$$\begin{aligned}\frac{\partial^2 h(a,z)}{\partial z^2} &= -a\frac{z^4(6+2a^2) + z^2(-5a^2+a^4) + 2a^4}{z^3\left(a^2-z^2\right)^{5/2}} \\ &= -a\frac{6(z^2 - a^2/2)^2 + 2a^2z^4 + a^2(a^2+1)z^2 + a^4/2}{z^3\left(a^2-z^2\right)^{5/2}}.\end{aligned} \tag{A.50}$$

It is easy to see that the second derivative is negative for any (positive) values of a. The same holds for Eq. (A.48), proving concavity.

Finally, it is obvious from Eq. (3.41) that $\theta_+(u_0, u_\tau, H)$ tends to ∞ as $H \to 0-$ and that $\theta_+(u_0, u_\tau, H_{\min})$ is finite and positive, resulting altogether in a monotonically increasing shape [see Fig. 3.14(b)] or a cubic shape [see Fig. 3.14(c)] for the graph of $\theta_+(u_0, u_\tau, H)$.

A.6 Eigenvalue problem for the pure dry friction case

Without viscous damping and driving Eq. (2.18) reads [see Eq. (4.2)]

$$-\Lambda u_\Lambda(v) = u''_\Lambda(v) + u'_\Lambda(v) \qquad \text{for } v > 0 \tag{A.51}$$

$$-\Lambda u_\Lambda(v) = u''_\Lambda(v) - u'_\Lambda(v) \qquad \text{for } a < v < 0. \tag{A.52}$$

Let

$$u_\Lambda(v) = e^{-|v|/2}\varphi_\Lambda(v), \tag{A.53}$$

then Eqs. (A.51) and (A.52) can be written as

$$\varphi''_\Lambda(v) = (1/4 - \Lambda)\varphi_\Lambda(v) \qquad \text{for } v \neq 0. \tag{A.54}$$

On the one hand, for $\Lambda < 1/4$ let us introduce the positive variable $\lambda = \sqrt{1/4 - \Lambda}$. Then the solution of Eq. (A.54) which results in a finite normalisation factor [see Eq. (2.22)] is given by

$$\varphi_\Lambda(v) = \begin{cases} A_\lambda e^{-\lambda v} & \text{for } v > 0 \\ B_\lambda e^{\lambda v} + C_\lambda e^{-\lambda v} & \text{for } a < v < 0. \end{cases} \tag{A.55}$$

Choose $A_\lambda = 2\lambda$ and use the matching conditions (2.20) and (2.21) to determine the other two coefficients in Eq. (A.55) as

$$B_\lambda = 1, \qquad C_\lambda = 2\lambda - 1. \tag{A.56}$$

The eigenvalue is now determined by the absorbing boundary condition (2.19), i.e., $\varphi_\Lambda(a) = 0$, which results in Eq. (4.4).

On the other hand, for $\Lambda > 1/4$ the solution of Eq. (A.54) which vanishes at $v = a$, i.e., which satisfies the absorbing boundary condition (2.19), is given by

$$\varphi_\Lambda(v) = \begin{cases} \bar{A}_\kappa \sin(\kappa v) + \bar{B}_\kappa \cos(\kappa v) & \text{for } v > 0 \\ \bar{C}_\kappa \sin[\kappa(v - a)] & \text{for } a < v < 0, \end{cases} \tag{A.57}$$

where we have introduced the abbreviation $\kappa = \sqrt{\Lambda - 1/4} > 0$. Choose $\bar{C}_\kappa = \kappa$, then by using the matching conditions (2.20) and (2.21), the two parameters $\bar{A}_\kappa$ and $\bar{B}_\kappa$ are evaluated as

$$\bar{A}_\kappa = \kappa \cos(a\kappa) + \sin(a\kappa), \qquad \bar{B}_\kappa = -\kappa \sin(a\kappa). \tag{A.58}$$

Hence, Eq. (4.9) follows from substituting Eq. (A.57) into Eq. (A.53). For the normali-

sation, Eqs. (A.53) and (A.57) result in

$$\begin{aligned}\int_a^\infty u_\Lambda(v)u_{\Lambda'}(v)e^{|v|}dv &= \int_0^\infty [\bar{A}_\kappa \sin(\kappa v) + \bar{B}_\kappa \cos(\kappa v)][\bar{A}_{\kappa'} \sin(\kappa' v) + \bar{B}_{\kappa'} \cos(\kappa' v)]dv \\ &\quad + \int_a^0 \kappa\kappa' \sin[\kappa(v-a)] \sin[\kappa'(v-a)]dv \\ &= \int_0^\infty \Big\{ \frac{1}{2}\left(\bar{A}_\kappa \bar{A}_{\kappa'} + \bar{B}_\kappa \bar{B}_{\kappa'}\right) \cos[(\kappa-\kappa')v] \\ &\quad + \frac{1}{2}\left(\bar{B}_\kappa \bar{B}_{\kappa'} - \bar{A}_\kappa \bar{A}_{\kappa'}\right) \cos[(\kappa+\kappa')v] \\ &\quad + \frac{1}{2}\left(\bar{A}_\kappa \bar{B}_{\kappa'} - \bar{A}_{\kappa'} \bar{B}_\kappa\right) \sin[(\kappa-\kappa')v] \\ &\quad + \frac{1}{2}\left(\bar{A}_\kappa \bar{B}_{\kappa'} + \bar{A}_{\kappa'} \bar{B}_\kappa\right) \sin[(\kappa+\kappa')v] \Big\} dv - \frac{\kappa \bar{A}_\kappa \bar{B}_{\kappa'} - \kappa' \bar{A}_{\kappa'} \bar{B}_\kappa}{\kappa^2 - \kappa'^2} \\ &= \frac{\pi}{2}(\bar{A}_\kappa^2 + \bar{B}_\kappa^2)\delta(\kappa - \kappa'), \end{aligned} \tag{A.59}$$

which shows that the normalisation factor Z_Λ satisfies Eq. (4.10) if we take Eq. (A.58) into account. To derive Eq. (A.59), we have used the standard identities for the δ and the principal-value distribution:

$$\int_0^\infty \cos(\kappa v)dv = \pi\delta(\kappa), \qquad \int_0^\infty \sin(\kappa v)dv = P\left(\frac{1}{\kappa}\right) = \begin{cases} 0 & \text{for } \kappa = 0, \\ 1/\kappa & \text{for } \kappa \neq 0. \end{cases} \tag{A.60}$$

A.7 Eigenvalue problem for the full model

For the full model (1.2), the eigenvalue problem (2.18) reads [see Eq. (4.24)]

$$-\Lambda u_\Lambda(v) = [(v+\mu-b)u_\Lambda(v)]' + u_\Lambda''(v) \qquad \text{for } v > 0, \tag{A.61}$$

$$-\Lambda u_\Lambda(v) = [(v-\mu-b)u_\Lambda(v)]' + u_\Lambda''(v) \qquad \text{for } a < v < 0. \tag{A.62}$$

These two equations are a special case of the so-called Kummer's equation, which can be solved in terms of parabolic cylinder functions (see Ref. [88] and also appendix A.9). The solution of Eqs. (A.61) and (A.62) which vanishes at infinity is given by (see Refs. [19, 89])

$$u_\Lambda(v) = \begin{cases} A_\Lambda e^{-(v+\mu-b)^2/4} D_\Lambda(v+\mu-b) & \text{for } v > 0, \\ e^{-(v-\mu-b)^2/4}\left[B_\Lambda D_\Lambda(v-\mu-b) + C_\Lambda D_\Lambda(-v+\mu+b)\right] & \text{for } a < v < 0, \end{cases} \tag{A.63}$$

where $D_\Lambda(z)$ denotes the parabolic cylinder function. Here we have used a fundamental system in terms of $D_\nu(z)$ and $D_\nu(-z)$ to write down the solution. Such a fundamental system degenerates for ν being an integer. Thus, our expressions may contain spurious singularities at integer values of Λ which have to be taken care of. The coefficients A_Λ, B_Λ and C_Λ depend on the parameters b and μ as well, but are independent of v.

Using Eq. (A.63) the matching conditions (2.20) and (2.21) result in a set of linear homogeneous equations

$$B_\Lambda D_\Lambda(-\mu-b)+C_\Lambda D_\Lambda(\mu+b)=e^{\mu b}A_\Lambda D_\Lambda(\mu-b), \tag{A.64}$$

$$B_\Lambda D_{1+\Lambda}(-\mu-b)-C_\Lambda D_{1+\Lambda}(\mu+b)=e^{\mu b}A_\Lambda[D_{1+\Lambda}(\mu-b)-2\mu D_\Lambda(\mu-b)], \tag{A.65}$$

when the property (A.84) of the parabolic cylinder function is employed. For A_Λ we choose

$$A_\Lambda=\sqrt{2\pi}e^{-\mu b}. \tag{A.66}$$

Then, the other two coefficients in Eq. (A.63) follow as

$$B_\Lambda=\Gamma(1-\Lambda)[D_\Lambda(\mu+b)D_{\Lambda-1}(\mu-b)+D_\Lambda(\mu-b)D_{\Lambda-1}(\mu+b)], \tag{A.67}$$

$$C_\Lambda=-\Gamma(1-\Lambda)[D_\Lambda(-\mu-b)D_{\Lambda-1}(\mu-b)-D_\Lambda(\mu-b)D_{\Lambda-1}(-\mu-b)], \tag{A.68}$$

where we have used the identities (A.80) and (A.85) to simplify the above two expressions.

The characteristic equation simply follows from the boundary condition (2.19), and is thus given by

$$B_\Lambda D_\Lambda(a-\mu-b)+C_\Lambda D_\Lambda(-a+\mu+b)=0\,, \tag{A.69}$$

which results in Eq. (4.25) if we take Eqs. (A.67) and (A.68) into account.

For the integral over the eigenfunction which enters the FPT distribution (4.29) we obtain by using the differential identity (A.84)

$$\begin{aligned}\int_a^\infty u_\Lambda(v)dv=\;&e^{-(a-\mu-b)^2/4}[B_\Lambda D_{\Lambda-1}(a-\mu-b)-C_\Lambda D_{\Lambda-1}(-a+\mu+b)]\\&-e^{-(\mu+b)^2/4}[B_\Lambda D_{\Lambda-1}(-\mu-b)-C_\Lambda D_{\Lambda-1}(\mu+b)]\\&+A_\Lambda e^{-(\mu-b)^2/4}D_{\Lambda-1}(\mu-b).\end{aligned} \tag{A.70}$$

Finally to compute the normalisation let us consider the integral

$$
\begin{aligned}
&(\Lambda-\Lambda')\int_a^\infty e^{[v+\mu\sigma(v)]^2/2-bv}u_\Lambda(v)u_{\Lambda'}(v)dv\\
&\quad=e^{-\mu b-b^2/2}(\Lambda-\Lambda')\int_a^0[B_\Lambda D_\Lambda(v-\mu-b)+C_\Lambda D_\Lambda(-v+\mu+b)]\\
&\qquad\times[B_{\Lambda'}D_{\Lambda'}(v-\mu-b)+C_{\Lambda'}D_{\Lambda'}(-v+\mu+b)]dv\\
&\qquad+e^{\mu b-b^2/2}(\Lambda-\Lambda')A_\Lambda A_{\Lambda'}\int_0^\infty D_\Lambda(v+\mu-b)D_{\Lambda'}(v+\mu-b)dv\\
&\quad=e^{-\mu b-b^2/2}(\Lambda-\Lambda')\int_{a-\mu-b}^{-\mu-b}[B_\Lambda D_\Lambda(v)+C_\Lambda D_\Lambda(-v)][B_{\Lambda'}D_{\Lambda'}(v)+C_{\Lambda'}D_{\Lambda'}(-v)]dv\\
&\qquad+e^{\mu b-b^2/2}(\Lambda-\Lambda')A_\Lambda A_{\Lambda'}\int_{\mu-b}^\infty D_\Lambda(v)D_{\Lambda'}(v)dv\\
&\quad=e^{-\mu b-b^2/2}\big\{-B_\Lambda D_{\Lambda+1}(a-\mu-b)[B_{\Lambda'}D_{\Lambda'}(a-\mu-b)+C_{\Lambda'}D_{\Lambda'}(\mu-a+b)]\\
&\qquad+B_{\Lambda'}D_{\Lambda'+1}(a-\mu-b)[B_\Lambda D_\Lambda(a-\mu-b)+C_\Lambda D_\Lambda(\mu-a+b)]\\
&\qquad+C_\Lambda D_{\Lambda+1}(\mu-a+b)[B_{\Lambda'}D_{\Lambda'}(a-\mu-b)+C_{\Lambda'}D_{\Lambda'}(\mu-a+b)]\\
&\qquad-C_{\Lambda'}D_{\Lambda'+1}(\mu-a+b)[B_\Lambda D_\Lambda(a-\mu-b)+C_\Lambda D_\Lambda(\mu-a+b)]\big\}.
\end{aligned}
\tag{A.71}
$$

For the last computational step we have used the properties (A.83) and (A.84). Indeed, if we choose for Λ and Λ' two different eigenvalues we obtain (bi-)orthogonality of the eigenfunctions if the characteristic equation (A.69) is taken into account. Furthermore, dividing Eq. (A.71) on both sides by $\Lambda-\Lambda'$ and taking the limit $\Lambda'\to\Lambda$ we end up with the normalisation factor

$$
\begin{aligned}
Z_\Lambda=e^{-\mu b-b^2/2}&\left[B_\Lambda D_{\Lambda+1}(a-\mu-b)-C_\Lambda D_{\Lambda+1}(\mu-a+b)\right]\\
&\times\partial_\Lambda\left[B_\Lambda D_\Lambda(a-\mu-b)+C_\Lambda D_\Lambda(\mu-a+b)\right].
\end{aligned}
\tag{A.72}
$$

A.8 Moments of the occupation time

Substituting Eq. (6.28) into Eq. (6.19) results in the first moment of the occupation time:

$$
\widetilde{M}_1(s,v_0)=\begin{cases}1/s^2+C_1^+\varphi(s,v_0) & \text{for } v_0>0,\\ C_1^-\varphi(s,v_0) & \text{for } v_0<0,\end{cases}
\tag{A.73}
$$

where the coefficients $C_1^\pm$ are determined by the first-order smooth matching condition at $v_0=0$ [see Eqs. (6.15) and (6.17)]. Then using the property (6.27) it is easy to derive

from Eq. (6.19) that the second moment can be expressed as

$$\widetilde{M}_2(s,v_0)=\begin{cases}2/s^3-2C_1^+\frac{\partial}{\partial s}\varphi(s,v_0)+C_2^+\varphi(s,v_0) & \text{for } v_0>0,\\ C_2^-\varphi(s,v_0) & \text{for } v_0<0.\end{cases} \tag{A.74}$$

Similarly, the third moment reads

$$\widetilde{M}_3(s,v_0)=\begin{cases}3/s^4+3C_1^+\frac{\partial^2}{\partial s^2}\varphi(s,v_0)-3C_2^+\frac{\partial}{\partial s}\varphi(s,v_0)+C_3^+\varphi(s,v_0) & \text{for } v_0>0,\\ C_3^-\varphi(s,v_0) & \text{for } v_0<0.\end{cases} \tag{A.75}$$

Here the coefficients $C_2^\pm$ and $C_3^\pm$ are again determined by the matching conditions (6.15) and (6.17). By observing the first three moments presented here, we can already guess that the n-th moment has the form as shown in Eq. (6.29). Indeed, using the inductive method it is easy to prove our guess since the moments defined in Eq. (6.29) satisfy Eq. (6.11) with

$$U(v_0)=\theta(v_0)=\begin{cases}1 & \text{for } v_0>0,\\ 0 & \text{for } v_0\leqslant 0.\end{cases} \tag{A.76}$$

A.9 Properties of parabolic cylinder function

The parabolic cylinder functions are a class of functions sometimes called Weber functions (see, e.g., Refs. [33, 19, 28]). Here we denote them as $D_\nu(z)$, which satisfy the following differential equation

$$\frac{d^2D_\nu(z)}{dz^2}-\left(\frac{z^2}{4}-\nu-\frac{1}{2}\right)D_\nu(z)=0 \tag{A.77}$$

and read

$$D_\nu(z)=\begin{cases}\dfrac{e^{-z^2/4}}{\Gamma(-\nu)}\displaystyle\int_0^\infty t^{-\nu-1}e^{-zt-t^2/2}dt & \text{for } \mathrm{Re}(\nu)<0,\\ \dfrac{e^{z^2/4}}{\sqrt{\pi/2}}\displaystyle\int_0^\infty t^{\nu}e^{-t^2/2}\cos(zt-\nu\pi/2)dt & \text{for } \mathrm{Re}(\nu)>-1,\end{cases} \tag{A.78}$$

where $\Gamma(z)$ denotes the Gamma function [28]. The two branches of this formula agree for $-1<\mathrm{Re}(\nu)<0$. From the expression (A.78) it is easy to see that if $\nu<0$ then $D_\nu(z)>0$ for any real values of z. If ν is not an integer, $D_\nu(z)$ and $D_\nu(-z)$ are independent and the solutions of Eq. (A.77) can be expressed in terms of this fundamental system. Moreover,

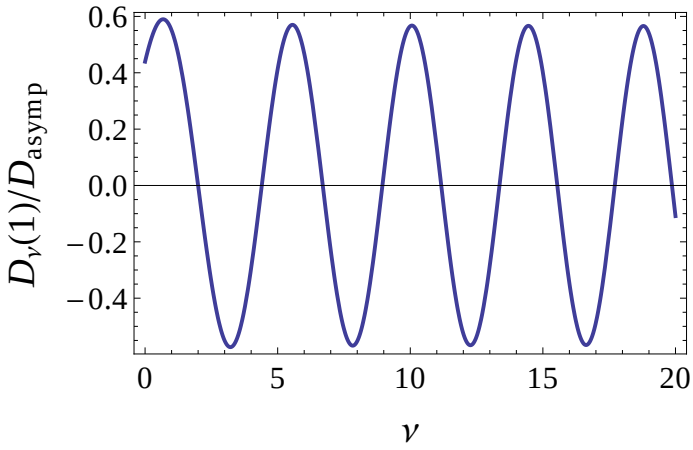

Figure A.1: Parabolic cylinder function $D_\nu(z)$ for z = 1 normalised by the asymptotic growth D_{asymp} (A.79) for large ν. The resulting expression remains bounded.

if we consider $D_\nu(z)$ as a function of the index ν for fixed z, it is useful to normalise it by the asymptotic growth

$$D_{\text{asymp}} = 2^{\nu/2}\Gamma((1+\nu)/2) \tag{A.79}$$

for large ν (see Refs. [3, 88] and also Fig. A.1)

For the parabolic cylinder functions, we have the following recurrence relation

$$D_{\nu+1}(z) = zD_\nu(z) - \nu D_{\nu-1}(z), \tag{A.80}$$

and the differential identity

$$D'_\nu(z) + \frac{z}{2}D_\nu(z) = \nu D_{\nu-1}(z). \tag{A.81}$$

By using Eq. (A.80), we can obtain another differential identity from Eq. (A.81), i.e.,

$$D'_\nu(z) - \frac{z}{2}D_\nu(z) = -D_{\nu+1}(z). \tag{A.82}$$

Then from Eqs. (A.81) and (A.82) it is straightforward to derive the following two

standard differential identities

$$\frac{de^{z^2/4}D_\nu(z)}{dz} = \nu e^{z^2/4}D_{\nu-1}(z), \tag{A.83}$$

$$\frac{de^{-z^2/4}D_\nu(z)}{dz} = -e^{-z^2/4}D_{\nu+1}(z), \tag{A.84}$$

which are the essential properties used to prove the orthogonal properties of the eigenfunctions in chapter 4. In addition, we have the following property for the fundamental system $(D_\nu(z), D_\nu(-z))$:

$$D_\nu(z)D_{\nu+1}(-z) + D_\nu(-z)D_{\nu+1}(z) = \frac{\sqrt{2\pi}}{\Gamma(-\nu)}. \tag{A.85}$$

In particular, we have

$$D_{-1}(z) = \frac{\pi}{2}e^{z^2/4}\mathrm{erf}\left(\frac{z}{\sqrt{2}}\right), \tag{A.86}$$

$$D_0(z) = e^{-z^2/4}. \tag{A.87}$$

Based on these two equations, all other expressions for the parabolic cylinder functions with integer index ν can be obtained by using the recurrence relation (A.80). For instance, we have

$$D_{-2}(z) = D_0(z) - zD_{-1}(z) = e^{-z^2/4} - \frac{\pi z}{2}e^{z^2/4}\mathrm{erf}\left(\frac{z}{\sqrt{2}}\right), \tag{A.88}$$

$$D_1(z) = zD_0(z) = ze^{-z^2/4}, \tag{A.89}$$

$$D_2(z) = zD_1(z) - D_0(z) = (z^2-1)e^{-z^2/4}. \tag{A.90}$$

Bibliography

[1] J. Abate and P. P. Valkó. Multi-precision Laplace transform inversion. *Int. J. Numer. Meth. Engng*, 60:979–993, 2004.

[2] J. Abate and W. Whitt. A unified framework for numerically inverting Laplace transforms. *INFORMS J. Comput.*, 18:408–421, 2006.

[3] M. Abramowitz and I. A. Stegun. *Handbook of Mathematical Functions*. Dover Publications, New York, 1968.

[4] L. Alili, P. Patie, and J. L. Pedersen. Representations of the first hitting time density of an Ornstein-Uhlenbeck process. *Stoch. Models*, 21:967–980, 2006.

[5] J. D. Atkinson and J. K. Dienes. First order piecewise linear systems with random parametric excitation. *Int. J. Non-Linear Mech.*, 3:399–411, 1968.

[6] A. Baule, E. G. D. Cohen, and H. Touchette. A path integral approach to random motion with nonlinear friction. *J. Phys. A: Math. Theor.*, 43:025003, 2010.

[7] A. Baule and P. Sollich. Singular features in noise-induced transport with dry friction. *Europhys. Lett.*, 97:20001, 2012.

[8] A. Baule and P. Sollich. Rectification of asymmetric surface vibrations with dry friction: An exactly solvable model. *Phys. Rev. E*, 87:032112, 2013.

[9] A. Baule, H. Touchette, and E. G. D. Cohen. Stick-slip motion of solids with dry friction subject to random vibrations and an external field. *Nonlinearity*, 24:351–372, 2011.

[10] V. E. Benes, L. A. Shepp, and H. S. Witsenhausen. Some solvable stochastic control problems. *Stochastics*, 4:39–83, 1980.

[11] E. J. Berger. Friction modeling for dynamic system simulation. *Appl. Mech. Rev.*, 55:535–577, 2002.

[12] M. Bernardo, C. Budd, A. R. Champneys, and P. Kowalczyk. *Piecewise-Smooth Dynamical Systems: Theory and Applications*. Springer, Berlin, 2008.

[13] J. J. B. Biemond, N. van de Wouw, and H. Nijmeijer. Bifurcations of equilibrium sets in mechanical systems with dry friction. *Physica D: Nonlinear Phenomena*, 241:1882–1894, 2012.

[14] I. F. Blake and W. C. Lindsey. Level-crossing problems for random processes. *IEEE Trans. Inf. Theory*, IT-19:295–315, 1973.

[15] M. Boué, P. Dupuis, and R. S. Ellis. Large deviations for small noise diffusions with discontinuous statistics. *Prob. Theory Relat. Fields*, 116:125–149, 2000.

[16] F. P. Bowden and D. Tabor. *The Friction and Lubrication of Solids*. Oxford University Press, Oxford, 1950.

[17] A. J. Bray, S. N. Majumdar, and G. Schehr. Persistence and first-passage properties in nonequilibrium systems. *Adv. Phys.*, 62:225–361, 2013.

[18] S. Browne and W. Whitt. Piecewise-linear diffusion processes. In J. H. Dshalalow, editor, *Advances in Queueing*, pages 463–480, Boca Raton, 1995. CRC Press.

[19] H. Buchholz. *The Confluent Hypergeometric Function with Special Emphasis on its Applications*. Springer, Berlin, 1969.

[20] W. Cassing and J. Knoll. Path integral approach to the solution of Fokker-Planck equations. *Phys. Lett. B*, 106:443–448, 1981.

[21] T. K. Caughey and J. K. Dienes. Analysis of a nonlinear first-order system with a white noise input. *J. Appl. Phys.*, 32:2476–2479, 1961.

[22] M. Chaichian and A. Demichev. *Path Integrals in Physics: Stochastic Processes and Quantum Mechanics*, volume I. Institute of Physics Publishing, London, 2001.

[23] M. K. Chaudhury and S. Mettu. Brownian motion of a drop with hysteresis dissipation. *Langmuir*, 24:6128–6132, 2008.

[24] T.-S. Chiang and S.-J. Sheu. Large deviations for diffusion processes and occupation times with discontinuous drift. *Ann. Prob.*, 28:140–165, 2000.

[25] A. Colombo, M. di Bernardo, S. J. Hogan, and M. R. Jeffrey. Bifurcations of piecewise smooth flows: perspectives, methodologies and open problems. *Physica D*, 241:1845–1860, 2012.

[26] S. Condamin, O. Bénichou, V. Tejedor, R. Voituriez, and J. Klafter. First-passage times in complex scale-invariant media. *Nature*, 450:77–80, 2007.

[27] R. M. Corless, G. H. Gonnet, D. E. G. Hare, D. J. Jeffrey, and D. E. Knuth. On the Lambert W function. *Adv. Comp. Math.*, 5:329–359, 1996.

[28] A. Cuyt, V. B. Petersen, B. Verdonk, H. Waadeland, and W. B. Jones. *Handbook of Continued Fractions for Special Functions*. Springer, New York, 2008.

[29] D. A. Darling and A. J. F. Siegert. The first passage problem for a continuous Markov process. *Ann. Math. Stat.*, 24:624–639, 1953.

[30] P.-G. de Gennes. Brownian motion with dry friction. *J. Stat. Phys.*, 119:953–962, 2005.

[31] D. DeBlassie and R. Smits. The influence of a power law drift on the exit time of Brownian motion from a half-line. *Stoch. Proc. Appl.*, 117:629–654, 2007.

[32] F.-J. Elmer. Nonlinear dynamics of dry friction. *J. Phys. A: Math. Gen.*, 30:6057–6063, 1997.

[33] A. Erdélyi, W. Magnus, F. Oberhettinger, and F. G. Tricomi. *Higher Transcendental Functions*. based on notes left by H. Bateman, McGraw-Hill, New York, 1953.

[34] A. F. Filippov. *Differential Equations with Discontinuous Righthand Sides*. Kluwer, Dordrecht, 1988.

[35] M. I. Freidlin and A. D. Wentzell. *Random Perturbations of Dynamical Systems*, volume 260 of *Grundlehren der Mathematischen Wissenschaften*. Springer, New York, 1984.

[36] C. W. Gardiner. *Handbook of Stochastic Methods for Physics, Chemistry and the Natural Sciences*. Springer, Berlin, 1990.

[37] A. Gnoli, A. Petri, F. Dalton, G. Pontuale, G. Gradenigo, A. Sarracino, and A. Puglisi. Brownian ratchet in a thermal bath driven by Coulomb friction. *Phys. Rev. Lett.*, 110:120601, 2013.

[38] A. Gnoli, A. Puglisi, and H. Touchette. Granular Brownian motion with dry friction. *Europhys. Lett.*, 102:14002, 2013.

[39] A. Göing-Jaeschke and M. Yor. A survey and some generalizations of Bessel processes. *Bernoulli*, 9:313–349, 2003.

[40] P. S. Goohpattader and M. K. Chaudhury. Diffusive motion with nonlinear friction: apparently Brownian. *J. Chem. Phys.*, 133:024702, 2010.

[41] P. S. Goohpattader and M. K. Chaudhury. Random motion with interfacial contact: driven diffusion vis-á-vis mechanical activation. *Eur. Phys. J. E*, 35:67, 2012.

[42] P. S. Goohpattader, S. Mettu, and M. K. Chaudhury. Experimental investigation of the drift and diffusion of small objects on a surface subjected to a bias and an external white noise: roles of Coulombic friction and hysteresis. *Langmuir*, 25:9969–9979, 2009.

[43] M. Gradinaru, S. Herrmann, and B. Roynette. A singular large deviations phenomenon. *Ann. Inst. Poincaré B*, 37:555–580, 2001.

[44] R. Graham. Macroscopic potentials, bifurcations and noise in dissipative systems. In F. Moss and P. V. E. McClintock, editors, *Noise in Nonlinear Dynamical Systems*, volume 1, pages 225–278, Cambridge, 1989. Cambridge University Press.

[45] H. Guclu and G. Korniss. Extreme fluctuations in small-world networks with relaxational dynamics. *Phys. Rev. E*, 69:065104, 2004.

[46] E. Hairer, C. Lubich, and G. Wanner. *Geometric Numerical Integration: Structure-Preserving Algorithms for Ordinary Differential Equations*. Springer, Berlin, 2006.

[47] P. Hänggi, P. Talkner, and M. Borkovec. Reaction-rate theory: fifty years after Kramers. *Rev. Mod. Phys.*, 62:251–341, 1990.

[48] H. Hayakawa. Langevin equation with Coulomb friction. *Physica D*, 205:48–56, 2005.

[49] M. R. Jeffrey. Nondeterminism in the limit of nonsmooth dynamics. *Phys. Rev. Lett.*, 106:254103, 2011.

[50] M. Kac. On distribution of certain wiener functionals. *Trans. Amer. Math. Soc.*, 65:1–13, 1949.

[51] I. Karatzas and S. E. Shreve. Trivariate density of Brownian motion, its local and occupation times, with application to stochastic control. *Ann. Prob.*, 12:819–828, 1984.

[52] I. Karatzas and S. E. Shreve. *Brownian Motion and Stochastic Calculus*. Springer, Berlin, 1991.

[53] A. Kawarada and H. Hayakawa. Non-Gaussian velocity distribution function in a vibrating granular bed. *J. Phys. Soc. Jpn.*, 73:2037–2040, 2004.

[54] M. J. Kearney and S. N. Majumdar. On the area under a continuous time Brownian motion till its first-passage time. *J. Phys. A: Math. Gen.*, 38:4097–4104, 2005.

[55] P. E. Kloeden and E. Platen. *Numerical Solution of Stochastic Differential Equations*. Springer, Berlin, 1992.

[56] A. P. Korostelev and S. L. Leonov. Action functional for diffusions in discontinuous media. *Prob. Theory Relat. Fields*, 94:317–333, 1993.

[57] H. A. Kramers. Brownian motion in a field of force and the diffusion model of chemical reactions. *Physica*, 7:284–304, 1940.

[58] B. Leblanc and O. Scaillet. Path dependent options on yields in the affine term structure model. *Finance Stochast.*, 2:349–367, 1998.

[59] Q. Li, Y. Dong, D. Perez, A. Martini, and R. W. Carpick. Speed dependence of atomic stick-slip friction in optimally matched experiments and molecular dynamics simulations. *Phys. Rev. Lett.*, 106:126101, 2011.

[60] V. Linetsky. Computing hitting time densities for CIR and OU diffusions: applications to mean-reverting models. *J. Comput. Finance*, 7:1–22, 2004.

[61] S. N. Majumdar. Brownian functionals in physics and computer science. *Curr. Sci.*, 89:2076–2093, 2005.

[62] S. N. Majumdar and A. Comtet. Exact asymptotic results for persistence in the Sinai model with arbitrary drift. *Phys. Rev. E*, 66:061105, 2002.

[63] S. N. Majumdar and A. Comtet. Local and occupation time of a particle diffusing in a random medium. *Phys. Rev. Lett.*, 89:060601, 2002.

[64] S. N. Majumdar and A. Comtet. Airy distribution function: from the area under a Brownian excursion to the maximal height of fluctuating interfaces. *J. Stat. Phys.*, 119:777–826, 2005.

[65] O. Makarenkov and J. S. W. Lamb. Dynamics and bifurcations of nonsmooth systems: a survey. *Physica D: Nonlinear Phenomena*, 241:1826–1844, 2012.

[66] A. Manacorda, A. Puglisi, and A. Sarracino. Coulomb friction driving Brownian motors. *arXiv:1402.5266*, 2014.

[67] J. Masoliver and J. M. Porrà. Exact solution to the mean exit time problem for free inertial processes driven by Gaussian white noise. *Phys. Rev. Lett.*, 75:189–192, 1995.

[68] J. Masoliver and J. M. Porrà. Exact solution to the exit-time problem for an undamped free particle driven by Gaussian white noise. *Phys. Rev. E*, 53:2243–2256, 1996.

[69] A. Mauger. Anomalous motion generated by the Coulomb friction in the Langevin equation. *Physica A*, 367:129–135, 2006.

[70] A. M. Menzel and N. Goldenfeld. Effect of Coulombic friction on spatial displacement statistics. *Phys. Rev. E*, 84:011122, 2011.

[71] J. D. Murray. *Asymptotic Analysis*. Clarendon Press, Oxford, 1974.

[72] J. D. Noh and H. Rieger. Random walks on complex networks. *Phys. Rev. Lett.*, 92:118701, 2004.

[73] B. N. J. Persson. *Sliding Friction: Physical Principles and Applications*. Springer, Berlin, 1998.

[74] S. Redner. *A Guide to First-Passage Processes*. Cambridge University Press, Cambridge, 2001.

[75] P. Reimann. Brownian motors: noisy transport far from equilibrium. *Phys. Rep.*, 361:57–265, 2002.

[76] H. Risken. *The Fokker-Planck Equation: Methods of Solution and Applications*. Springer, Berlin, 1989.

[77] S. Sabhapandit, S. N. Majumdar, and A. Comtet. Statistical properties of functionals of the paths of a particle diffusing in a one-dimensional random potential. *Phys. Rev. E*, 73:051102, 2006.

[78] T. G. Sano and H. Hayakawa. Roles of dry friction in the fluctuating motion of an adiabatic piston. *Phys. Rev. E*, 89:032104, 2014.

[79] A. Sarracino. Time asymmetry of the Kramers equation with nonlinear friction: fluctuation-dissipation relation and ratchet effect. *Phys. Rev. E*, 88:052124, 2013.

[80] A. Sarracino, A. Gnoli, and A. Puglisi. Ratchet effect driven by Coulomb friction: The asymmetric Rayleigh piston. *Phys. Rev. E*, 87:040101, 2013.

[81] A. J. F. Siegert. On the first passage time probability problem. *Phys. Rev.*, 81:617–623, 1951.

[82] D. J. W. Simpson and R. Kuske. The positive occupation time of brownian motion with two-valued drift and asymptotic dynamics of sliding motion with noise. *Stoch. Dyn.*, 14:1450010, 2014.

[83] D. J. W. Simpson and R. Kuske. Stochastically perturbed sliding motion in piecewise-smooth systems. *Discrete Contin. Dyn. Syst. Ser. B*, 19:2889–2913, 2014.

[84] A. Talbot. The accurate numerical inversion of Laplace transforms. *IMA J. Appl. Math.*, 23:97–120, 1979.

[85] J. Talbot and P. Viot. Effect of dynamic and static friction on an asymmetric granular piston. *Phys. Rev. E*, 85:021310, 2012.

[86] J. Talbot, R. D. Wildman, and P. Viot. Kinetics of a frictional granular motor. *Phys. Rev. Lett.*, 107:138001, 2011.

[87] H. Touchette. The large deviation approach to statistical mechanics. *Phys. Rep.*, 478:1–69, 2009.

[88] H. Touchette, E. V. der Straeten, and W. Just. Brownian motion with dry friction: Fokker-Planck approach. *J. Phys. A: Math. Theor.*, 43:445002, 2010.

[89] H. Touchette, T. Prellberg, and W. Just. Exact power spectra of Brownian motion with solid friction. *J. Phys. A: Math. Theor.*, 45:395002, 2012.

[90] H. C. Tuckwell, F. Y. M. Wan, and J.-P. Rospars. A spatial stochastic neuronal model with ornstein-uhlenbeck input current. *Biol. Cybernet.*, 86:137–145, 2002.

[91] M. C. Wang and G. E. Uhlenbeck. On the theory of the Brownian motion II. *Rev. Mod. Phys.*, 17:323–342, 1945.

[92] A. J. Weymouth, D. Meuer, P. Mutombo, T. Wutscher, M. Ondracek, P. Jelinek, and F. J. Giessibl. Atomic structure affects the directional dependence of friction. *Phys. Rev. Lett.*, 111:126103, 2013.

[93] J. Whitehouse, M. R. Evans, and S. N. Majumdar. Effect of partial absorption on diffusion with resetting. *Phys. Rev. E*, 87:022118, 2013.

[94] E. Wong. The construction of a class of stationary Markoff processes. In R. Bellman, editor, *Stochastic Processes in Mathematical Physics and Engineering*, pages 264–276, Providence, R.I., 1964. American Mathematical Society.

[95] W. Zhang. Transition density of one-dimensional diffusion with discontinuous drift. *IEEE Trans. Aut. Cont.*, 35:980–985, 1990.

List of Abbreviations

SDE	stochastic differential equation
SPA	saddle-point approximation
SPA(0)	saddle-point approximation with zeroth-order action
SPA(1)	saddle-point approximation with first-order action
MCS	Monte Carlo simulation
DF	exact analytic solution of the pure dry friction model
FPT	first-passage time
MFPT	mean first-passage time
MVD	distribution of maximum velocity
ODE	ordinary differential equation

Index